

DK9901154

RECEIVED
MAR 10 1999
OSTI



Particle Transport

in

Inclined Annuli

Erik Kurtzhals

Ph.D. thesis

1993

DISTRIBUTION OF THIS DOCUMENT IS UNLIMITED
FOREIGN SALES PROHIBITED
al

Department of Chemical Engineering
The Technical University of Denmark (DTH)
DK-2800 Lyngby

DISCLAIMER

Portions of this document may be illegible in electronic image products. Images are produced from the best available original document.

Particle Transport in Inclined Annuli

Abstract:

A new model for the formation and behaviour of deposits in inclined wellbores is formulated. The annular space is divided into two layers, separated by a distinct plane boundary. While the lower layer is taken to consist of closely packed cuttings, the upper layer is presumed to behave as a pure fluid. A force balance for the lower layer decides whether it is stationary or slides in the upwards- or downwards direction. The position of the deposit surface is governed by the fluid shear stress at the deposit surface. The proposed model represents a major improvement compared to an earlier model by *Gavignet & Sobey*¹⁵.

The predictions from the SCSB-model are in good qualitative agreement with experimental results obtained by the author, and results published by research groups in the U.S.A, United Kingdom and Germany. The quantitative agreement is variable, presumably because the SCSB-model is a somewhat simplified description of particle behaviour in inclined annuli. However, the model provides a clearer understanding of the physical background for previously published experimental results.

In order to couple the theoretical work with experimental observations, an annular flow loop has been constructed. A characteristic feature in the flow loop design is the application of load cells, which permits determination of the annular particle content at steady state as well as under transient conditions. Due to delays in the constructional work, it has only been possible to perform a limited number of investigations in the loop. However, the results produced are in agreement with results published by other research groups.

Partikeltransport i Skråtstillede Annuli

Abstract:

En ny model for partikelaflejringers dannelse og opførsel i afvigelsesboringer præsenteres. Det annulære rum inddeles i to lag, der adskilles af en plan grænseflade. Mens det nedre lag antages at bestå af tæt pakkede boreskærver, antages det øvre lag at opføre sig som en ren væske. En kraftbalance for det nedre lag afgør om dette er stationært eller skrider op- eller nedover. Grænsefladens position bestemmes af den forskydningskraft hvormed borevæsken påvirker partikelaflejringens overflade. Den angivne model repræsenterer en væsentlig forbedring af en tidligere model fremsat af *Gavignet & Sobey*¹⁵.

Modellens forudsigelser er i god kvalitativ overensstemmelse med eksperimentelle resultater der er opnået i forbindelse med Ph.D.-arbejdet, samt resultater, der er blevet publiceret af forskningsgrupper i U.S.A., Storbritannien og Tyskland. Den kvantitative overensstemmelse varierer med de eksperimentelle parametre, formodentlig fordi modellen er en noget forenklet beskrivelse af partiklers opførsel i skråtstillede annuli. Modellen giver dog en klarere forståelse af den fysiske baggrund for tidligere publicerede resultater.

Med henblik på kombinere det teoretiske arbejde med eksperimentelle undersøgelser er der blevet opbygget et anlæg til studier af annulær tofasestrømning. Et karakteristisk træk ved anlæggets udformning er anvendelsen af vejeceller, der tillader bestemmelse af det annulære rums partikelindhold under såvel steady state betingelser som i forbindelse med transiente forløb. På grund af forsinkelser i opbygningsarbejdet har det kun været muligt at foretage få målinger i anlægget. Imidlertid er de opnåede resultater i overensstemmelse med resultater publiceret af andre forskningsgrupper.

TABLE OF CONTENTS

CHAPTER 1 : INTRODUCTION	1
1.1 An introduction to cuttings transport	2
1.2 A definition of cuttings transport	2
1.3 Quantification of steady state cuttings transport	3
1.4 Quantification of transient cuttings transport	4
CHAPTER 2 : PREVIOUS INVESTIGATIONS OF CUTTINGS TRANSPORT - A CHRONOLOGICAL REVIEW	5
2.1 Cuttings transport in vertical wellbores	6
2.2 Cuttings transport in deviated wellbores	8
CHAPTER 3 : SOME VARIABLES AFFECTING CUTTINGS TRANSPORT AND BEHAVIOUR	10
3.1 Annular inclination	11
3.2 Fluid Rheology	12
3.2.1 Annular flow regime	14
3.3 Particle size and- shape	15
3.4 Particle- and fluid density	16
3.5 Fluid flowrate	17
3.6 Annular eccentricity	18
3.7 Inner pipe rotation	20
3.8 Particle feed concentration	22
3.9 Annular dimensions	22
CHAPTER 4 : MODELLING WORK	23
4.1 Background	24
4.2 The SCSB-model	24
4.2.1 Geometry	24
4.2.2 Force balances for the fluid	25
4.2.3 Shear stress relations	26
4.2.4 Friction factor relations	27
4.2.5 A volumetric balance	28
4.2.6 The Shields concept	28
4.2.7 Criteria for deposit motion	29

4.2.8	Solution procedure	30
4.3	Introduction of non-Newtonian behavior in the SCSB-model	33
4.3.1	The flow of Power Law fluids in smooth- and rough pipes	33
4.3.2	The flow of Power Law fluids through granular beds	34
4.3.3	The effect of non-Newtonian rheology on the solution procedure	34
4.4	Some general comments to the SCSB-model	38

CHAPTER 5 : A COMPARISON OF PREDICTIONS FROM THE SCSB-MODEL WITH EXPERIMENTAL RESULTS	42
--	-----------

5.1	$c(\phi)$ -plots	44
5.1.1	General remarks	44
5.1.2	Specific remarks	45
5.2	$c(v)$ -plots	51
5.2.1	General remarks	51
5.2.2	Specific remarks	52
5.3	$v(\phi)$ -plots	61
5.3.1	General remarks	61
5.3.2	Specific remarks	61

CHAPTER 6 : THE FLOW LOOP	62
----------------------------------	-----------

6.1	Specifications	63
6.2	Equipment	63
6.3	A description of the loop	63
6.3.1	A comment on the use of load cells in the flow loop	66
6.4	Limitations	66
6.4.1	General limitations	66
6.4.2	Specific limitations	68

CHAPTER 7 : CONCLUSIONS	69
--------------------------------	-----------

APPENDIX 1 : GEOMETRICAL RELATIONS IN THE SCSB-MODEL	71
APPENDIX 2 : FRICTION BETWEEN THE DEPOSIT AND THE ANNULAR WALLS	73
APPENDIX 3 : THE SHIELDS CONCEPT FOR INCLINED DEPOSITS	78
APPENDIX 4 : THE ARTYUSHKOV ET AL. THEORY FOR THE FLOW OF NON-NEWTONIAN FLUIDS IN SMOOTH AND ROUGH PIPES	83
APPENDIX 5 : COMPUTER PROGRAMS	92
APPENDIX 6 : SUBROUTINE DESCRIPTIONS	112
REFERENCES	142
SYMBOLS	147

Chapter 1

Introduction.

1.1 An introduction to cuttings transport.

The material being liberated by the impact of a drilling tool on a geological formation is denoted *cuttings*.

During drilling or *hole cleaning*^a a drilling fluid is circulated down through the drill pipe and back up the annular space on the outside. The drilling fluid has several functions, but one of the most important is to remove cuttings from the wellbore. If cuttings accumulate in the hole, drilling becomes inefficient. Energy is devoted to grind the cuttings into smaller particles, causing slower progress, contamination of the drilling fluid with debris, increased torque loads on the drill pipe and increased wear on the drill pipe and –bit. The accumulation may eventually create a resistance to drill string motion which cannot be overcome, a situation denoted *stuck pipe*. Insufficient cuttings removal during hole cleaning may also lead to problems in *cementing operations*^b and *hole completion*^c.

Compared to the vertical– or near vertical wellbore, the inclined or horizontal wellbore permits a larger– or otherwise inaccessible area of exploitation to be reached from a single drilling rig. Furthermore, the highly deviated wellbore allows a parallel entry into thin oil conducting layers, providing an increased contact surface between the hole and the potential production zone. However, the drilling of deviated wellbores also presents an increased frequency of difficulties which, if they occur at all, are not experienced as markedly in vertical holes. The physical background for these problems is not always firmly established, but it is a general perception that at least some of them are caused by an insufficient removal of drilled cuttings from the hole.

1.2 A definition of cuttings transport.

A definition of cuttings transport in a wellbore could be as follows:

Cuttings transport occur if a plane perpendicular to the hole axis in a given interval of time is passed by a larger volume of cuttings from one side than from the other.

Cuttings transport under steady state conditions always produces a net transport of cuttings in a given axial direction at any time. The volume of cuttings entering a section of the wellbore must equal the volume leaving, and consequently the overall transport efficiency is 100%. However, it is possible to influence the particle concentration, –behaviour and –distribution in the annular space by changing variables such as fluid rheology, flowrate, inner pipe eccentricity, etc.

Under transient conditions the direction of net transport and the volume of cuttings transported may vary with time. The time dependency makes it possible to define a transport efficiency, i.e. to compare how fast cuttings are removed from a wellbore in a given period of time, when the characteristics of the system are varied.

-
- a *Hole cleaning* is the process where cuttings are circulated out of the hole after drilling has been stopped.
 - b *Cementing* is the application of a liquid slurry of cement and water to seal off the casing from the surrounding formation.
 - c *Hole completion* is the activities and methods used to prepare the well for the production of oil or gas.

1.3 Quantification of steady state cuttings transport

Vertical annuli

In vertical annuli, the difference between the fluid velocity and the particle slip velocity reflects the *carrying capacity* of a drilling fluid. However, the fluid velocity and the particle slip velocity may vary with position in the annular space, and the carrying capacity is generally not calculated according to a well defined procedure. While the local fluid velocity normally is replaced by the average linear fluid velocity, the determination of an average or net particle slip velocity for the annular cross section is relatively difficult. Therefore the work concerning cuttings transport in vertical wellbores has largely been a study of particle slippage with respect to the surrounding fluid and the development and/or application of more or less empirical relations, predicting a characteristic particle slip velocity under given conditions (see for example *Hall et al.* ¹⁸, *Hopkin* ²¹, *Zeidler* ⁴⁹, *Walker & Mayes* ⁴³, *Sifferman et al.* ³⁸, *Sample & Bourgoyne* ³⁴).

Sifferman et al. ³⁸ suggested a non-dimensional measure for the carrying capacity of a drilling fluid in the form of a transport ratio:

$$R_t = \frac{v_a - v_s}{v_a} = \frac{v_p}{v_a} = \frac{C_f}{C_a} \quad (1.3-1)$$

where v_p is the average linear particle transport velocity, v_a the average linear fluid velocity and v_s the average particle slip velocity. If the annular cuttings concentration is small, the transport ratio is approximately equal to the ratio between the annular feed concentration, c_f , and the annular cuttings concentration, c_a .

Inclined annuli

In deviated wellbores there is no simple coupling between the slip velocity of freely suspended particles and the annular cuttings concentration. Various quantities have been used as a measure for the cuttings behaviour under given conditions.

Iyoho ²³, *Okrajni & Azar* ²⁸, *Seeberger et al.* ³⁶, *Becker et al.* ⁵ and *Grossmann* ¹⁷ all used annular cuttings concentration as the only- or major dependent variable in their work.

Grossmann ¹⁷ also described cuttings behaviour in terms of an "*austragswirkungsgrad*", defined as the ratio between cuttings feed concentration and annular cuttings concentration (i.e. analogous to the transport ratio defined by *Sifferman et al.* ³⁸ for vertical annuli). He pointed out that this quantity displays a more marked response to changes in the experimental variables than cuttings concentration does, when the latter is small.

Finally, steady state cuttings transport may be characterized by a critical annular fluid velocity. *Peden et al.* ²⁹ considered the smallest nominal annular fluid velocities needed to keep cuttings in full suspension or in an upwards sliding/rolling deposit. Also *Hemphill* ²⁰ determined the smallest flowrate keeping particles in suspension while *Martin et al.* ²⁵ considered the minimum fluid velocity required in order to transport a single particle up an annulus.

1.4 Quantification of transient cuttings transport

The quantities of interest in transient removal of cuttings from vertical as well as deviated wellbores, are the particle recovery rate and the cumulative recovery fraction.

In a plot of the recovery fraction vs. time, the recovery rate may be determined as the slope of the curve (*Williams & Bruce* ⁴⁴, *Zeidler* ⁴⁸, *Hemphill* ²⁰). This allows a detailed description of the cleaning process as function of time. A more primitive approach is to define cleaning rate as the mass of particles present in the annular space divided by the time required to clean them out (*Okrajni & Azar* ²⁸, *Brown et al.* ⁷). Finally, *Martin et al.* ²⁵ measured the minimum flowrate required to attain a given recovery fraction in a given period of time.

Chapter 2

**Previous investigations
of cuttings transport.
- A chronological review.**

2.1 Cuttings transport in vertical wellbores.

*Pigott*³² (1941), as part of a paper concerning the flow of drilling fluids in wellbores and mud handling equipment, briefly considered the lift of spherical- and disc shaped particles in water and a few typical drilling fluids. Particle slip velocities were calculated from relations derived from *Stokes law* and *Rittingers equation*. However, no experimental verification of the relations was performed.

*Hall et al.*¹⁸ (1950) performed measurements of particle slip velocities in two vertical laboratory columns (33 ft. 4" & 9 ft. 1 $\frac{1}{4}$ ") with fluid circulation. Various particle shapes and fluids of different densities and rheological properties were included in the work. Relations expressing particle slip velocity as function of slip regime (see chapter 3.2), particle characteristics and fluid properties were derived on the basis of experimental data. The applicability of the relations were tested in a field scale annular flow loop (1000 ft. 9 $\frac{5}{8}$ "/4 $\frac{1}{2}$ ").

*Williams & Bruce*⁴⁴ (1951) performed field- and laboratory investigations of cuttings transport in vertical annuli. The field investigations were carried out in a 500 ft. 7 $\frac{1}{2}$ " & 27 $\frac{7}{8}$ " wellbore, and concerned particle recovery as function of time. The particles were aluminium discs of varying thickness and diameter. The slope of recovery vs. time curves was taken as a measure for the cuttings transport efficiency. The effect of drill string rotation and fluid rheology was considered. The laboratory investigations were performed in a 5 ft. 4 $\frac{1}{8}$ "/1" concentric annulus, in which the fluid could be circulated and the inner pipe rotated. Here, the effects of particle shape, fluid velocity profile and inner pipe rotation were considered.

*Hopkin*²¹ (1967), in a 8 ft 4 $\frac{1}{2}$ " diameter vertical column investigated particle slip velocities in fluids circulating up the column. The effects of particle shape and non-Newtonian fluid rheology were considered. The results were coupled with field experience in order to estimate the annular fluid velocities needed to ensure adequate cuttings removal in a wellbore.

*Chien*⁹ (1971), in a purely theoretical work, developed a correlation between the annular particle concentration and the nominal annular fluid velocity, the densities of the particles and the fluid, the dimensions of the particles, the dimensions of the wellbore and the rate of penetration. *Chien* pointed out that a more efficient use of the drill bit is achieved when the bottom hole pressure is minimized and showed that the bottom hole pressure displays a minimum at a specific flowrate.

*Zeidler*⁴⁸ (1972) investigated the transport of drilled cuttings, graded according to sieve size. In a 15 ft. 3" vertical column, particle settling in quiescent Newtonian fluids was investigated. Semiempirical relations for the settling velocity of the particles were derived and applied in an empirical expression for the cumulative recovery of particles exposed to turbulent flow of water in a 65 ft. 8 $\frac{1}{8}$ "/4 $\frac{1}{2}$ " vertical concentric annulus. The effects of non-Newtonian rheology and inner pipe rotation on the annular particle transport were treated qualitatively.

*Zeidler*⁴⁹ (1974), in a Ph.D.-thesis, continued and elaborated his theoretical and experimental work on the transport of drilled particles. The thesis contains the perhaps most ambitious attempt ever performed to produce a model for the transport of particles in vertical annular flow. *Zeidler* developed theoretical relations for the average axial velocity and equilibrium concentration of particles being transported in viscous concentric annular flow of a Power Law fluid. Due to the complexity of the subject, the

resulting expressions were semiempirical in nature and later researchers (*Thomas et al.* ³⁹ *Hussaini & Azar* ²²) have only to some degree been able to confirm the validity of the model.

Sifferman et al. ³⁸ (1974) introduced the transport ratio, R_t , defined as the ratio between the net particle transport velocity, v_p , and the nominal fluid velocity, v_a . For small annular cuttings concentrations the transport ratio is equal to the ratio between the annular cuttings feed concentration, c_f , and the cuttings concentration in the annular volume, c_a , i.e. as previously given in eq. (1.3-1)

$$R_t = \frac{v_p}{v_a} = \frac{c_f}{c_a}$$

A comprehensive experimental programme was carried out in field scale vertical annuli. The results were described in terms of transport ratio vs. annular fluid velocity plots. Discrete variables were fluid rheology, fluid density, cuttings size, cuttings feed rate, annular dimensions, inner pipe eccentricity and inner pipe rotational speed.

Walker & Mayes ⁴³ (1975) made the approximation that drilled cuttings in general are disc shaped and settles flatwise, and developed simple relations for the particle settling velocity in the turbulent-, transition- and viscous slip regimes (see chapter 3.2). In order to verify their relations, *Walker & Mayes* conducted measurements of the terminal settling velocities of disc shaped particles in a 5 ft. 6" diameter static fluid column. The density of the particles and the rheology of the fluid were varied in order to obtain results in all particle slip regimes.

Sample & Bourgoyne ³⁴ (1977) adopted the transport ratio, originally proposed by *Sifferman et al.* ³⁸, in the form:

$$R_t = \frac{v_p}{v_a} = \frac{v_a - v_s}{v_a} = 1 - v_s \left(\frac{1}{v_a} \right) \quad (2.1-1)$$

Where v_p , v_a and v_s are the net particle transport velocity, the nominal annular fluid velocity and net particle slip velocity respectively. Experimental data indicated that the particle slip velocity was largely independent of annular fluid velocity, resulting in a linear relationship between the transport ratio and the inverse annular fluid velocity. Transport ratios obtained experimentally in annular flow were compared to the corresponding ratios based on particle slip velocities measured in quiescent fluids, and calculated from theoretical relations given by previous investigators.

Thomas et al. ³⁹ (1982), using the same flow loop as *Zeidler* ⁴⁸ ⁴⁹ except for a larger diameter inner pipe, attempted to verify the model outlined by *Zeidler* for vertical annuli. The attempt was performed in connection to a study of the effects of inner pipe rotation and -eccentricity on cuttings behaviour in vertical annular flow.

Hussaini & Azar ²² (1983), also by means of a slightly modified version of the *Zeidler* flow loop, pursued a further verification of the *Zeidler* model. The work also treated the effects of fluid flowrate and rheology on the annular particle concentration.

*Peden & Luo*³⁰ (1987) noted that the drag coefficient for a sphere moving through a Power Law fluid could be expressed in the general form:

$$C_d = \frac{\lambda}{(Re'_p)^\zeta} \quad (2.1-2)$$

where λ and ζ depends only on the particle slip regime and the Power Law flow behaviour index. Re'_p is a particle Reynolds number defined for a Power Law fluid. The expression was adapted to discs and rectangular plates.

2.2 Cuttings transport in deviated wellbores

*Iyoho*²³ (1980) was the first to perform comprehensive experimental investigations of steady state cuttings transport in inclined annuli. The experimental work was carried out in a large scale (40 ft/5"/1.9") annular flow loop located at the University of Tulsa. Apart from annular inclination, the work treated the effect of annular fluid velocity, fluid rheology, annular flow regime, annular eccentricity, inner pipe rotation and particle feed concentration. The effect of the mentioned variables was quantified in terms of the annular cuttings concentration and a generalized transport ratio.

*Becker*³ (1982) used the Tulsa University flow loop facility to investigate the effect of fluid density and annular geometry on steady state cuttings transport in inclined annuli. Dependent variables were annular cuttings concentration and the torque required in order to rotate the inner pipe at 50 rpm.

*Okrajni & Azar*²⁸ (1985) used the Tulsa University flow loop to perform investigations of steady state transport and transient removal of cuttings in an inclined annulus. The effects of fluid rheology, annular flowrate, annular flow regime, annular eccentricity and inner pipe rotation were considered. Dependent variables were annular cuttings concentration and transient cleaning rates.

*Gavignet & Sobey*¹⁵ (1986) presented a simple "two layer model" for the steady state transport of cuttings in deviated wellbores. In the model, the cuttings are presumed to be transported in a closely packed deposit, sliding up the wellbore, driven by the fluid shear stress exerted on the deposit surface. Resistance to cuttings transport appear in the form of friction between the sliding deposit and the annular walls. The model predictions showed an order of magnitude agreement with experimental results by *Iyoho*²³.

*Martin et al.*²⁵ (1987) pointed out that the model outlined by *Gavignet & Sobey*¹⁵ contains parameters which in practice are inaccessible. As a countermeasure a model based on directly accessible variables was proposed. The model utilizes the experience that the non-dimensional quantity

$$K = \sqrt{Re} Fr \quad (2.2-1)$$

where Re is a Reynolds number and Fr a Froude number, depends largely on annular inclination and fluid viscosity. Input to the model are annular dimensions, annular inclination, fluid rheology, fluid density and particle density. Output is the minimum annular flowrate needed in order to obtain a given recovery fraction during a given period

of time. The model was based partly on experimental results obtained in a 16 ft. 10⁵/₈" annulus and a 10 ft. 4⁵" cylindrical pipe respectively, partly on field data.

*Grossmann*¹⁷ (1988), used the Buckingham Π-theorem and similarity theory to build a laboratory scale flow loop (3 m. 50 mm/32 mm) and select operational parameters which should produce results identical to the ones obtainable with field parameters in a full scale geometry. A comprehensive experimental programme was carried out, and detailed qualitative and quantitative descriptions of the transport phenomena under different steady state conditions were outlined. Variables were nominal annular fluid velocity, annular inclination, fluid viscosity, annular eccentricity, inner pipe rotation, particle size and particle feed rate. Dependent variables were the annular particle concentration, a particle transport ratio ("*Austragswirkungsgrad*"), the axial annular pressure gradient, the average particle transport velocity and the part of the annular cross sectional area not occupied by a deposit.

*Seeberger et al.*³⁶ (1989) performed experiments which indicated that an oil based- and a polymer water based drilling fluid with similar rheological properties, produce identical cuttings behaviour in inclined wellbores.

*Brown et al.*⁷ (1989), in a field scale annular flow loop (50 ft. 8"/5"), considered the transient cleaning of a wellbore annulus as function of inclination, fluid flowrate, fluid rheology and inner pipe eccentricity. Two quantities were determined: 1) The minimum annular velocity required in order to initiate the removal of particles from the annulus and 2) the cleaning rate once particle transport was initiated. The experimentally determined fluid velocities, required to initiate cuttings removal, were compared with predictions from the *Gavignet & Sobey*¹⁵ model.

*Becker et al.*⁵ (1989) performed experiments in the Tulsa University flow loop facility in order to investigate the correlation between annular cuttings concentration and various quantities used to characterize the rheology of drilling fluids in field practice.

*Peden et al.*²⁹ (1990) quantified the cuttings transport process in terms of the minimum annular fluid velocity keeping cuttings in upwards motion. Two types of minimum transport velocity were considered: 1) The lowest nominal fluid velocity keeping particles in full suspension, and 2) the lowest nominal fluid velocity needed to keep a particle deposit in forwards/upwards motion. The dependence on annular inclination, annular dimensions, fluid rheology, inner pipe eccentricity, inner pipe rotation and particle size was investigated in a 22 ft. (outer pipe diameter not reported)/2.5" & 3.5" flow loop, located at the Heriot-Watt University in Edinburgh.

*Hemphill*²⁰ (1990) used the Tulsa University flow loop facility to investigate the effect of oil based drilling fluids on steady state cuttings behaviour and transient cuttings removal. In the steady state experiments, the minimum annular flowrate keeping particles in upwards sliding/rolling motion was determined as function of annular inclination, fluid rheology and oil to water ratio. In the transient cuttings removal experiments, the dependence of particle recovery on time was determined as function of annular inclination, oil to water ratio, fluid rheology and inner pipe rotational speed.

Chapter 3

**Some variables affecting
cuttings transport and
behaviour.**

Cuttings transport is a two phase solid-liquid flow in an annular geometry. A rather large number of variables affect particle behaviour in a wellbore. Among these are:

- 3.1 Annular inclination
- 3.2 Fluid rheology
- 3.2.1 Annular flow regime
- 3.3 Particle size- and shape
- 3.4 Particle- and fluid density
- 3.5 Fluid flowrate
- 3.6 Annular eccentricity
- 3.7 Inner pipe rotational speed
- 3.8 Particle feed concentration
- 3.9 Annular dimensions

Please note that in this thesis, inclination always is measured relative to vertical, unless it is otherwise specified.

3.1 Annular inclination

In a deviated wellbore, gravity and buoyancy may be separated into axial- and radial components. Even if fluid dynamic forces to some extent act in the radial direction, these radial forces are weak compared to the radial body forces under most drilling conditions, and the net gravitational force makes cuttings settle out of the fluid and form a deposit on the low side of the wellbore.

The appearance and behaviour of a deposit depend on the physical conditions in the wellbore and are often complex. For a detailed description of the various patterns of behaviour, the reader is referred to the works of *Iyoho*²³ and *Grossmann*¹⁷.

*Iyoho*²³, *Becker*³, *Okrajni & Azar*²⁸ and *Grossmann*¹⁷ observed that annular cuttings concentration increased with annular inclination. Under some experimental conditions the growth was monotonous, while under other conditions it reached a maximum, typically between 40 and 50 degrees, decreasing slightly with a further increase in inclination.

*Peden et al.*²⁹ observed that the minimum transport velocities (see chapter 1.3.2) increased with hole angle, typically reaching a maximum value between 40 and 60 degrees, whereupon they decreased with a further increase in inclination. *Hemphill*²⁰ reported similar results for a number of oil based muds.

*Martin et al.*²⁵ found that the minimal fluid velocity required to transport a single particle up an annulus displayed a maximum between 30 and 60 degrees.

*Brown et al.*⁷, in transient cuttings removal, noted that the interval around 50-60 degrees represented the most difficult annular inclinations to clean. *Hemphill*²⁰ reported similar results.

3.2 Fluid rheology

The force on a freely suspended particle in an infinite fluid may be given by the expression:

$$F_{fd} = C_d A_p (\frac{1}{2} \rho_m u_p^2) \quad (3.2-1)$$

where A_p is a characteristic surface area for the particle, ρ_m the fluid density and u_p the velocity of the particle relative to the fluid. The expression defines the *drag coefficient*, C_d .

The drag coefficient is normally plotted against a particle Reynolds number, Re_p , defined in a manner suitable for the particle and fluid in question. In a range of low Re_p viscous forces dominate the fluid-particle interaction, and the particle is said to be in viscous slip. If Re_p is gradually increased, the particle enters a transitional regime where neither viscous nor momentum forces can be ignored. With a further increase in Re_p the particle slip becomes turbulent, and momentum forces dominate the interaction between the fluid and the particle. The behaviour of a particle in turbulent slip is independent of fluid rheology.

Due to the difference in physical background it is necessary to discern between annular flow regime and particle slip regime. However, they are not independent. In the viscous fluid flow regime, particle motion may take place in either the viscous-, transitional- or turbulent particle slip regime. In the transitional fluid flow regime, particle motion may take place in the transitional- or turbulent particle slip regime, while in turbulent fluid flow regime, particle slip always takes place in the turbulent regime. It is not always simple to determine the particle slip regime for freely suspended particles in annular flow, and often it is attempted to relate particle behaviour to the fluid flow regime instead.

The particle slip velocity is largely constant in Newtonian annular flow. However, particles in viscous- or transitional slip through non-Newtonian fluids "feel" a local fluid viscosity which is a result of shear from annular flow, particle slippage and inner pipe rotation. Consequently the slip velocity varies with annular position in these slip regimes.

Under normal drilling conditions, the number of particles in free slip is small in inclined annuli. The effect of rheology on particles sliding or saltating along the deposit surface/annular wall is not well defined. However, it is expected to be related to the effect of rheology on wall shear stress in rough pipes (compare fig. A3/1 and fig. 4.2.4/1).

For the particles in the interior of a deposit, the effect of rheology in viscous interstitial flow may be given in terms of the *Ergun equation*. (see eqs. (4.2.2-2) and (4.3.2-1))

Reported results – Vertical annuli

The difficulties in handling non-Newtonian rheology are reflected in papers concerning cuttings transport in vertical annuli. *Williams & Bruce* ⁴⁴ outlined slip velocity relations valid for turbulent slip only, where particle behaviour is independent of fluid rheology. *Chien* ⁹ chose to define constant viscosities for non-Newtonian fluids. *Zeidler* ⁴⁸ proposed an effective viscosity based on the shear stress and shear rate at the annular wall. *Walker & Mayes* ⁴³ proposed to use the ratio between local fluid shear stress and shear rate as

viscosity in their relations for particle slip velocities, and outlined a partly empirical technique to estimate these quantities.

*Hopkin*²¹ found that the particle slip velocity decreased with increasing fluid viscosity in the viscous slip regime.

*Sifferman et al.*³⁸, in viscous annular flow and under steady state conditions, observed that cuttings transport ratios increased with viscosity.

Reported results - Inclined annuli

Both *Okrajni & Azar*²⁸ and *Becker et al.*⁵ reported that annular cuttings concentration was independent of fluid rheology in turbulent flow.

*Okrajni & Azar*²⁸ found that an increase in *plastic viscosity* resulted in lower cuttings concentrations at all inclinations.

*Becker et al.*⁵ investigated the effects of a number of rheological parameters commonly applied in the field. These were *yield point*, *plastic viscosity*, *yield point to plastic viscosity ratio*, Power Law flow behaviour index, Power Law consistency index, *Fann V-G readings*, an effective viscosity and *initial- and 10 minute gel strengths*. A general trend for the results obtained in viscous annular flow was that annular cuttings concentration decreased with an increase in the rheological parameters considered. However, *Hemphill*²⁰ found contradictory results for a number of oil based drilling fluids, where the annular flowrate needed to keep cuttings in an upwards rolling/sliding motion increased with some of the same rheological parameters.

*Peden et al.*²⁹, in addition to water, operated with a low-, a medium- and a high viscosity polymer solution, characterized in terms of *apparent viscosity* vs. shear rate plots. In a concentric annulus, the effect of fluid rheology on cuttings behaviour was observed to depend on the annular dimensions and the type of minimum transport velocity considered. However, no clear correlation was established between the minimum transport velocities and fluid rheology. *Peden et al.* pointed at transitions between the viscous- and turbulent flow regimes as a possible explanation for the observed inconsistencies. However, no effort was performed to check this hypothesis.

*Hemphill*²⁰ found that highly viscous "sweeps" in transient cuttings removal gave lower cuttings recovery rates and smaller cumulative cuttings recovery fractions than low viscosity "sweeps".

Authors comment

Drilling fluids are generally non-Newtonian, shear thinning, sometimes viscoelastic and may possess a yield stress or *gelling* properties. The inability to describe such fluids in terms of a few parameters is a serious restriction to experimental work where the effect of rheology is to be considered. Furthermore, even if a fluid could be characterized with a few rheological parameters, it is normally impossible to vary one of the parameters without affecting the value of the others, i.e. the rheological properties cannot be separated and investigated independently of each other. This makes the results of experimental work with non-Newtonian fluids inconsistent and difficult to interpret.

It is noteworthy that the simplest (and consistent) investigation of rheological effects on

cuttings transport and behaviour appears not to have been performed yet: The effect of variations in viscosity of Newtonian fluids in the viscous flow/slip regime.

3.2.1 Annular flow regime

A special case in the consideration of rheological effects on cuttings behaviour is the comparison of cuttings behaviour in viscous- and turbulent annular flow. The case is denoted "special" because there is negligible effect of rheology in turbulent annular flow, where fluid momentum forces are dominant, i.e. comparisons are made between a situation where rheology is significant and another, where it is not. The different flow regimes are normally obtained by varying the fluid rheology, while other variables such as densities and flowrate are kept constant.

In vertical or near vertical annuli, cuttings are more or less freely suspended in the annular space and particle slip regime is of importance. In viscous annular flow, particle slip may take place in the viscous-, transitional- or turbulent slip regimes. In turbulent annular flow particle slip always takes place in the turbulent slip regime, where the slip velocity attains a maximum value. It is therefore expected that viscous flow produces a lower annular cuttings concentration than turbulent in vertical/near vertical annuli.

In deviated wellbores with a deposit, the majority of the cuttings are transported in a narrow zone on- and immediately above the deposit surface, and the distribution of the fluid dynamic forces in the annular space becomes important. The turbulent fluid velocity profile displays considerably larger fluid velocities than the viscous profile in the layer immediately above the deposit surface. Therefore, turbulent annular flow is expected to produce a lower annular particle concentration than viscous annular flow, when a well defined deposit is present.

Reported results – Vertical annuli

*Hopkin*²¹ in low viscosity fluids found that the particle slip velocity was constant and independent of rheology. However, if the viscosity was raised beyond some point, the particle slip velocity became dependent on rheology and decreased towards zero with further increases in viscosity. This behaviour presumably reflects a shift from turbulent to viscous slip.

*Williams & Bruce*⁴⁴ found that low viscosity muds gave better cuttings removal than high viscosity muds. This was apparently due to the interaction between the disc shaped particles and the velocity profile in turbulent and viscous flow respectively. In turbulent flow the particles were observed to be transported smoothly and flatwise, while in viscous flow they performed recirculatory movements, which prolonged their residence time in the annular section.

Reported results – Inclined annuli

*Okrajni & Azar*²⁸ found that viscous annular flow gave lower annular cuttings concentrations than turbulent at inclinations between 0 and 45 degrees. Between 45 and 55 degrees, the two flow regimes performed equally well, while turbulent flow gave the lowest annular concentrations for inclinations between 55 and 90 degrees. Very similar observations were made by *Becker et al.*⁵.

*Iyoho*²³, for a single annular inclination of 40 degrees, observed that a low viscosity fluid in turbulent flow produced largely the same annular cuttings concentrations as a high viscosity mud in viscous flow.

*Grossmanns*¹⁷ results showed that in vertical annuli, there was only negligible difference between the annular cuttings concentration obtained with a high viscosity fluid in viscous flow and a low viscosity fluid in turbulent flow. However, at inclinations of 45 and 90 degrees, the high viscosity fluid gave markedly higher annular cuttings concentrations than the low viscosity fluid, at practically all the flowrates considered.

*Okrajni & Azar*²⁸ in transient cuttings removal observed a pattern similar to the one observed for steady state cuttings transport. Between 0 and 45 degrees cleaning rates were highest in viscous flow, between 45 and 55 degrees hole cleaning in the two regimes was equally efficient, while between 55 and 90 degrees cleaning rates were highest in the turbulent regime.

*Brown et al.*⁷, in transient cuttings removal, observed that water in turbulent flow gave higher cleaning rates than a polymer solution in viscous flow at all-, and in particular the low annular inclinations.

3.3 Particle size and -shape.

Particle size is normally accounted for through some characteristic dimension. A frequent choice is the diameter of a sphere with the same volume as the particle in question.

Cuttings are generally of irregular shape, and a simple geometrical characterization is difficult. Several methods have been proposed (see for example *Garde & Ranga Raju*¹⁴ p.16) but the concept of *sphericity* introduced by *Wadell*⁴² appears to be of fundamental importance. Sphericity is defined as the surface area of a sphere with the same volume as the particle in question, divided by the actual surface area of the particle.

Particles with three mutually perpendicular axes of symmetry are orientationally stable in free viscous slip, i.e. they tend to preserve the orientation originally imposed on them. This was experimentally confirmed by *Pettyjohn & Christiansen*³¹. *Heiss & Coull*¹⁹ showed that the resistance to viscous slip depends on the shape and orientation of the particle.

Outside the viscous slip regime, the orientation of freely settling particles is in general not arbitrary. In the transition from viscous to turbulent particle slip regime, the particles gradually attain a preferred orientation with the largest possible cross sectional area perpendicular to the direction of motion. For isometric particles the resistance to particle motion increases with decreasing sphericity, the sphere meeting the smallest resistance of all particle shapes (see for example *Pettyjohn & Christiansen*³¹). Above some particle Reynolds number in the turbulent slip regime, non-spherical particles tend to develop a spinning or pitching motion (*Willmarth et al.*⁴⁵).

While the influence of particle size in inclined annuli with a deposit has been treated by several researchers, the effect of particle shape does not appear to have received any attention.

Reported results – Vertical annuli

The described behaviour of non-spherical particles in free slip has largely been confirmed in experiments related to cuttings transport. An exception is the lack of a preferred orientation at low particle Reynolds numbers. *Peden & Luo*³⁰, for discs and rectangular plates in quiescent fluids and with a suitably defined particle Reynolds number, found that for $Re_p < 1$ the preferred orientation was edgewise, for $1 < Re_p < 10$ the particle tended to perform unstable zig-zag movements in the transition to flatwise slip, which occurred for $Re_p > 10$. These observations were largely in accordance with earlier observations by *Walker & Mayes*⁴³ for disc shaped particles and by *Zeidler*⁴⁹ for ellipsoidal particles.

Particle slip in viscous shear flow may give rise to complex particle behaviour. A noticeable example was given by *Williams & Bruce*⁴⁴, who observed and proposed a hypothesis for the fact that disc shaped particles may perform recycling movements along the annular walls. The recycling phenomenon, which also is described by *Zeidler*⁴⁹, was considered the reason why large particles in transient cuttings removal sometimes are more easily removed from the wellbore than small. This *reverse order effect* is presumed to occur when the size and shape of the small particles make them more exposed to recycling than particles with a larger size and/or different shape. The small particles must then travel a longer virtual distance than the latter, before they reach the surface of Earth.

Reported results – Inclined annuli

*Peden et al.*²⁹ considered two different particle size fractions. For low viscosity fluids in turbulent flow they observed that the large particles required higher minimum transport velocities than the small, at all inclinations. However, for a high viscosity fluid in viscous flow, the large particles required lower minimum transport velocities than the small, in a range of annular inclinations.

*Grossmann*¹⁷ conducted experiments in turbulent flow with three particle size fractions, one containing small particles, another large particles and a third containing a mixture of the small and large particles. The behaviour of the mixed particle fraction was largely similar to the fraction with large particles alone, while the small particle fraction gave lower annular particle concentrations than the large- and mixed fraction.

*Martin et al.*²⁵ studied the transient recovery of particles transported in pipe flow. With a thixotropic fluid in viscous flow they observed that large particles were transported more easily than small particles at all inclinations. They suggested this phenomenon to be caused by the embedment of the small particles in a stagnant sublayer at the pipe wall.

3.4 Particle- and fluid density.

The difference in density between the cuttings and the drilling fluid affects the buoyancy of the cuttings. The less the difference, the less the net gravity on the cuttings.

For particles moving in the transitional- or turbulent slip regime, the response to an increase in drilling fluid density is twofold: The cuttings become easier to transport due

to the increase in buoyancy, and the ability of the drilling fluid to transport the cuttings grows due to the increase in fluid momentum.

In deviated wellbores where a deposit has formed, the large resistance to flow through the interstitial voids normally ensures viscous flow in the interior of the deposit. Consequently the influence of fluid momentum on the deposit is restricted to the cuttings on- and above the deposit surface. However, an increase in fluid density increases the buoyancy of the cuttings, reducing the intergranular friction as well as the friction between the deposit and the annular walls. This reduces the stability of the deposit, making it more exposed to erosion and sliding.

Reported results – Vertical annuli

Sifferman et al. ³⁸, under steady state conditions, observed that increasing the density of the fluid led to higher particle transport ratios, especially at relatively low annular fluid velocities.

Williams & Bruce ⁴⁴ in transient cuttings removal found that increasing the density of the fluid gave higher particle recovery rates.

Reported results – Inclined annuli

Becker ^{3 4} investigated the effect of fluid density variations on annular particle concentration. He solely treated viscous annular flow, and consequently his results should reflect the effect of buoyancy, but not of fluid momentum. He observed that an increase in fluid density led to reductions in annular particle concentrations at all inclinations considered and that weighted fluids produced a less steep rise in annular particle concentration with inclination, than less- or unweighted fluids.

3.5 Fluid flowrate

Annular flowrate has a marked effect on cuttings behaviour in vertical as well as inclined annuli. If the flowrate is too low, cuttings accumulate in the annular space until the fluid velocity becomes large enough to ensure a net transport of cuttings. While the cuttings remain suspended in vertical annuli, the accumulation in inclined annuli occurs in the form of a deposit.

Reported results – Vertical annuli

Sifferman et al. ³⁸, under steady state conditions and for all combinations of system variables considered, observed that the particle transport ratio increased with annular flowrate. While the slope of a transport ratio vs. flowrate curve was steep at relatively low fluid flowrates, it levelled out at higher flowrates. This reflects that there is an upper limit to the particle slip velocity (attained in turbulent slip), while there in principle is no upper bound for the fluid velocity.

Hussaini & Azar ²², under steady state conditions and in viscous annular flow, observed that annular cuttings concentration decreased with increasing flowrate in all the rheologically different fluids considered.

Reported results – Inclined annuli

Iyoho ²³ observed that the higher the fluid flowrate, the lower the annular cuttings concentration at all inclinations, fluid viscosities and flow regimes. Similar results were reported by Okrajni & Azar ²⁸.

Grossmann ¹⁷ observed that the higher the annular flowrate, the lower the annular cuttings concentration at all inclinations, annular eccentricities, fluid viscosities, inner pipe rotational speeds, particle sizes and particle feed rates.

3.6 Annular eccentricity

An eccentric annulus is characterized by variations in the distance across the annular gap with angular position. The annular fluid velocity distribution is strongly affected by annular eccentricity. Some examples of velocity distributions for a Newtonian fluid in viscous eccentric annular flow are shown in fig.3.6/1.

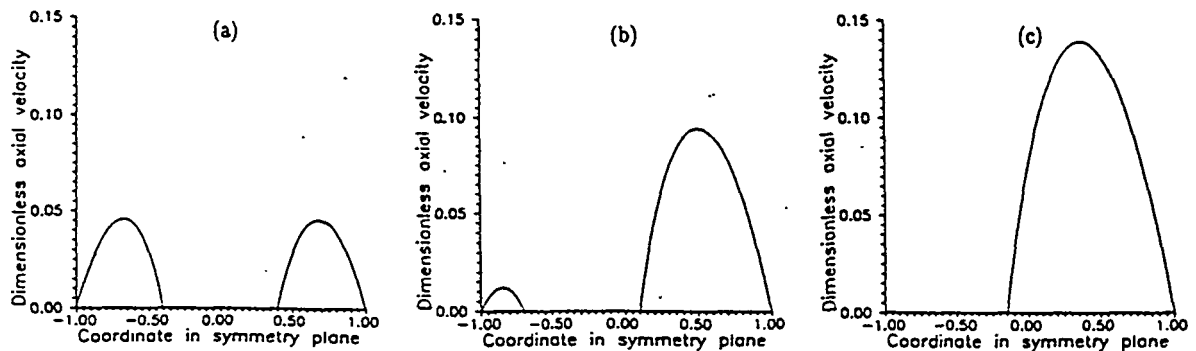


Fig. 3.6/1 The distribution of fluid velocities for a Newtonian fluid along the symmetry axis of an eccentric annulus. The eccentricities shown are: (a) 0% (concentric), (b) 50%, (c) 90%. The ratio between the inner- and outer pipe radius is 0.4. The non dimensional axial fluid velocity on the ordinate is defined as v/v_0 , where v is the annular fluid velocity and $v_0 = (-dP/dz)R^2/\mu$.

The asymmetric distribution of the fluid velocity leads to variations in particle transport velocity and behaviour with position in annular space. In vertical annuli the reduced particle transport velocities in the narrow parts of the annulus may to some degree be compensated for by a corresponding increase in the transport velocities in the wide parts. In inclined annuli, the creation of a narrow low fluid velocity regions enhances the deposition of particles.

Reported results – Vertical annuli

Sifferman et al. ³⁸, under steady state conditions and in viscous flow, observed that a 100% eccentric drill pipe (i.e. placed against the wall) resulted in slightly higher transport ratios than a concentric pipe.

Thomas et al. ³⁹, under steady state conditions and in viscous flow, varied the annular eccentricity. The effect on particle transport velocities and annular particle concentration was observed to be weak and inconsistent.

Williams & Bruce ⁴⁴ investigated transient cuttings removal in a 500 ft. experimental wellbore and observed that with highly viscous fluids, the cumulative recovery fractions were larger for a concentric– than for an eccentric drill string, i.e. cuttings were being retained in the eccentric wellbore.

Reported results – Inclined annuli

Iyoho ²³, with water in turbulent flow, observed that the effect of eccentricity was small for low annular inclinations, while at larger inclinations, a +50% (i.e. 50%–downwards) eccentric annulus resulted in the highest annular particle concentrations, followed by a –50% (i.e. 50%–upwards) eccentric annulus and a concentric annulus in the mentioned order.

Okrajni & Azar ²⁸ observed that a +50% eccentric position of the inner pipe gave increased annular cuttings concentrations compared to a concentric annulus, at all inclinations and in both flow regimes. The effect was slight for relatively low annular inclinations, while it became more marked at higher inclinations.

Peden et al. ²⁹ considered three annular eccentricities: –50%, 0% and +50%. At all inclinations and in viscous flow, the lowest minimum transport velocities occurred in the –50% eccentric annulus. However, which of the two annular configurations, concentric– or +50% eccentric, that displayed the lowest minimum transport velocities, appeared to depend on annular inclination.

Grossmann ¹⁷ considered a broad range of annular flowrates in the turbulent regime. He observed that eccentricity had only negligible effect on annular particle concentration in vertical annuli. However, in inclined annuli, the experimental results showed that, compared to the concentric configuration, a +90% eccentric inner pipe could result in both increased and reduced annular particle concentrations.

Brown et al. ⁷, in transient cuttings removal, observed that a shift from a concentric to a +75% eccentric annular configuration resulted in reduced cleaning rates. In turbulent flow the reduction was relatively small at low annular inclinations while it became more marked at higher inclinations. In viscous annular flow the reduction was very pronounced at all inclinations.

Authors comment

The experimental results concerning the effect of annular eccentricity is ambiguous. However, Fig. 3.6/2 should illustrate that in inclined annuli with a deposit, a change in annular eccentricity may result in a different effect, depending on the relationship between the deposit and the inner pipe. The deposit shown in fig. 3.6/2 (a) and (b)

occupies 5% of the annular volume, while in (c) and (d) it occupies 50%. In (a) and (c) the eccentricity is -50% , while in (b) and (d) it is $+50\%$.

It is presumed that particle deposition is related to the fluid velocity and that the reduced fluid velocity in the narrow regions of the annular space enhances the deposition of particles.

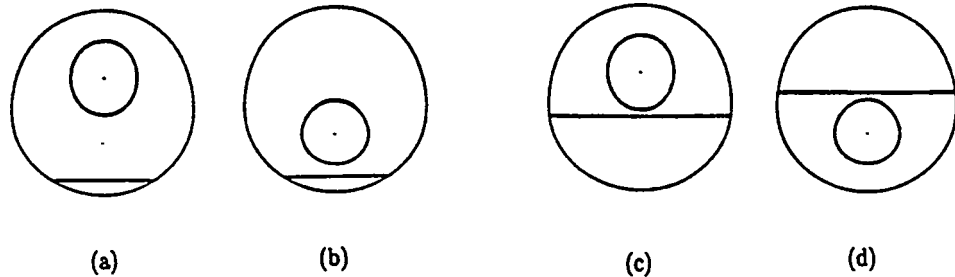


Fig.3.6/2 The relationship between deposit and inner pipe at various combinations of eccentricity and deposit size. (a) Ecc.: -50% , deposit: $5\% v/v$; (b) Ecc.: $+50\%$, deposit: $5\% v/v$; (c) Ecc.: -50% , deposit: $50\% v/v$; (d) Ecc.: $+50\%$, deposit: $50\% v/v$.

When the eccentricity is changed from -50% to $+50\%$ in fig. 3.6/2 (a) & (b), it creates a narrow region above the deposit, promoting further deposition. However, in fig. 3.6/1 (c) & (d) the same change in eccentricity eliminates a narrow region, making the deposit more exposed to erosion. Consequently, a given change may result in a decrease as well as an increase in annular cuttings concentration, depending on the position of the inner pipe with respect to the deposit, prior to the change.

In transient cleaning of a wellbore, the gradual removal of cuttings from the annular space means that no particular position of the inner pipe with respect to the deposit is characteristic for the interaction between the particles and the fluid. However, the situation where the drill pipe is displaced towards the low side of the wellbore requires the largest relative increase in fluid flowrate in order to induce particle motion below the pipe. Consequently, this configuration is expected to be harder to clean than the concentric or negatively eccentric annulus.

3.7 Inner pipe rotation

Inner pipe rotation changes the character of annular flow from axial to helical, imposing a tangential force on the particles in vertical annuli. The fluid shear stress in simple couette flow of a Newtonian fluid is inversely proportional to the radial distance from the rotating pipe squared, and consequently the effect of inner pipe rotation on freely suspended cuttings is expected to decrease rapidly with distance from the pipe.

In inclined annuli the non-axial fluid dynamic forces caused by inner pipe rotation are normally weak compared to the net gravity acting on the cuttings. Furthermore, the helical nature of the flow disappears if the deposit gets in contact with the inner pipe. Therefore, the largest effect of inner pipe rotation is expected to occur when there is a

direct interaction between the pipe and the deposit, i.e. where the deposit structure is disrupted and cuttings pulled out of the deposit surface by the rotating inner pipe.

Reported results – Vertical annuli

Sifferman et al. ³⁸, under steady state conditions and in viscous flow, observed that transport ratios increased with inner pipe rotary speed. For water in turbulent flow, a slight reduction in transport ratios was reported.

Thomas et al. ³⁹, under steady state conditions and in viscous flow, found that inner pipe rotation increased the particle transport velocity and reduced annular particle concentration slightly. An increase in rotational speed beyond some point produced no further effects.

Williams & Bruce ⁴⁴ in transient cuttings removal observed that particle recovery rates increased with inner pipe rotation. The effect of inner pipe rotation was pronounced at low rotational speeds, while an increase in rotational speed beyond some point produced no further effects.

Zeidler ⁴⁸, in transient particle removal with water in turbulent flow, obtained markedly increased particle recovery rates with inner pipe rotation.

Williams & Bruce ⁴⁴, *Zeidler* ⁴⁸ and *Thomas et al.* ³⁹ all suggested various mechanisms for the effect of inner pipe rotation. One was that the tangential motion of the particles in helical flow gives rise to centrifugal forces, which displace the particles into annular regions with higher fluid velocities. Another was that the inner pipe rotation changes the fluid velocity profile, making particles less exposed to recirculatory patterns of motion or sticking to the inner pipe wall.

Reported results – Inclined annuli

Iyoho ²³ found the effects of inner pipe rotation to be negligible for various combinations of annular inclination, annular eccentricity, inner pipe rotational speed and flow regime. So did *Hemphill* ²⁰ for a single combination of the mentioned variables.

Peden et al. ²⁹, for viscous flow in concentric annuli, observed that the effect of inner pipe rotation was negligible in an annulus with a wide clearance, while the minimum transport velocities were significantly reduced in an annulus with a narrow clearance.

Grossmann ¹⁷ observed that inner string rotation reduced the annular particle concentration at all flowrates in the viscous- as well as the turbulent flow regime, and at all eccentricities and inclinations considered. The effect was generally weak in vertical annuli, while it became increasingly pronounced with annular inclination.

Martin et al. ²⁵ reported that inner pipe rotation had little influence on the transport velocity of a single particle in turbulent annular flow, while it had significant influence in viscous annular flow.

Okrajni & Azar ²⁸, in transient particle removal and in viscous annular flow, observed that cleaning rates increased with increasing inner pipe rotational speed. The effect gradually became more pronounced with increasing inclination.

3.8 Particle feed concentration

If cuttings were transported with the same average velocity as the fluid, the annular cuttings concentration would equal the concentration generated at the drill bit, i.e. the annular feed concentration. However, accumulation caused by particle slip, recirculatory particle movements and deposit formation results in annular cuttings concentrations which always are larger than the particle feed concentration.

Reported results – Vertical annuli

Sifferman et al. ³⁸, under steady state conditions and in viscous flow, observed no consistent effect of variations in the particle feed concentration on transport ratios. However, due to the definition of the transport ratio ($R_t \approx c_f/c_a$), this result must reflect that the annular particle concentration grows in proportion to the feed concentration.

Reported results – Inclined annuli

Grossmann ¹⁷, in turbulent annular flow, observed that the annular cuttings concentration increased with particle feed concentration in a concentric as well as an eccentric annulus, with or without inner pipe rotation and at all inclinations. The effect was weak at low inclinations, while it became marked at large inclinations.

3.9 Annular dimensions

A change in annular dimensions has, apart from a very significant influence on the annular fluid velocity, consequences for the relationship between the inner pipe and a deposit.

Reported results – Inclined annuli

Brown et al. ⁷ noted that there is a marked difference in the geometrical appearance of a deposit in two different annular configurations.

Becker ³ investigated the effect of varying the inner pipe diameter, keeping the nominal linear fluid velocity constant. Increasing the inner pipe diameter from 1¹/₈" to 2³/₁₆" in a 5" outer pipe produced a slight increase in annular particle concentration at all inclinations.

Peden et al. ²⁹ showed that the minimum particle transport velocities were smaller in a narrow annulus than in a wide. Furthermore, the effect of inner pipe rotation was strongly affected by the annular dimensions, ranging from a large effect in a narrow gap configuration to an insignificant effect in a wide gap configuration.

Chapter 4

Modelling work.

4.1 Background.

The theoretical work in this dissertation was spurred by a critical examination of a model for the steady state transport of cuttings in deviated wellbores, published by *Gavignet & Sobey*¹⁵ in 1986.

Gavignet & Sobey proposed a simple two layer model where the cuttings are presumed to be transported in a closely packed deposit, sliding upwards along the low side of the wellbore. The deposit is driven by the fluid shear stress exerted on its surface, while the friction between the deposit and the annular walls offers resistance to the motion.

However, the model contains at least two defects:

- 1) Upwards sliding deposits are not the only transport pattern reported from experimental work. Stationary or downwards sliding deposits are frequently observed (see for example *Iyoho*²³ or *Grossmann*¹⁷). With a stationary or downwards sliding deposit, the net transport of cuttings in the upwards direction takes place in suspension above- or in saltation along the surface of the deposit, a behaviour which cannot be described by the *Gavignet & Sobey* model.
- 2) The friction between the deposit and the annular walls is presumed to be the only resistance to deposit motion, i.e. the model does not account for the presence of an axial component of gravity in the inclined wellbore.

Even if the predictions from the model are reported to show an order of magnitude agreement with experimental results published by *Iyoho*²³, the model by *Gavignet & Sobey* must be considered to be inadequate in its physical description of the cuttings transport process.

In the following an improved two layer model is outlined. The new model allows particles to be transported in suspension above the deposit and the deposit to be either static or sliding in the upwards- or downwards direction. For reasons which will become obvious, the model has been named the Shields Concept Sliding Bed model or, in short, the SCSB-model.

4.2 The SCSB-model

The two layer concept is not new, but has previously been used in theoretical works concerning solid-liquid flow in pipes. The SCSB-model is in several respects similar to models published by *Wilson*⁴⁷, *Shook*¹³ and *Doron et al.*¹¹. However, major differences between this work and the ones mentioned are the annular geometry, the inclination with respect to vertical and the application of the *Shields concept*³⁷ to determine the position of the deposit surface.

4.2.1 Geometry

Before any equations are given, the idealized geometry which forms the basis for the SCSB-model should be described.

The annular space is divided into two layers separated by a distinct, plane surface (see fig. 4.2.1/1). The lower layer represents a closely packed particle deposit, while the upper layer represents the mixture of fluid and particles flowing above the deposit.

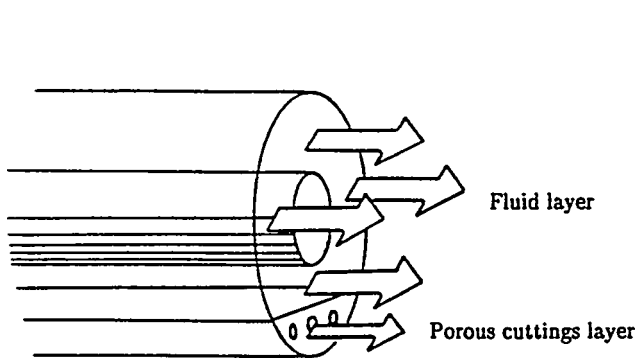


Fig. 4.2.1/1 The two-layer geometry in the SCSB-model.

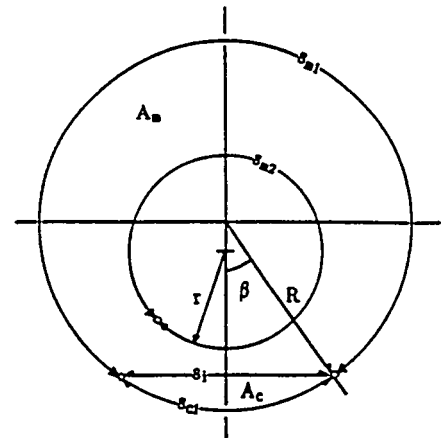


Fig. 4.2.1/2 Geometrical variables in the SCSB-model.

A number of geometrical variables are defined in fig. 4.2.1/2 (See also Appendix 1). The terminology is largely in accordance with the one of *Gavignet & Sobey*¹⁵. The parts of the outer pipe perimeter in contact with the upper- and lower layer are denoted s_{m1} and s_{c1} respectively. Analogously, the parts of the inner pipe perimeter in contact with the upper- and lower layer are denoted s_{m2} and s_{c2} . The length of the interface between the two layers is denoted s_i . The overall cross sectional area of the annulus is divided in two: The cross sectional area of the lower layer, A_c , and the cross sectional area of the upper layer, A_m .

4.2.2 Force balances for the fluid.

Initially, the fluid in the solid-liquid annular flow is taken to be Newtonian (an expansion of the model to non-Newtonian fluid behaviour is performed in chapter 4.3). Furthermore, it is presumed that the flow is fully developed and purely axial. Finally it is presumed that the particle diameter, d_c , particle density, ρ_c , deposit porosity, ϵ , fluid density, ρ_m , and fluid viscosity, μ_m , all are known parameters.

For the fluid in each of the two layers a force balance may be written. The force balances of the present work are:

$$\text{upper layer: } -\frac{dP}{dz} = \frac{1}{A_m} \left[\tau_m (s_{m1} + s_{m2}) + \tau_i s_i \right] \quad (4.2.2-1)$$

$$\text{lower layer: } -\frac{dP}{dz} = 150 \frac{\mu_m u_c (1-\epsilon)^2}{d_c^2 \epsilon^3} + 1.75 \frac{\rho_m u_c |u_c| (1-\epsilon)}{d_c \epsilon^3} \quad (4.2.2-2)$$

where z is the axial position, P the modified pressure ($P = p + \rho_m g z$), τ_m the fluid shear stress exerted on the annular walls, τ_i the fluid shear stress exerted on the deposit surface and u_c the nominal fluid velocity in the lower layer (calculated as if the particles occupied no volume).

Equation (4.2.2-1) states that the pressure gradient in the upper layer is caused by the fluid shear at the annular walls and the deposit surface. Equation (4.2.2-2) is the *Ergun equation* ⁶ and states that the pressure gradient in the lower layer is equivalent to the resistance to flow in a column of packed grains.

The elimination of dP/dz between the equations (4.2.2-1) and (4.2.2-2) leads to:

$$\frac{1}{A_m} \left[\tau_m (s_{m1} + s_{m2}) + \tau_i s_i \right] = 150 \frac{\mu_m u_c (1-\epsilon)^2}{d_c^2 \epsilon^3} + 1.75 \frac{\rho_m u_c |u_c| (1-\epsilon)}{d_c \epsilon^3} \quad (4.2.2-3)$$

This expression is the key equation in the SCSB-model. It is solved with respect to the deposit surface position. The solution requires a number of additional relations, which are given in chapters 4.2.3 – 4.2.7, while the solution procedure is treated in chapter 4.2.8.

4.2.3 Shear stress relations.

In the upper layer, the fluid shear stress on the annular walls, τ_m , and on the deposit surface, τ_i , are given by:

$$\tau_m = \frac{1}{2} f_m \rho_m u_m |u_m| \quad (4.2.3-1)$$

$$\tau_i = \frac{1}{2} f_i \rho_m (u_m \mp u_b) |(u_m \mp u_b)| \quad (4.2.3-2)$$

where u_m is the upper layer fluid velocity and u_b the deposit sliding velocity, both with respect to the annular walls. While eq. (4.2.3-1) defines the friction factor f_m for the interaction between the fluid and the annular walls, eq. (4.2.3-2) defines the friction factor f_i for the interaction between the fluid and the deposit surface.

For a stationary deposit u_b is zero, and the expressions (4.2.3-1) and (4.2.3-2) differ only with respect to the value of the friction factors.

If the deposit moves, u_b takes a non-zero value, and the upper layer fluid velocity relative to the annular walls and relative to the deposit surface respectively, will be different. In equation (4.2.3-2) the positive sign is applied for a downwards sliding deposit, while the negative is used if the deposit slides upwards.

4.2.4 Friction factor relations.

Fig. 4.2.4/1 is taken from *Schlichting*³⁵ (p.580). It shows a resistance number (equal to 400 times the friction factor) vs. the Reynolds number for a Newtonian fluid flowing through pipes of varying roughness. In laminar flow, the resistance is inversely proportional to the Reynolds number, but independent of pipe roughness.

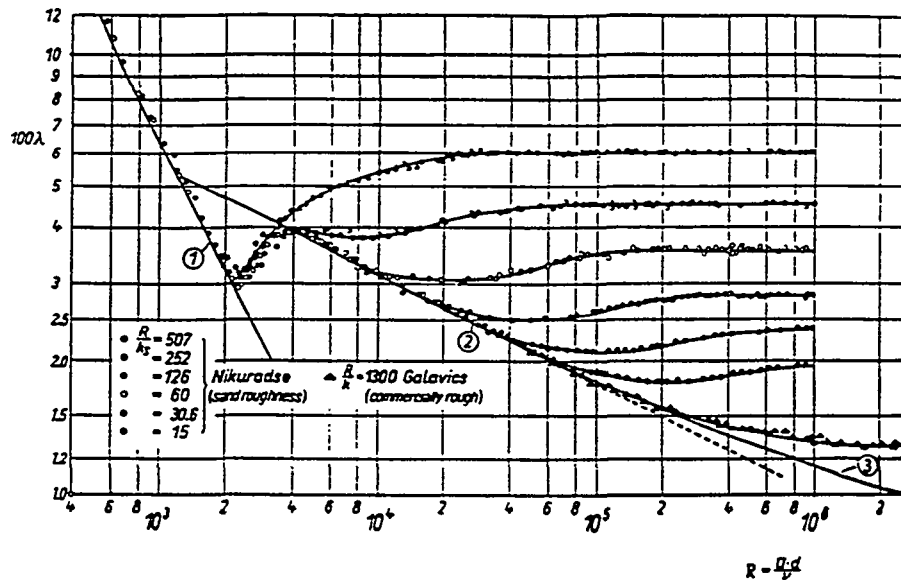


Fig. 4.2.4/1 Resistance to Newtonian fluid flow in rough pipes. (From *Schlichting*³⁵, p. 580).

When the Reynolds number exceeds approximately 2100 the flow becomes turbulent. In a range above 2100, the resistance remains independent of the pipe roughness, and the flow is said to be *hydraulically smooth*. However, beyond some Reynolds number the nature of the resistance gradually changes until it is dependent on the pipe roughness alone. In this situation the flow is said to be *completely rough*.

*Gavignet & Sobey*¹⁵ in their model presumed the flow in the upper layer to be turbulent and applied the following expressions for the friction factors:

$$f_m = \left[4.0 \log_{10}(\text{Re}_m \sqrt{f_m}) - 0.4 \right]^{-2} \quad (4.2.4-1)$$

$$f_i = 2.0 \left[4.0 \log_{10} \left[\frac{D_h}{d_c} \right] + 3.36 \right]^{-2} \quad (4.2.4-2)$$

Re_m is a Reynolds number defined as $\text{Re}_m = (\rho_m u_m D_h) / \mu_m$, D_h being the hydraulic diameter of the upper layer.

These relations originate from two works by *Nikuradse*^{26 27}, concerning the flow of Newtonian fluids in smooth and rough pipes. While (4.2.4-1) is identical to the original relation derived for hydraulically smooth flow, (4.2.4-2) is a slightly modified version of the original relation derived for completely rough flow.

If the friction factors f_m and f_i are calculated from eqs. (4.2.4-1) and (4.2.4-2) alone, the results derived from the SCSB-model are valid only for a situation, where the flow along the annular walls is hydraulically smooth, and the flow with respect to the deposit surface is completely rough. However, these limitations are removed with the introduction of the *Artyushkov et al.*^{1 2} theory in chapter 4.3.1.

4.2.5 A volumetric balance.

A volumetric balance for the fluid and particles in annular flow is given by:

$$V = A_m u_m + A_c(u_c \pm u_b) \quad (4.2.5-1)$$

Here V is the total volumetric flowrate. A_m and A_c are the cross sectional areas of the upper and lower layer respectively, u_c is the nominal fluid velocity in the deposit layer and u_b the deposit sliding velocity. The positive sign in the last term is applied for an upwards sliding deposit, while the negative sign is used for a downwards sliding deposit. When the deposit is stationary, u_b is zero.

In drilling operations, the volume of particles being transported is small compared to the volume of fluid transporting it, and the total volumetric flowrate may be approximated with the volumetric flowrate of the fluid alone. The latter is presumed to be a known parameter.

4.2.6 The Shields Concept.

*Shields*³⁷ treated the conditions for the incipient motion of a particle resting on a horizontal plane deposit surface. From theoretical considerations and experimental investigations, *Shields* derived the relationship:

$$\frac{\tau_0}{(\rho_p - \rho) g d_p} = 0.06 \quad (4.2.6-1)$$

where τ_0 denotes the fluid shear stress at the deposit surface at the point of incipient motion, ρ_p the particle density, ρ the fluid density, g the gravitational acceleration and d_p the particle diameter.

An adaptation of the Shields concept to the incipient motion of a particle resting on an inclined deposit is outlined in Appendix 3. If the modified *Shields* relation is presumed to be valid for cuttings deposits in inclined annuli, the following expression can be written:

$$\frac{\tau_0}{(\rho_c - \rho_m) g d_c} = \left[\frac{\cos(\varphi)}{\tan(\psi_r)} \pm \sin(\varphi) \right] 0.06 \quad (4.2.6-2)$$

where φ is the inclination with respect to vertical and ψ_r the angle of repose for the granular material in question. The dual sign on the R.H.S. of equation (4.2.6-2) reflects

that the particle may move in the uphill as well as the downhill direction. The positive sign between the brackets corresponds to a situation where the particle is on the verge of being pulled along by the fluid, while the negative sign corresponds to a situation where the fluid is barely able to prevent the particle from sliding downhill under the influence of net gravity (see Appendix 3 for details). In order to keep the model simple, it is presumed that the deposit generally tends to slide downwards before the particles on top of it. The negative sign has therefore been omitted in the present work.

4.2.7 Criteria for deposit behaviour.

In theory, three types of deposit behaviour are possible. The deposit may: 1) be stationary, 2) slide downwards or 3) slide forwards/upwards. While downwards sliding cannot take place in an horizontal annulus, due to the absence of an axial component of gravity, forwards sliding may occur due to the forces invoked by the fluid.

Two functions, f_1 and f_2 , are defined in order to determine the deposit behaviour.

$$f_1 = \tau_i s_i - A_c \frac{dP}{dz} - (\tau_{c1} s_{c1} + \tau_{c2} s_{c2}) - A_c (\rho_c - \rho_m) g \cos(\varphi) \quad (4.2.7-1)$$

$$f_2 = \tau_i s_i - A_c \frac{dP}{dz} + (\tau_{c1} s_{c1} + \tau_{c2} s_{c2}) - A_c (\rho_c - \rho_m) g \cos(\varphi) \quad (4.2.7-2)$$

τ_{c1} is the frictional shear stress between the deposit and the outer pipe wall, while τ_{c2} is the frictional shear stress between the deposit and the inner pipe wall (see Appendix 2). s_{c1} and s_{c2} are the lengths of the outer and inner pipe perimeter in contact with the deposit respectively. The term $(\tau_{c1} s_{c1} + \tau_{c2} s_{c2})$ quantifies the friction between the deposit and the annular walls, while $A_c (\rho_c - \rho_m) g \cos(\varphi)$ is the axial component of net gravity acting on the deposit (see fig. 4.2.7/1).

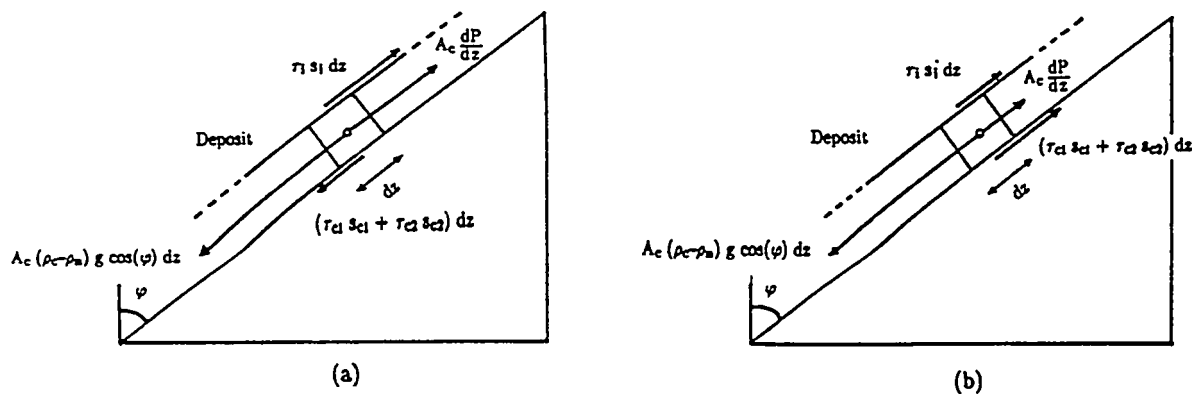


Fig. 4.2.7/1 A force balance for a subelement of the deposit. (a): Friction and net gravity act in the same direction, (b): Friction and net gravity act in opposite directions.

The equation $f_1=0$ is a force balance for the deposit per unit axial length, when the axial component of net gravity and the friction between the deposit and the annular walls act in the same direction (see fig. 4.2.7/1 (a)). The equation $f_2=0$ is the corresponding force balance when the net axial gravity and the friction between the deposit and the annular walls act in opposite directions (see fig.4.2.7/1 (b)).

In order to determine the behaviour of a given deposit, the values of f_1 and f_2 are calculated, using coefficients of static friction for τ_{c1} and τ_{c2} (see Appendix 2). If f_1 and f_2 both are positive, the deposit slides upwards. If they both are negative the deposit slides downwards. If the signs of f_1 and f_2 differ, the deposit is stationary. These relationships are shown graphically in fig. 4.2.7/2.

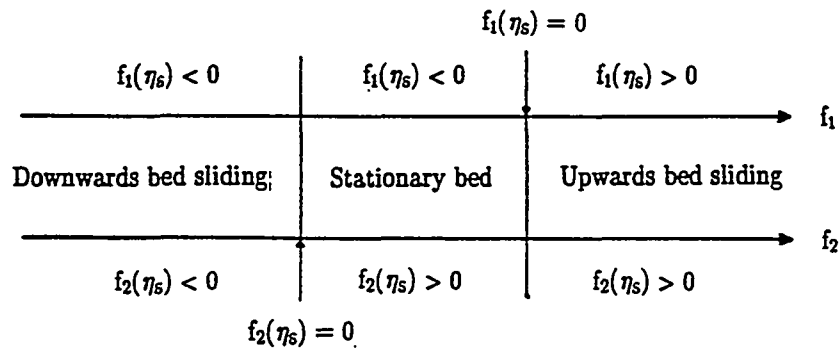


Fig. 4.2.7/2 Behavior of the deposit in terms of the functions f_1 and f_2 , defined in eqs. (4.2.7-1) and (4.2.7-2).

Note that f_2 always is larger than f_1 due to the sign in front of $(\tau_{c1} s_{c1} + \tau_{c2} s_{c2})$ and that according to the definition of η_s (see Appendix 2) the solution to $f_1=0$ or $f_2=0$ is valid only for a deposit at the verge of sliding.

4.2.8 Solution procedure.

The expressions given in the chapters 4.2.3 – 4.2.7 and the Appendices 1 and 2 make it possible to solve equation (4.2.2-3) in an iterative fashion.

The solution procedure is based on the fact that all of the defined geometrical quantities (i.e. s_{m1} , s_{m2} , s_{c1} , s_{c2} , s_i , A_m , A_c and D_H) may be expressed in terms of the angle β , corresponding to a given deposit surface position (see Appendix 1).

The deposit surface positions that satisfies the equation (4.2.2-3) are the ones which produce an equal axial pressure gradient in the upper and lower layer. The diagram in fig. 4.2.8/1 shows how solutions to eq. (4.2.2-3) are determined.

The β -interval between 0 (no deposit) and π (the deposit fills the annular space completely), is divided into a suitable number of subintervals, whereupon each interval is

tested for the presence of solutions. If a subinterval contains a solution, the exact position of the corresponding deposit surface is obtained by an enclosure technique.

For a given size of the deposit (i.e. value of β) the distribution of the fluid between the upper and lower layer is calculated. If the shear stress τ_i in equation (4.2.3-2) is taken to be equal to the surface shear stress at the point of incipient particle motion in eq. (4.2.6-2), i.e.

$$\tau_o = \tau_i \quad (4.2.8-1)$$

the fluid velocity with respect to the deposit surface is found to be:

$$(u_m \pm u_b) = \frac{+}{(-)} \sqrt{\frac{0.12 (\rho_c - \rho_m) g d_c \left[\frac{\cos(\varphi)}{\tan(\psi_r)} + \sin(\varphi) \right]}{f_i \rho_m}} \quad (4.2.8-2)$$

In order to determine the upper layer fluid velocity relative to the annular walls, u_m , it is necessary to determine the value of the deposit sliding velocity, u_b . This is achieved by using the functions f_1 and f_2 defined in chapter 4.2.7.

As a first guess, the deposit is presumed to be stationary, i.e. $u_b=0$. The upper layer fluid velocity u_m is then equal to the R.H.S. of eq. (4.2.8-2), and the nominal lower layer fluid velocity u_c is determined from the volumetric balance in eq. (4.2.5-1). The value of u_c is then used in the calculation of f_1 and f_2 .

If the signs of f_1 and f_2 confirm that the deposit is stationary, it is straightforward to obtain all the quantities occurring in eq. (4.2.2-3), and it is checked if the equation is satisfied for the given position of the deposit surface.

However, if the signs of f_1 and f_2 show that the deposit slides, the initial assumption that u_b is zero, is incorrect. Instead, the nominal lower layer fluid velocity u_c is calculated by solving the equation $f_1=0$ for an upwards sliding deposit, and by solving $f_2=0$ for a downwards sliding deposit (this is possible because the calculation of f_1 and f_2 does not require any knowledge of u_b , merely the upper layer fluid velocity with respect to the deposit surface, which is given by eq. (4.2.8-2)). The solution procedure is iterative and it should be noted that the coefficients of static friction are replaced by coefficients of kinematic friction in the calculations of τ_{c1} and τ_{c2} . When u_c has been determined, u_m and u_b are determined from eqs. (4.2.5-1) and (4.2.8-2), and it is again possible to check if eq. (4.2.2-3) is satisfied.

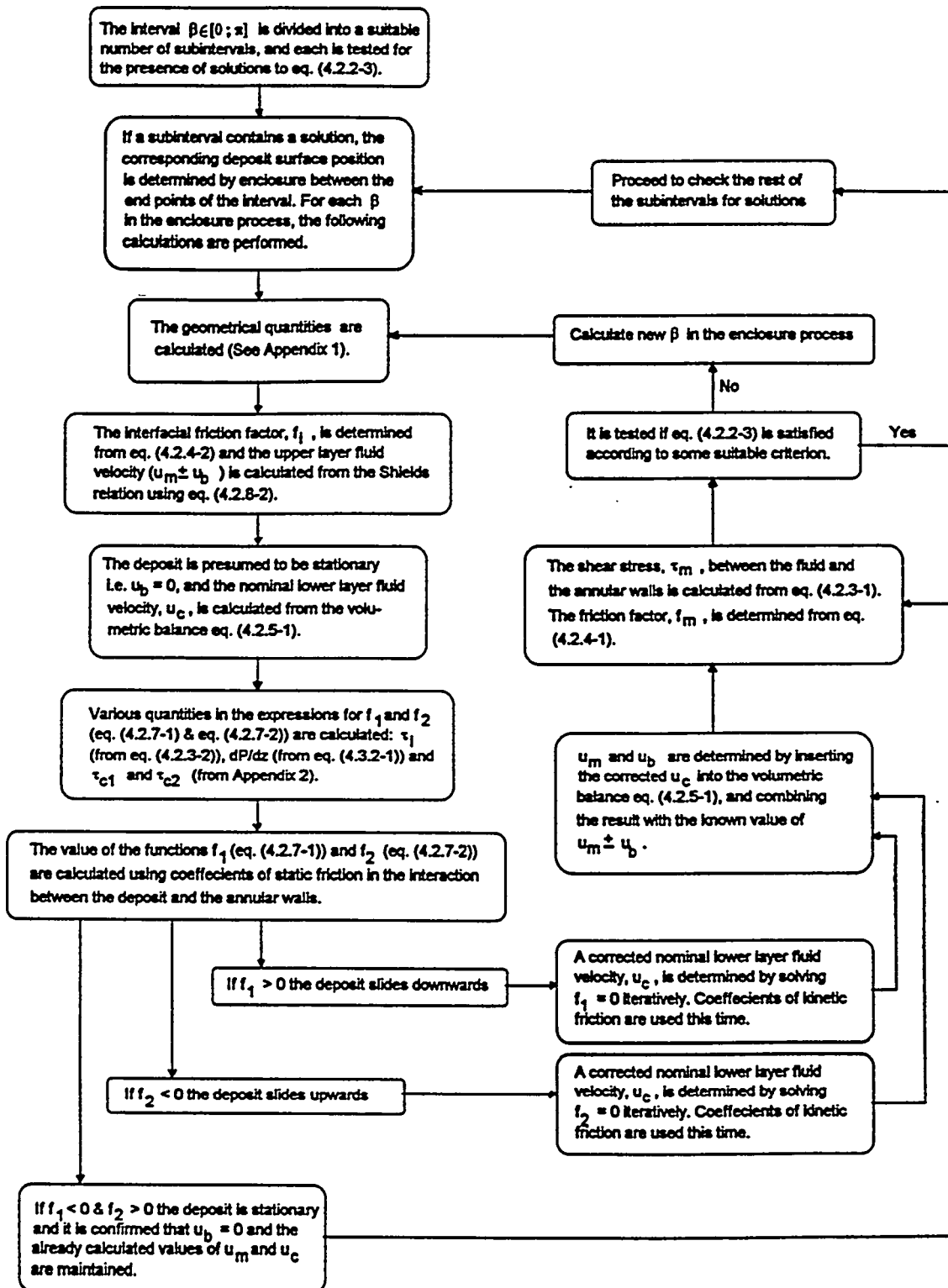


Fig. 4.2.8/1 Diagram showing the solution procedure in the SCSB-model with Newtonian fluid and friction factor expressions calculated from eqs. (4.2.4-1) and (4.2.4-2).

4.3 Introduction of non-Newtonian rheology in the SCSB-model.

In chapter 4.2.4 the fluid shear stresses exerted on the annular walls and the deposit surface were determined on the basis of friction factor relations originally developed for hydraulically smooth and completely rough pipe flow of Newtonian fluids (*Nikuradse* ²⁶ ²⁷). In chapter 4.2.2 the the *Ergun equation* was used to calculate the resistance to intergranular flow.

If the basic structure of the SCSB-model is to be maintained, the introduction of non-Newtonian rheology requires relations describing the flow of non-Newtonian fluids in smooth and rough pipes. A relation similar to the *Ergun equation*, quantifying the resistance to a non-Newtonian fluid in interstitial flow, will also be necessary.

4.3.1 The flow of Power Law fluids in smooth- and rough pipes.

Artyushkov et al. ¹ ² developed a semiempirical model for the flow of Power Law fluids in smooth- and rough pipes (see Appendix 4). The model makes it possible to relate the friction factors defined in (4.2.3-1) and (4.2.3-2) to a Reynolds number for Power Law fluids flowing in a pipe with a known wall roughness. The Reynolds number is defined as (see *Dodge & Metzner* ¹⁰):

$$\text{Re}' = \frac{\rho D^n u^{2-n}}{\left[\frac{3n+1}{4n}\right]^n k 8^{n-1}} \quad (4.3.1-1)$$

where ρ is the fluid density, D the pipe diameter, u the average fluid velocity, k the Power Law consistency index and n the Power Law flow behaviour index.

The *Artyushkov et al.* model covers hydraulically smooth and completely rough flow (for definitions see chapter 4.2.4) as well as the transition between these. Consequently, it is possible to avoid the restrictions tied to the relations (4.2.4-1) and (4.2.4-2). However, the model does not permit a direct determination of the friction factor for a given Reynolds number. A wall shear stress has to be prescribed, whereupon the corresponding friction factor and Reynolds number are determined. Therefore, corresponding values of Reynolds numbers and friction factors are calculated for a suitable range of wall shear stresses, and a friction factor vs. Reynolds number plot is then constructed.

4.3.2 The flow of Power Law fluids through granular beds

Kemblowski & Mertl ²⁴ developed a modified version of the *Ergun equation*, which is valid for the flow of Power Law fluids through a column of packed grains. The modified expression is:

$$-\frac{dP}{dz} = 150 \frac{\psi_k u_k (1-\epsilon)^2}{d_p^2 \epsilon^3} + 1.75 \frac{\rho u_k |u_k| (1-\epsilon)}{d_p \epsilon^3} \left[\frac{\mu_k \kappa_k^2}{\sqrt{\mu_k^2 (\kappa_k^2 - 1) + \kappa_k^2}} \right] \quad (4.3.2-1)$$

where:

$$\psi_k = \frac{k}{12} \left(9 + \frac{3}{n}\right)^n (150 s \epsilon^{1-2n})$$

$$s = \frac{d_p^2}{150} \frac{\epsilon^3}{(1-\epsilon)^2}$$

u_k is the nominal fluid velocity in the column, ϵ the porosity, d_p the diameter of the grains, ρ the fluid density and the term:

$$\left[\frac{\mu_k \kappa_k^2}{\sqrt{\mu_k^2 (\kappa_k^2 - 1) + \kappa_k^2}} \right]$$

is an empirical function, where μ_k and κ_k have been determined from experiments and described in a polynomial form, depending on the Power Law flow behaviour index and a Reynolds number defined by:

$$Re_{km} = \frac{\rho d_p u_k^{2-n}}{\psi_k (1-\epsilon)} \quad (4.3.2-2)$$

When the Power Law flow behaviour index is set to 1, the relation given by *Kemblowski & Mertl* returns to the original *Ergun equation*, derived for Newtonian fluids.

4.3.3 The effect of non-Newtonian rheology on the solution procedure.

In the non-Newtonian version of the SCSB-model, the *Artyushkov et al.* theory outlined in Appendix 4 replaces the relations (4.2.4-1) and (4.2.4-2), while the *Kemblowski & Mertl* relation, eq. (4.3.2-1), replaces the *Ergun equation*, eq. (4.2.2-2). These modifications do not change the fundamental structure of the SCSB-model, as it is described in chapters 4.2.2 - 4.2.8. They are merely refinements that allow the consideration of a wider range of Reynolds numbers and the greater rheological complexity contained in the Power Law model. However, they do create some complications in the solution procedure described in chapter 4.2.8.

The fact that the *Artyushkov et al.* model does not permit a direct determination of the friction factor for a given Reynolds number makes the application of the theory into the SCSB-model somewhat unhandy. A different $f(\text{Re}')$ -plot occurs for each discrete combination of wall roughness and Power Law flow behaviour index. This is unfortunate because the systematic variation in the deposit size in the iterative solution procedure affects the relative roughness of the deposit surface. Consequently, a new $f(\text{Re}')$ -plot has to be generated in each iterative step.

In order to simplify the calculation procedure, a series of $f(\text{Re}')$ -plots have been calculated in advance for discrete values of Power Law flow behaviour indices and roughnesses. Some plots of this type are shown in figs. 4.3.3/1 – 4.3.3/4.

If the constant value of the friction factor in completely rough flow is presumed to be valid for the transition to hydraulically smooth flow also, it is possible to construct a single friction factor vs. Reynolds number plot for the transitional/completely rough region (see fig. 4.3.3/5 (a) – (d)). Note the change in the abscissa between (b) and (c)).

For a number of discrete Power Law flow behaviour indices, *Forsythe polynomials* have been fitted to curves of the type given in figs. 4.3.1/1 and 4.3.1/5 (d), allowing a fast estimate of the friction factor for a given combination of Power Law flow behaviour index, surface roughness and Reynolds number.

The resistance to a Power Law fluid flowing in the upper annular layer now is determined in the following way:

- 1) If the flow is viscous, the friction factor is calculated from the well known relation $f = 16/\text{Re}'$. According to *Dowell Schlumberger*¹² the Reynolds number at transition between viscous and turbulent flow can be estimated from:

$$\text{Re}'_{\text{tr}} = 3470 - 1370 n$$

where n is the flow behaviour index.

- 2) If the flow is hydraulically smooth, the friction factor is determined from the friction factor vs. Reynolds number curve of the type shown in fig. 4.3.3/1. In the present work the curves have been generated for discrete values of the Power Law flow behaviour index n , the range 0.5 – 1.5 being covered in steps of 0.1. The curve corresponding to the flow behaviour index nearest to the one specified is used.
- 3) If the flow is in the transitional/completely rough region, the friction factor is determined from the friction factor vs. roughness curves given in fig. 4.3.3/5 (d). Again, the flow behaviour index range 0.5 – 1.5 is covered in steps of 0.1, and the curve for the index nearest to the one specified is used.

In Re' (see eq. (4.3.1-1)) the hydraulic diameter of the upper layer replaces the pipe diameter, the fluid density ρ_m replaces ρ and the the upper layer fluid velocity u_m replaces u . When the deposit is stationary, the same upper layer fluid velocity is used to determine the fluid shear stress exerted on the annular walls and the deposit surface. However, a sliding deposit leads to different upper layer fluid velocities relative to the annular walls and to the deposit surface respectively, and two different Reynolds numbers are calculated in order to determine the friction factors f_m and f_1 .

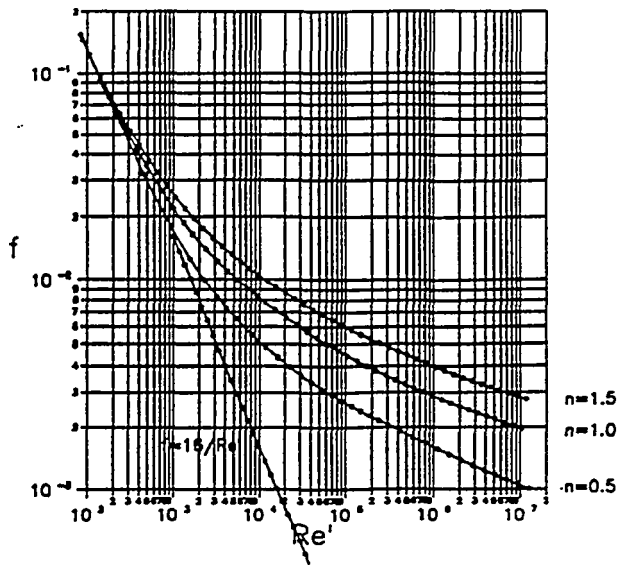


Fig. 4.3.3/1 Resistance to Power Law fluids in hydraulically smooth pipe flow. The curves are calculated on the basis of Artyushkov et al. theory in App. 4.

Fig. 4.3.3/2 Resistance to Power Law fluid flow in rough pipes ($k=10^{-3}$ Pa secⁿ, $n=0.5$). The curves are calculated on the basis of the Artyushkov et al. theory in App. 4. The discrete variable h/R is the relative roughness, h being the height of the roughness protrusions and R the pipe radius.

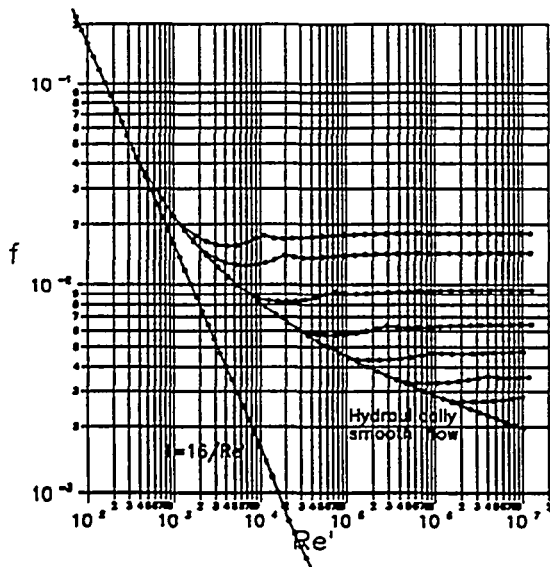
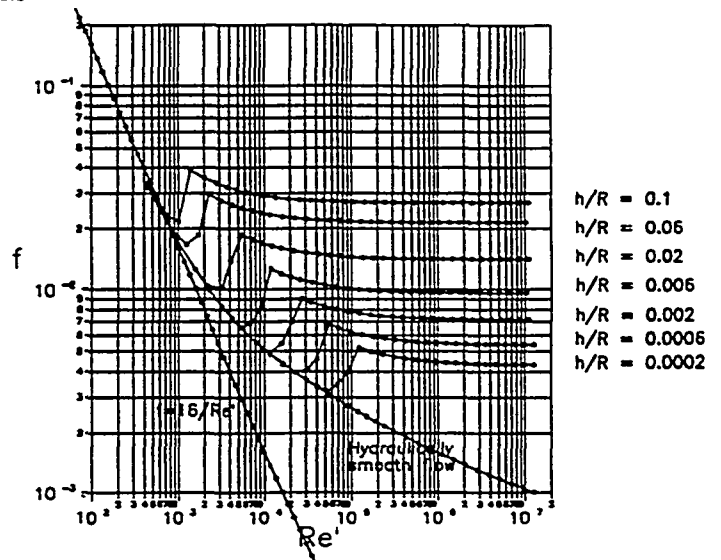
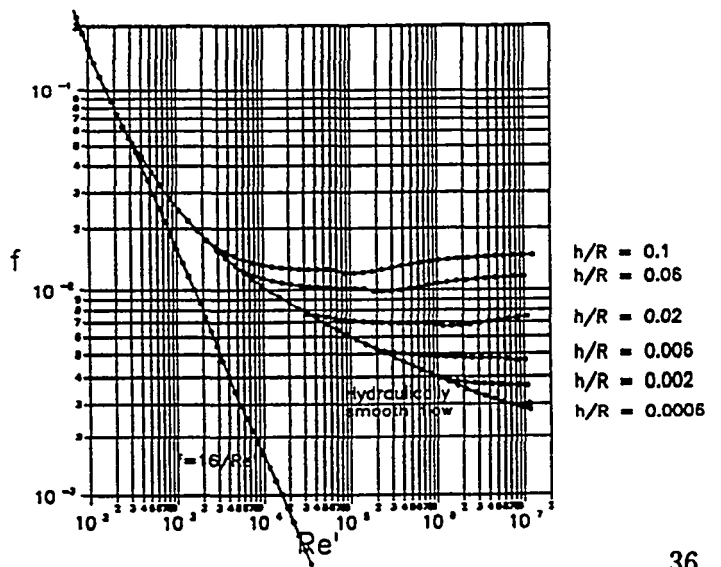


Fig. 4.3.3/3 Resistance to Power Law fluid flow in rough pipes ($k=10^{-3}$ Pa secⁿ, $n=1.0$). The curves are calculated on the basis of the Artyushkov et al. theory in App. 4. The discrete variable h/R is the relative roughness, h being the height of the roughness protrusions and R the pipe radius.

Fig. 4.3.3/4 Resistance to Power Law fluid flow in rough pipes ($k=10^{-3}$ Pa secⁿ, $n=1.5$). The curves are calculated on the basis of the Artyushkov et al. theory in App. 4. The discrete variable h/R is the relative roughness, h being the height of the roughness protrusions and R the pipe radius.



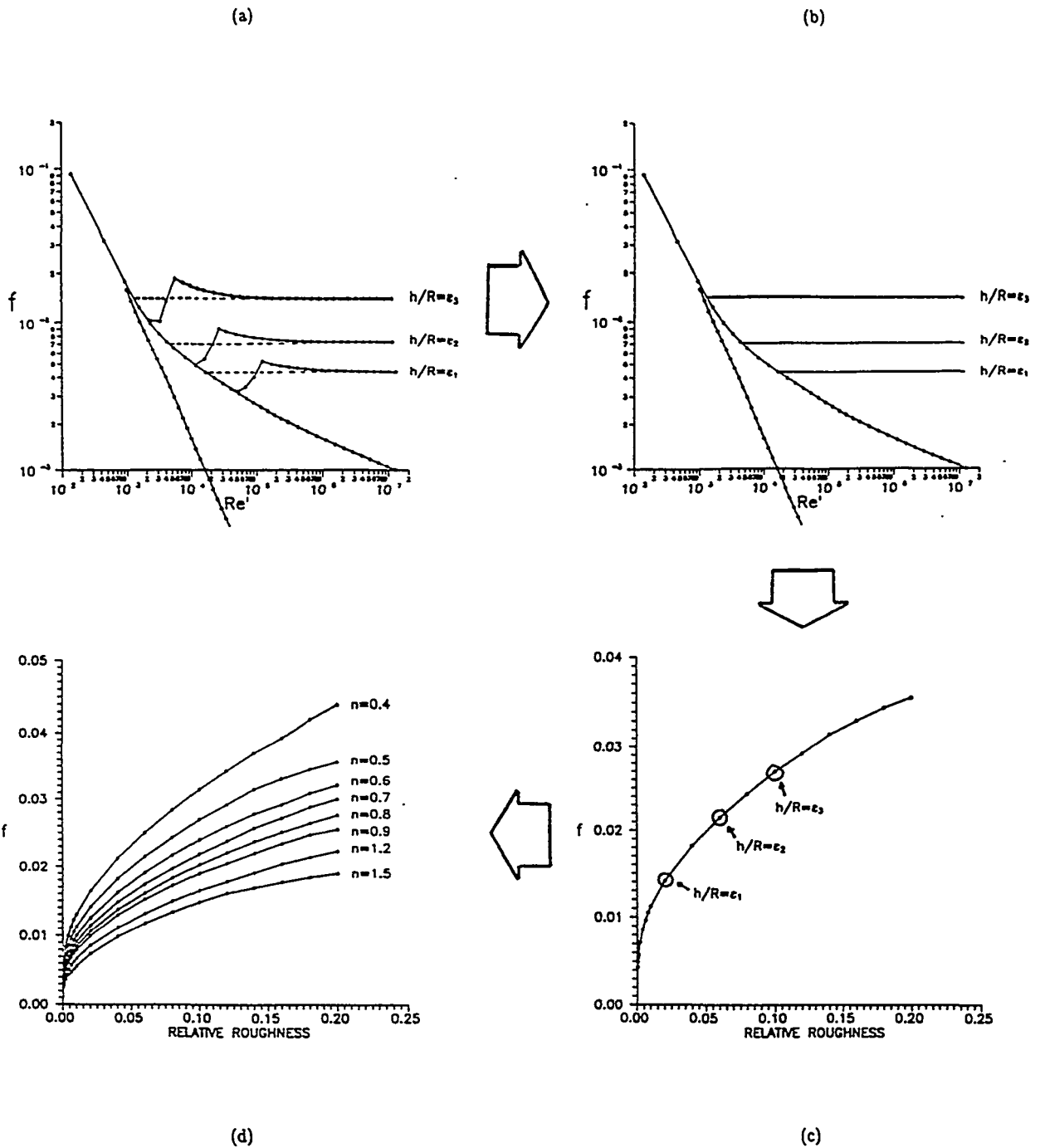


Fig. 4.3.3/5 Construction of a friction factor vs. roughness plot covering completely rough flow and the transition to hydraulically smooth flow. The values for completely rough pipe flow is presumed to be valid in the transition regions too (dashed lines in (a)), leading to the simplified plot shown in (b). The independence of the Reynolds number makes it possible to establish the interpolation curve shown in (c). In (d) interpolation curves for a range of flow behaviour indices are shown.

The application of the *Kemblowski & Mertl* relation on the lower layer in the SCSB-model is straightforward. In eqs. (4.3.2-1) and (4.3.2-2), u_m replaces u_k , d_c replaces d_p and ρ_m replaces ρ .

Fig. 4.3.3/6 shows the solution procedure after the introduction of non-Newtonian fluid rheology. The major differences compared to fig. 4.2.8/1 are:

- that the interfacial friction factor, f_i , is determined from the *Artyushkov et al.* theory and not from the *Nikuradse* relation eq. (4.2.4-2). Note that the determination of an interfacial friction factor in the *Artyushkov et al.* model requires an upper layer fluid velocity, which is determined from eq. (4.2.8-2). However, eq. (4.2.8-2) requires the interfacial friction factor to be known, and consequently the determination of the interfacial friction factor and the corresponding upper layer fluid velocity has to be performed iteratively.
- that the lower layer pressure gradient now is given by the modified Ergun equation given by *Kemblowski & Mertl*, i.e. eq. (4.3.2-1) replaces eq. (4.2.2-2).
- that the friction factor f_m is determined from the *Artyushkov et al.* ^{1 2} theory and not from the *Nikuradse* relation eq. (4.2.4-1).

Table 4.3.3/a lists the differences between the "simple" Newtonian version of the SCSB-model outlined in chapters 4.2.2 - 4.2.8, and the more complex version resulting from the introduction of non-Newtonian rheology.

4.4 Some general comments to the SCSB-model.

It is important to realize that the SCSB-model is based on a simplified description of the cuttings transport process. Before the predictions from the SCSB-model are compared with experimental results in chapter 5, a number of limitations in the model should be mentioned.

- 1) In the SCSB-model, the deposit is described with a distinct plane surface between the upper and lower layer. However, experimental evidence shows that plane bed surfaces exist only under some conditions, while the formation of movable bedforms (i.e. ripples and dunes) is common (see for example *Gonzalez* ¹⁶, *Garde & Ranga Raju* ¹⁴). The occurrence of moveable bedforms increases the resistance to fluid flow compared to the resistance displayed by the plane deposit surface.
- 2) The SCSB-model is valid only when a distinct deposit has formed, i.e. at relatively large annular inclinations relative to vertical. At low inclinations, the weak radial body forces tend to make a deposit unstable, and downwards sliding slugs and intermittent breakups of the deposit occur. This is reflected in a poor agreement between the SCSB-model predictions and experimental results at low inclinations (see chapter 5).
- 3) Consider fig. 4.4/1. The contours outlined in the annular cross sectional area are regions through which some given proportion of the total volumetric flowrate passes. When the upper layer cross sectional area is of a regular shape as in fig. 4.4/1 (a), a description of the upper layer geometry in terms of the hydraulic diameter is reasonable. However, in fig. 4.4/1 (b), the shape of the upper layer is complex. The

inner pipe tend to create narrow regions, where the local fluid velocities will be strongly reduced compared to the velocities in the wider parts (see fig. 3.6/1), and the description of the geometry in terms of the hydraulic diameter is poor. In the SCSB-model the position of the deposit surface is governed by the fluid shear stress at the surface, but the reduced shear stresses in narrow regions are not reflected in a model using a hydraulic diameter. Consequently, in situations where the inner pipe "shields" the deposit from the impact of bulk flow, it is expected that the SCSB-model predicts a smaller deposit than the one actually occurring.

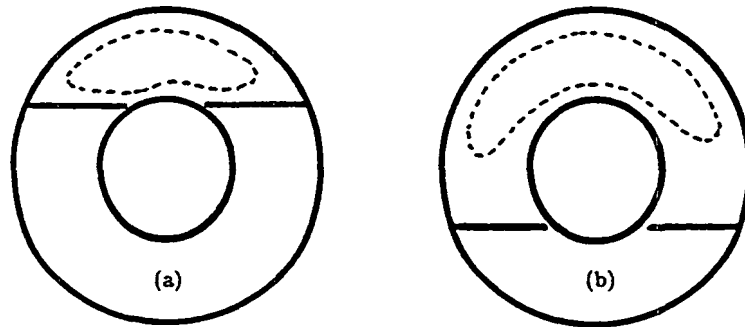


Fig. 4.4/1 Sketched contours of the annular regions through which the majority of the volumetric flowrate passes (e.g. 80%). (a) unshielded deposit, (b) shielded deposit.

- 4) The determination of two different Reynolds numbers in the space above the deposit at the same time, when the deposit slides, may be considered a somewhat dubious arrangement.
- 5) It should be noted that the annular particle feed concentration does not enter the SCSB-model, even if the annular cuttings concentration has been reported to depend on it (*Grossmann*¹⁷, *Sifferman et al.*³⁸).

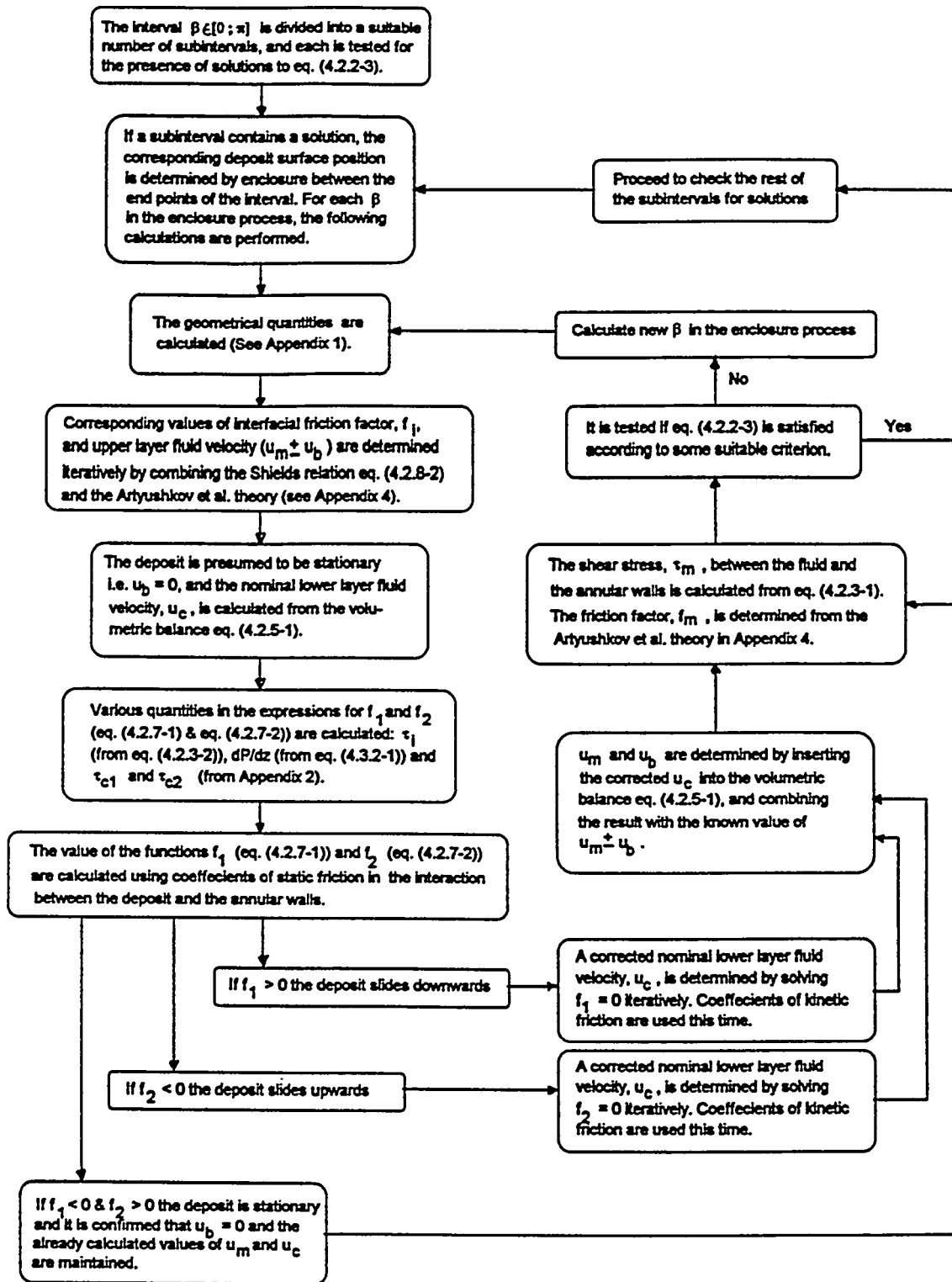


Fig. 4.3.3/6 Diagram showing the solution procedure in the SCSB-model after the introduction of the Artyushkov et al.^{1,2} theory and the Kemblowski & Mertl²⁴ modification of the Ergun equation.

	Simple version Newtonian fluids (Chap. 4.2)	Complex version Power Law fluids (Chap. 4.3)
Basic equation	$\frac{1}{A_m} [\tau_m (s_{m1} + s_{m2}) + \tau_1 s_1] =$ $150 \frac{\mu_m u_c (1-\epsilon)^2}{d_c^2 \epsilon^3} + 1.75 \frac{\rho_m u_c u_c (1-\epsilon)}{d_c \epsilon^3}$	$\frac{1}{A_m} [\tau_m (s_{m1} + s_{m2}) + \tau_1 s_1] = 150 \frac{\psi_k u_c (1-\epsilon)^2}{d_c^2 \epsilon^3}$ $+ 1.75 \frac{\rho_m u_c u_c (1-\epsilon)}{d_c \epsilon^3} \left[\frac{\mu_k \kappa_k^2}{\sqrt{\mu_k^2 (\kappa_k^2 - 1)^2 + \kappa_k^2}} \right]$
Geometrical relations	App. 1	identical
Shear stress relations	$\tau_m = \frac{1}{2} f_{m1} \rho_m u_m u_m $ $\tau_1 = \frac{1}{2} f_1 \rho_m (u_m^2 + u_b^2) (u_m^2 + u_b^2) $	identical
Friction factor relations	$f_m = \left[4.0 \log_{10} (Re_w \sqrt{f_m}) - 0.4 \right]^{-2}$ $f_1 = 2.0 \left[4.0 \log_{10} \left[\frac{D_h}{d_c} \right] + 3.36 \right]^{-2}$	Artyushkov et al. ^{1,2} theory (App. 4)
Volumetric balance	$V = A_m u_m + A_c (u_c^2 + u_b)$	identical
The Shields concept (modified form)	$\frac{\tau_o}{(\rho_c - \rho_m) g d_c} = \left[\frac{\cos(\varphi)}{\tan(\psi_r)} \right] \sin(\varphi) 0.06$	identical
Criteria for deposit sliding	$f_1 = \tau_1 s_1 - A_c \frac{dP}{dz} - (\tau_{c1} s_{c1} + \tau_{c2} s_{c2})$ $- A_c (\rho_c - \rho_m) g \cos(\varphi)$ $f_2 = \tau_1 s_1 - A_c \frac{dP}{dz} + (\tau_{c1} s_{c1} + \tau_{c2} s_{c2})$ $- A_c (\rho_c - \rho_m) g \cos(\varphi)$	identical (but dP/dz given by the <i>Kemblowski et al.</i> ²⁴ modification of the Ergun equation.)

Table 4.3.3/a A comparison of the elements in the simple Newtonian version of the SCSB-model and the more complex version resulting from the introduction of the Artyushkov et al.^{1,2} theory and the Kemblowski & Mertl²⁴ modification of the Ergun equation.

Chapter 5

**A comparison of
predictions from the
SCSB-model with
experimental results.**

In this chapter, The predictions from the SCSB-model are compared with experimental results obtained by the author and selected results from the works of *Brown et al.* ⁷, *Iyoho* ²³ and *Grossmann* ¹⁷.

The predictions from the SCSB-model are produced as output from the computer programs described in Appendix 5. It is important to realize that these programs make a sharp distinction between the possible flow regimes for the upper layer fluid. One version operates under the precondition of viscous flow, another under the precondition of turbulent flow. If a transition takes place somewhere in the range of the independent variable being investigated, a shift in the program used for the calculation is required.

While *Iyoho* ²³ and *Grossmann* ¹⁷ performed their experiments under steady state conditions, where cuttings were fed continuously to an annular section, the experimental procedure used by *Brown et al.* ⁷ was different: The annulus was loaded with cuttings until they occupied 15% of the total annular volume, and the maximum flowrate allowing the cuttings to remain in the annulus was determined, without cuttings being fed to the annulus. However, this variation in experimental approach makes no difference to the SCSB-model, as it does not account for the influence of particles on the properties of the fluid flowing above the deposit surface.

Iyoho ²³ observed that when fluid circulation was stopped, downwards sliding deposits in a Perspex annulus occurred for annular inclinations below approximately 60 degrees relative to vertical. It indicates a coefficient of static friction for the deposit/wall interaction of approximately 0.6. This value is adopted in the present work. The corresponding coefficient of kinetic friction is estimated to be approximately 0.3.

The relative wall roughness in the *Artyushkov et al.* theory is determined as the height of the roughness protrusions divided by the pipe radius. In the SCSB-model, the analogous quantity would be d_c/D_h . However, cuttings are of irregular shape, and it is expected that they will be positioned so their largest dimension is parallel to the surface plane. Therefore the deposit surface roughness in the present calculations has been estimated to $0.5 d_c/D_h$.

Due to the presentation in the original works, three different types of plots will occur in the comparison between the predictions from the SCSB-model and experimental data:

- 1) Plots of annular cuttings concentration vs. annular inclination for discrete values of the volumetric flowrate (in the following denoted $c(\varphi)$ -plots). The SCSB-model predictions in these plots are obtained from the programs SCSB-CT and SCSB-CV described in Appendix 5.
- 2) Plots of annular cuttings concentration vs. nominal annular fluid velocity for discrete values of the annular inclination (in the following denoted $c(v)$ -plots). The SCSB-model predictions in these plots are obtained from slightly modified versions of the programs SCSB-CT and SCSB-CV described in Appendix 5.
- 3) Plots of the nominal annular fluid velocity required in order to sustain a given annular cuttings concentration vs. annular inclination for discrete values of annular eccentricity. In the following, this type of plot is denoted a $v(\varphi)$ -plot and the SCSB-model predictions are obtained from the program SCSB-VT described in Appendix 5.

from the H-I branch) appear. They reflect that apart from a "free" deposit below the inner pipe, two more deposit sizes are possible due to frictional stabilization from the pipe.

Below D, the stationary deposit keeps on growing with decreasing annular inclination. Between the inclinations E and F, the SCSB-model again predicts multiple solutions. The various possible patterns of motion is (1): Large forwards/upwards moving deposit, (2): Stationary deposit, (3): A relatively large but slowly downwards sliding deposit, and (4): A relatively small but fast downwards sliding deposit. Between F and G the slowly sliding deposit solution disappears.

The inclination G is the smallest inclination where a stationary deposit can occur. Below the inclination G, the frictional forces between the deposit and the annular walls are unable to keep the former from sliding, and the SCSB-model allows only a large upwards- or a small downwards sliding deposit. In chapter 5.1.2, the agreement between the SCSB-model and the experimental results are poor for the lower annular inclinations. When the deposit slides downwards, it tends to form sliding slugs, which is intermittently formed and dissolved again. This complex behaviour is not well described by the SCSB-model, where a well defined plane deposit is presumed to occur at all inclinations. However, the predicted breakdown of the deposit below G in fig. 5.1.1/1 is reflected by steep decreases in the experimentally measured cuttings concentrations.

In the intervals of annular inclinations where the SCSB-model predicts more than one solution, it is generally not known if a given solution is more stable than another. However, the experimental evidence outlined in chapter 5.1.2 indicates that there is only one annular cuttings concentration corresponding to a given inclination, and that a large stationary deposit is favoured whenever this is possible.

5.1.2 Specific remarks

Due to numerous difficulties in the construction of the flow loop described in chapter 6, only few experimental data have been obtained from it. However, even if no comprehensive experimental programme has been carried out, the results obtained by the author are very similar to results reported by other researchers.

In figs. 5.1.2/1 and 5.1.2/2 the predictions from the SCSB-model are compared with experimental results obtained in the flow loop at DTH. While the results plotted in fig. 5.1.2/1 have been obtained with a concentric inner pipe, the results in fig. 5.2.1/2 have been obtained with an +50% eccentric configuration. In fig. 5.1.2/2, the experimental conditions are close to the ones used by *Iyoho*²³, and his results are included in the figure for comparison. It should be noted that despite the large difference in annular particle feed rate, the results obtained by the author and *Iyoho* do not differ significantly, i.e. it indicates that the size of the deposit is only weakly dependent on this variable.

Figs. 5.1.2/3 - 5.1.2/6 are $c(\varphi)$ -plots based on experimental parameters and results reported by *Iyoho*²³.

Fig. 5.1.2/3 concerns cuttings behaviour in a Carbopol solution. The predictions from the SCSB-model are characterized by the sudden disappearance of solutions when the annular cuttings concentration exceeds some given value. The reason for this behaviour is

that the deposit size forces a shift from viscous- to turbulent flow above the deposit surface. For the lowest of the discrete volumetric flowrates, the flow regime does not become turbulent before downwards deposit sliding is initiated. The predictions in fig. 5.1.2/3 have been obtained with a computer program valid for viscous flow only, and it might be expected that supplementary sections to the theoretical curves could be obtained with further calculations, using the version of the computer program valid for turbulent flow. However, an attempt of this type fails, presumably because the applied model of *Artyushkov et al.*^{1 2} tends to overestimate the interfacial friction factor in the transition from laminar to turbulent flow (compare the *Artyushkov et al.* model predictions in fig. A4/2 with the *Nikuradse* data plotted in fig. 4.2.4/1). However, if the annular cuttings concentration is presumed to decrease gradually with annular inclination after the onset of turbulence (i.e after the disappearance of solutions), some qualitative agreement between model and the experimental results is seen.

Fig 5.1.2/4 and fig. 5.1.2/5 concern cuttings behaviour in two different Bentonite suspensions, where the flow regimes are different. Fig. 5.1.2/6 concerns cuttings behaviour in water in turbulent flow. The amount of experimental data is small in these figures. However, the experiments show cuttings concentrations within the same order of magnitude as the model predictions. A slightly poorer quantitative agreement between theory and experiments at the high volumetric flowrates may be explained by a shielding of the deposit below the inner pipe (see chapter 4.4).

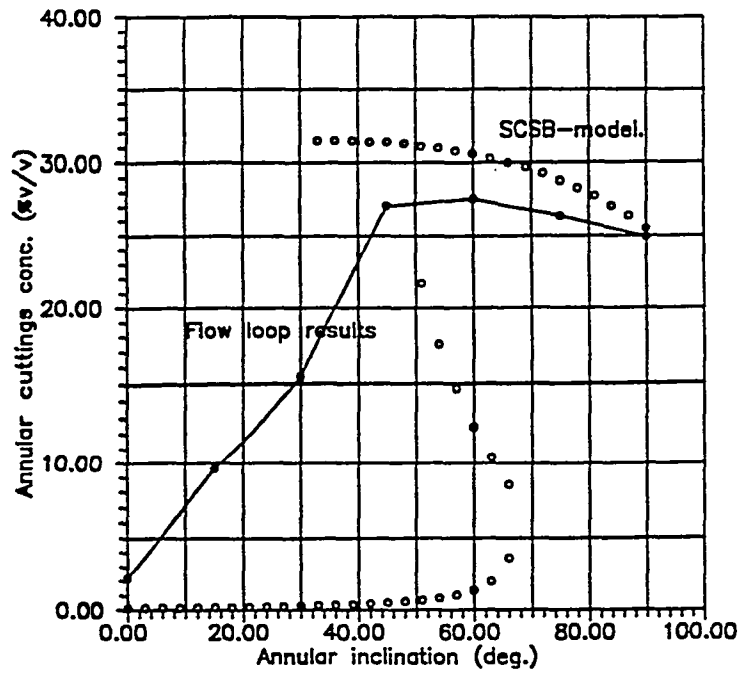


Fig. 5.1.2/1 Comparison of experimental results obtained in the flow loop at DTH with the corresponding predictions from the SCSB-model.

$D=0.127$ m, $d=0.051$ m, $\rho_c=2680$ kg/m³, $\rho_m=1000$ kg/m³, $\mu_m=10^{-3}$ Pa sec (water), ecc.=0%, rot.=0 rpm, $d_c=0.006$ m (5.0-7.0 mm), $\psi_i=36$ deg., $\eta_k=0.6$, $\eta_d=0.3$, $c_b=0.44$, $m_{feed}=0.025$ kg/sec, $V=5.56 \cdot 10^{-3}$ m³/sec.

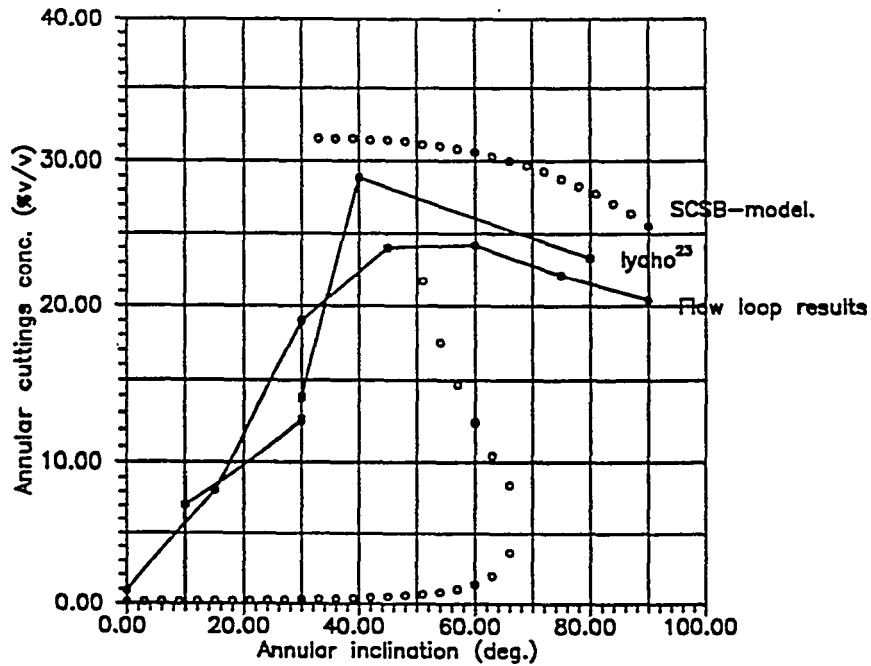


Fig. 5.1.2/2 Comparison of experimental results obtained in the flow loop with predictions from the SCSB-model and experimental results reported by Iyoho²³ for largely the same experimental parameters.

$D=0.127$ m, $d=0.051$ m, $\rho_c=2680$ kg/m³, $\rho_m=1000$ kg/m³, $\mu_m=10^{-3}$ Pa sec (water), ecc.=+50%, rot.=0 rpm, $d_c=0.006$ m (5.0-7.0 mm), $\psi_i=36$ deg., $\eta_k=0.6$, $\eta_d=0.3$, $c_b=0.44$, $m_{feed}=0.025$ kg/sec, $V=5.56 \cdot 10^{-3}$ m³/sec.

(Iyoho: $D=0.127$ m, $d=0.048$ m, $\rho_c=2620$ kg/m³, $\rho_m=1000$ kg/m³, $\mu_m=10^{-3}$ Pa sec (water), ecc.=+50%, rot.=0 rpm, $d_c=0.00635$ m, $\psi_i=36$ deg. (est.), $\eta_k=0.6$, $\eta_d=0.3$, $c_b=0.5$ (est.), $m_{feed}=0.15$ kg/sec, $V=6.31 \cdot 10^{-3}$ m³/sec.)

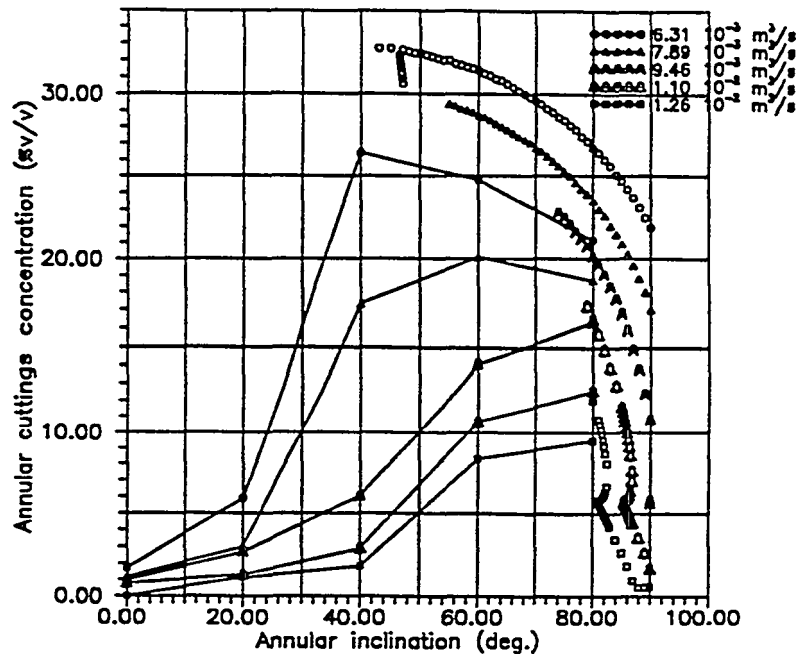


Fig. 5.1.2/3 Annular cuttings concentration vs. inclination for discrete volumetric flowrates. Fluid: Carbopol. Flow regime: Viscous. Unconnected data points: Predictions from the SCSB-model. Fully drawn curves: Experimental results by Iyoho ²³.

$D=0.127$ m, $d=0.0482$ m, $\rho_c=2620$ kg/m³, $\rho_m=1000$ kg/m³, $d_c=0.00635$ m, $k=0.271$ Pa sec^a, $n=0.64$, ecc.=+50%, rot.=50 rpm, $\psi_r=36$ deg., $c_b=0.5$, $\eta_s=0.6$, $\eta_d=0.3$, $m_{feed}=0.15$ kg/sec.

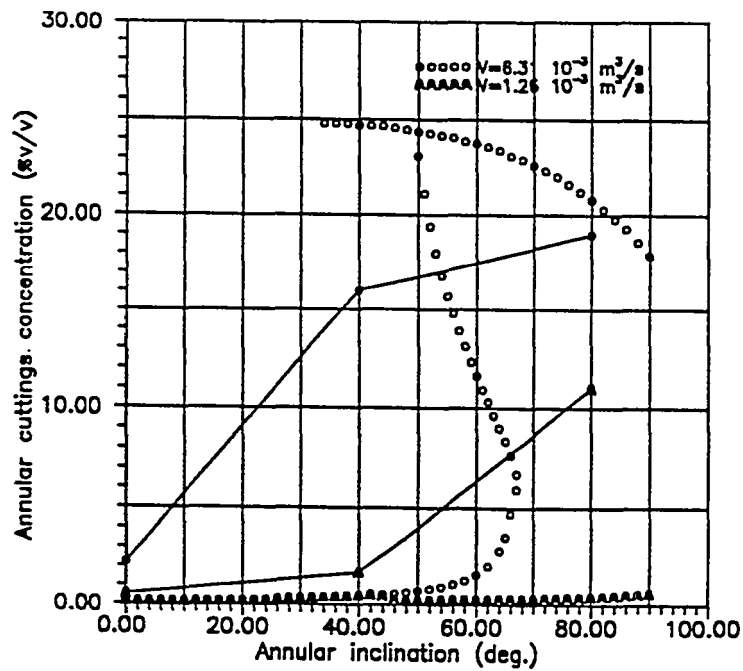


Fig. 5.1.2/4 Annular cuttings concentration vs. inclination for discrete volumetric flowrates. Fluid: Bentonite suspension. Flow regime: Turbulent. Unconnected data points: Predictions from the SCSB-model. Fully drawn curves: Experimental results by Iyoho ²³.

$D=0.127$ m, $d=0.0482$ m, $\rho_c=2620$ kg/m³, $\rho_m=1000$ kg/m³, $d_c=0.00635$ m, $k=0.039$ Pa sec^a, $n=0.68$, ecc.=+50%, rot.=50 rpm, $\psi_r=36$ deg., $c_b=0.5$, $\eta_s=0.6$, $\eta_d=0.3$, $m_{feed}=0.15$ kg/sec.

Fig. 5.1.2/5

Annular cuttings concentration vs. inclination for discrete volumetric flowrates. Fluid: Bentonite suspension. Flow regime: viscous. Unconnected data points: Predictions from the SCSB-model. Fully drawn curves: Experimental results by Iyoho 23.

$D=0.127$ m, $d=0.0482$ m, $\rho_c=2620$ kg/m³, $\rho_m=1000$ kg/m³, $d_c=0.00635$ m, $k=0.437$ Pa sec^a, $n=0.61$, $ecc.=+50\%$, $rot.=50$ rpm, $\psi_r=36$ deg., $c_b=0.5$, $\eta_s=0.6$, $\eta_d=0.3$, $m_{feed}=0.15$ kg/sec.

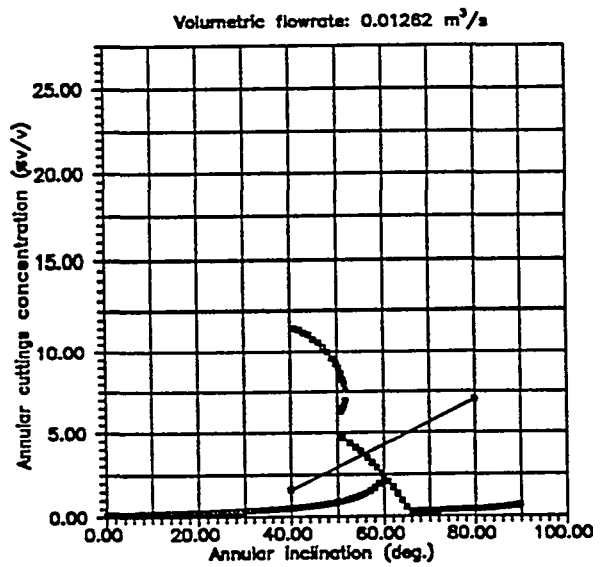
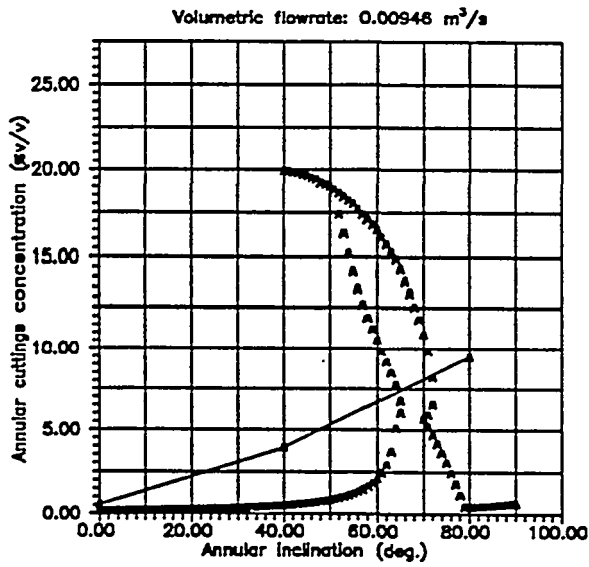
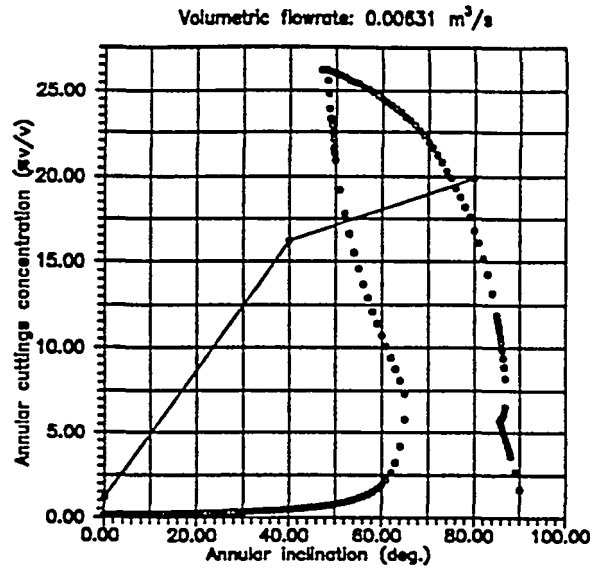
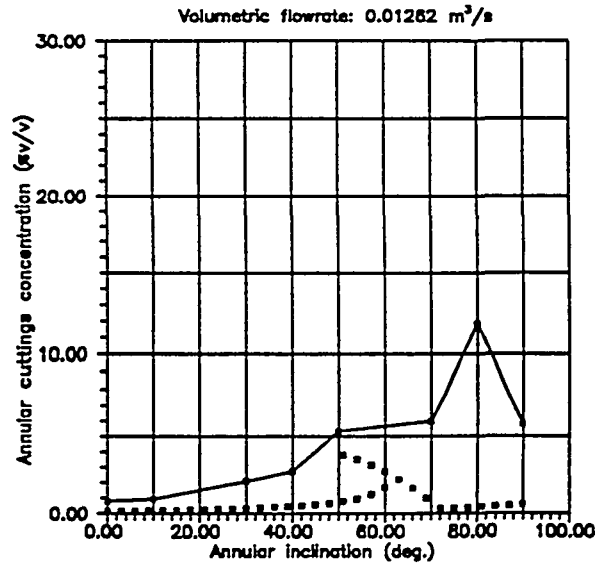
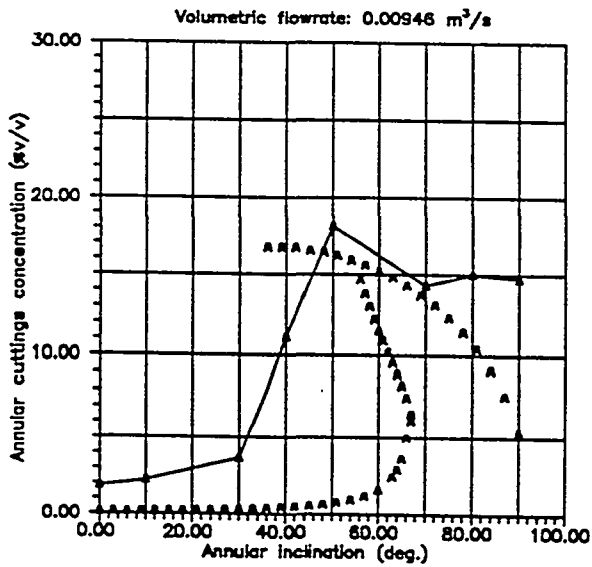
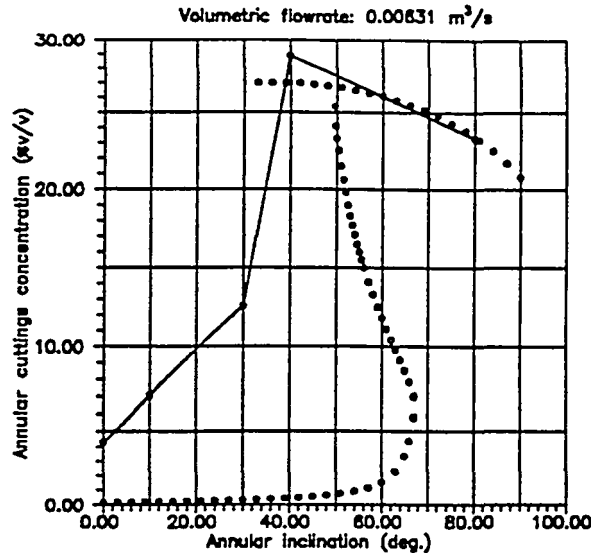


Fig. 5.1.2/6

Annular cuttings concentration vs. inclination for discrete volumetric flowrates. Fluid: Water. Flow regime: Turbulent. Unconnected data points: Predictions from the SCSB-model. Fully drawn curves: Experimental results by Iyoho²³.

$D=0.127$ m, $d=0.0482$ m, $\rho_c=2620$ kg/m³, $\rho_m=1000$ kg/m³, $d_c=0.00635$ m, $k=0.001$ Pa sec, $n=1.0$, ecc.=+50%, rot.=50 rpm, $\psi_r=36$ deg., $c_b=0.5$, $\eta_s=0.6$, $\eta_d=0.3$, $m_{feed}=0.15$ kg/sec.



5.2 $c(v)$ -plots

5.2.1 General remarks

A general form of a $c(v)$ -plot as predicted by the SCSB-model is shown in fig. 5.2.1/1. Not all of the branches outlined occur at the same time. Some of them are present at one inclination, while they are absent at another. However, parts of this general form occur in all $c(v)$ -plots derived from the SCSB-model.

In analogy with the $c(\varphi)$ -plots, a separate upper branch (G-H on fig. 5.2.1/1) frequently appears. It represents an extensive forwards/upwards sliding deposit, filling out most of the annular space. However, this type of behaviour has not been observed in any experiment and in order to attain greater clarity, the branch is omitted in the figures given in chapter 5.2.2.

The branch A-B represents a relatively fast downwards sliding deposit. The branch is absent at large annular inclinations with respect to vertical, where downwards deposit sliding cannot take place.

The branch D-E is of variable length and typically appears for annular inclinations around 45–50 degrees. The solutions on this branch corresponds to a slowly downwards sliding deposit.

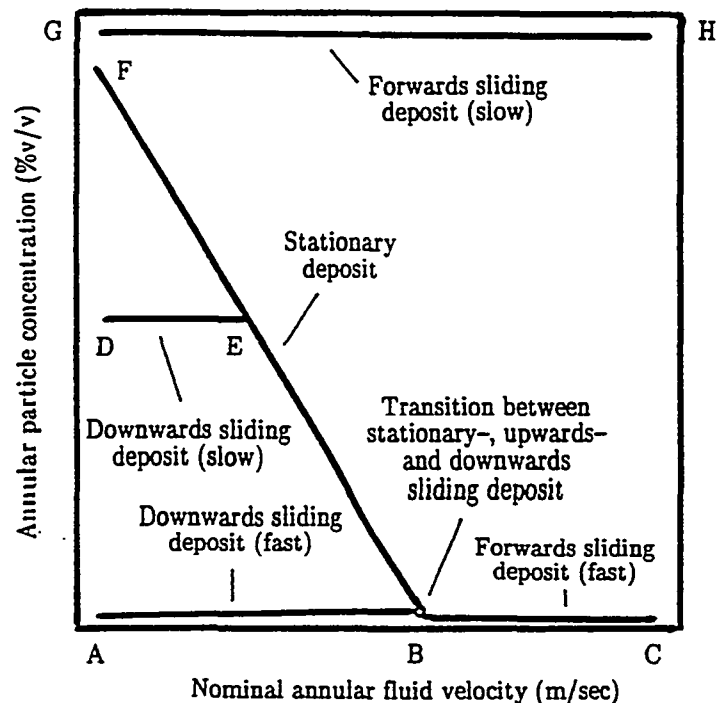


Fig. 5.2.1/1 $c(v)$ -plot, general form.

The branch F-B represents a stationary deposit. At relatively large annular inclinations, the branch passes continuously into the branch B-C, which corresponds to an upwards sliding deposit. However, below some annular inclination, the two branches detach from

each other, and void gaps of variable size occur (see for example figs. 5.2.2/3, 5.2.2/6 and 5.2.2/7). The SCSB-model does not predict any solutions in these gaps.

The disappearance of solutions in branch F-B may be caused by the transition from viscous to turbulent flow. As mentioned in chapter 5.1.2, the *Artyushkov et al.* theory tends to overestimate the interfacial friction factor in this region, and the required shift in computer program may not produce continuous solutions.

However, the void gaps described also occur in situations where there is no change in flow regime. The reason for this phenomenon presumably is, that a stationary deposit can be eroded only until some critical point, where the annular wall friction no longer is large enough to prevent the deposit from sliding downwards. When the deposit starts to slide against the direction of fluid flow, the fluid velocity relative to the deposit surface is increased, enforcing further erosion of the deposit. The erosion of the deposit will continue until it has disappeared completely, or it has attained a new equilibrium size. The replacement of a relatively large stationary deposit with a relatively small downwards sliding deposit would be analogous to the situation in in fig. 5.1.1/1, where the annular inclination is reduced below the point G.

If the abrupt disappearance of predicted solutions from the SCSB-model corresponds to a deposit that becomes unstable and rapidly is broken down, it would be in reasonable accordance with the experimental results given in chapter 5.2.2. The evidence of a breakdown is supported by the fact that the gaps in branch F-B are absent or small at large annular inclinations, while they get larger and larger with decreasing inclination (see for example fig. 5.2.2/3 or fig. 5.2.2/6). This is expected because the friction between the deposit and the annular walls decreases with inclination, while the axial component of gravity acting on the deposit increases. Furthermore, the gaps in F-B seem to be larger in a concentric- than in an eccentric annulus (compare figs. 5.2.2/6 with 5.2.2/7 and 5.2.2/8 with 5.2.2/9), which could be caused by the stronger frictional interaction between the deposit and the annular walls in the latter configuration.

The appearance of (small) gaps at high inclinations (see figs. 5.2.2/6, 5.2.2/7 and 5.2.2/9), where downwards sliding deposits cannot occur, is not fully understood, but it may lie within the formulation of the SCSB-model.

Around the point B in fig. 5.2.1/1, a transition from an upwards- to a downwards sliding deposit (or *vice versa*) takes place. According to the diagram in fig. 4.2.7/2 a direct transition should not be possible. However, the range of nominal annular fluid velocities where a stationary deposit exists, depends on the size of $(\tau_{c1} s_{c1} + \tau_{c2} s_{c2})$ compared to the other terms in the equations (4.2.7-1) and (4.2.7-2). If it is small, the transition may appear to take place directly.

5.2.2 Specific remarks

Figs. 5.2.2/1, 5.2.2/2, 5.2.2/3, 5.2.2/4 and 5.2.2/5 are based on experimental parameters and results reported by *Iyoho*²³. The parameters being varied are fluid rheology, annular inclination and annular fluid velocity.

Fig. 5.2.2/1 concerns cuttings behaviour in a Carbopol solution in viscous flow. The disappearance of solutions above approximately 0.70 m/sec for $\varphi=40$ and $\varphi=60$ deg. is caused by a transition from viscous to turbulent flow, similar to the one described for fig. 5.1.2/3 in chapter 5.1.2 (note: there is no transition for $\varphi=80$). It is noteworthy that the

disappearance of theoretical solutions is reflected in a slight increase in the slope of the corresponding experimental curves. If there is a connection, it indicates that *Iyoho* for the mentioned inclinations traversed the boundary between viscous and turbulent flow, even if the experimental data was reported to have been obtained in the viscous flow regime. Furthermore, it indicates that turbulent flow produces lower annular cuttings concentrations than viscous flow in inclined annuli. However, this is contradicted by the experimental evidence summarized in chapter 3.2.1, where turbulent and viscous flow were found to be equally efficient in cuttings removal for the annular inclinations around 50 degrees.

Fig 5.2.2/2 concerns cuttings behaviour in a Bentonite suspension in viscous flow. Figs. 5.2.2/3 and 5.2.2/4 concern cuttings behaviour in water in turbulent flow, while fig. 5.2.2/5 concerns cuttings behaviour in a Bentonite suspension in turbulent flow. The somewhat crude nature of the SCSB-model taken into consideration, the qualitative and quantitative agreement between theoretical predictions and experimental results are found to be good, except for combinations of high annular inclinations and large annular fluid velocities.

Figs. 5.2.2/6, 5.2.2/7, 5.2.2/8 and 5.2.2/9 are based on experimental parameters and results reported by *Grossmann* ¹⁷. All data are obtained with Newtonian fluids in turbulent flow. The parameters being varied are annular fluid velocity, annular inclination, particle size and inner pipe eccentricity.

The qualitative accordance between *Grossmanns* experimental data and the predictions from the SCSB-model is good, while the quantitative agreement seems to depend on the experimental conditions.

If the abrupt disappearance of predicted solutions from the SCSB-model corresponds to a deposit that becomes unstable and rapidly is broken down, the quantitative agreement between theory and experiment is good for the low inclinations in the concentric as well as the eccentric annulus.

In analogy with the plots in figs. 5.2.2/3, 5.2.2/4 and 5.2.2/5, the quantitative agreement between model predictions and experimental results are generally poor for combinations of large inclinations and large fluid velocities. The divergences do not appear to be strongly related to eccentricity (compare fig. 5.2.2/6 (ecc.=0%) with fig.5.2.2/7 (ecc.=+90%) and fig. 5.2.2/8 (ecc.=0%) with fig.5.2.2/9 (ecc.=+90%)), while it to some degree seems associated with particle diameter, as the divergence is more pronounced for the smaller particle size than for the large (compare fig. 5.2.2/6 ($d_c=0.74$ mm) with fig.5.2.2/8 ($d_c=0.4$ mm) and fig. 5.2.2/7 ($d_c=0.74$ mm) with fig.5.2.2/9 ($d_c=0.4$ mm)).

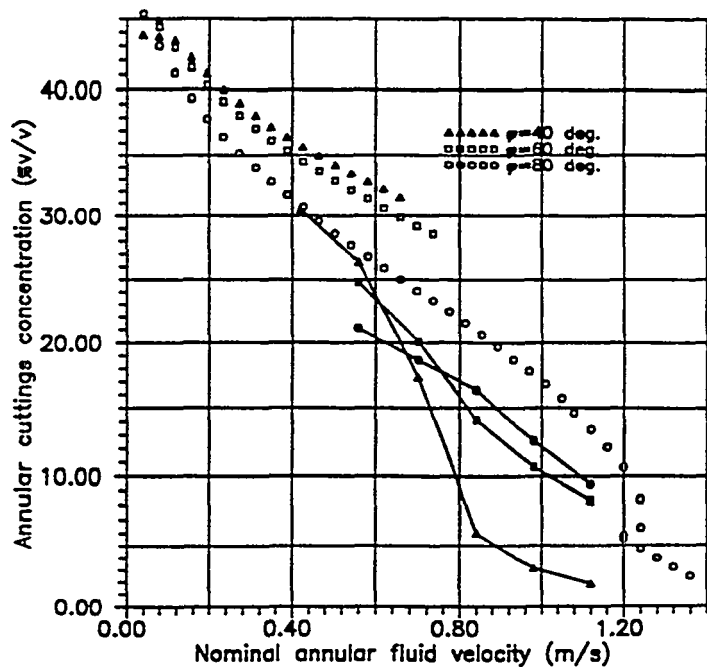


Fig. 5.2.2/1 Annular cuttings concentration vs. nominal fluid velocity for discrete inclinations. Fluid: Carbopol. Flow regime: Viscous. Unconnected data points: Predictions from the SCSB-model. Fully drawn curves: Experimental results by Iyoho et al.

$D=0.127$ m, $d=0.0482$ m, $\rho_c=2620$ kg/m³, $\rho_m=1000$ kg/m³, $d_c=0.00635$ m, $k=0.271$ Pa secⁿ, $n=0.64$, ecc.=+50%, rot.=50 rpm, $\psi_r=36$ deg., $c_b=0.5$, $\eta_s=0.6$, $\eta_d=0.3$, $m_{feed}=0.15$ kg/sec.

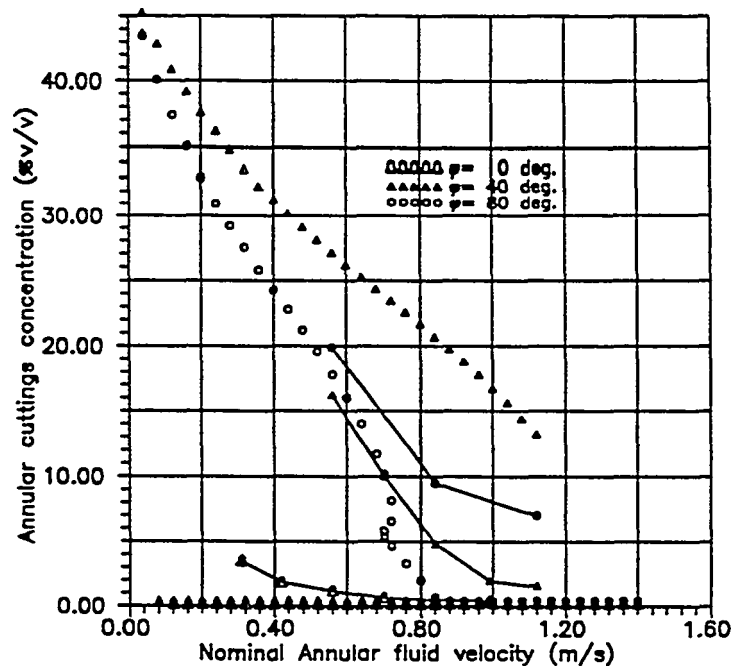


Fig. 5.2.2/2 Annular cuttings concentration vs. nominal fluid velocity for discrete inclinations. Fluid: Bentonite suspension. Flow regime: Viscous. Unconnected data points: Predictions from the SCSB-model. Fully drawn curves: Experimental results by Iyoho et al.

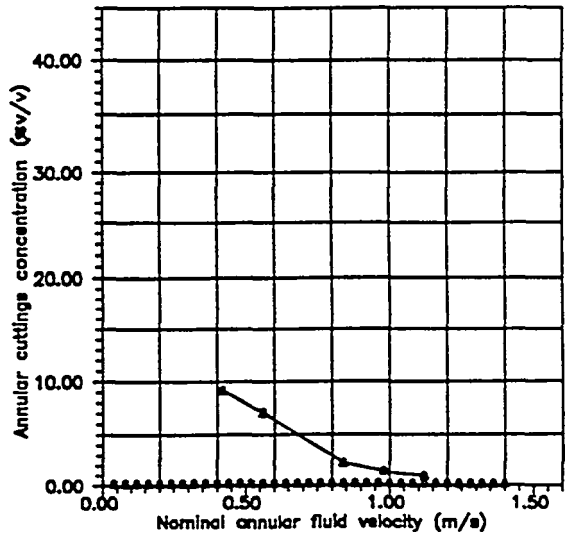
$D=0.127$ m, $d=0.0482$ m, $\rho_c=2620$ kg/m³, $\rho_m=1000$ kg/m³, $d_c=0.00635$ m, $k=0.437$ Pa secⁿ, $n=0.61$, ecc.=+50%, rot.=50 rpm, $\psi_r=36$ deg., $c_b=0.5$, $\eta_s=0.6$, $\eta_d=0.3$, $m_{feed}=0.15$ kg/sec.

Fig. 5.2.2/3

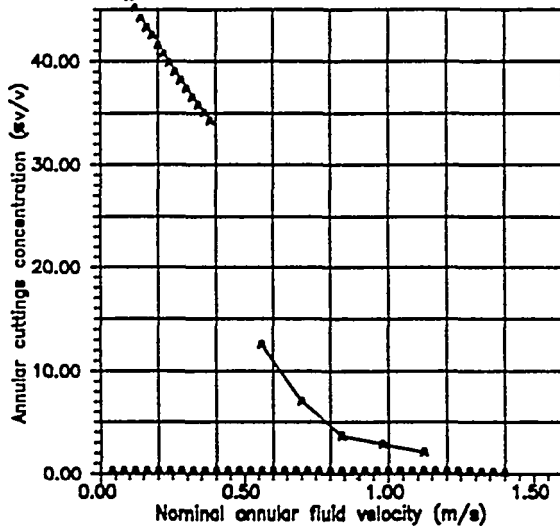
Annular cuttings concentration vs. nominal fluid velocity for discrete inclinations. Fluid: Water. Flow regime: Turbulent. Unconnected data points: Predictions from the SCSB-model. Fully drawn curves: Experimental results by Iyoho²³.

$D=0.127$ m, $d=0.0482$ m, $\rho_c=2620$ kg/m³, $\rho_m=1000$ kg/m³, $d_c=0.00635$ m, $k=0.001$ Pa sec, $n=1.0$, ecc.=+50%, rot.=0-100 rpm, $\psi_r=36$ deg., $c_b=0.5$, $\eta_s=0.6$, $\eta_d=0.3$, $m_{feed}=0.15$ kg/sec.

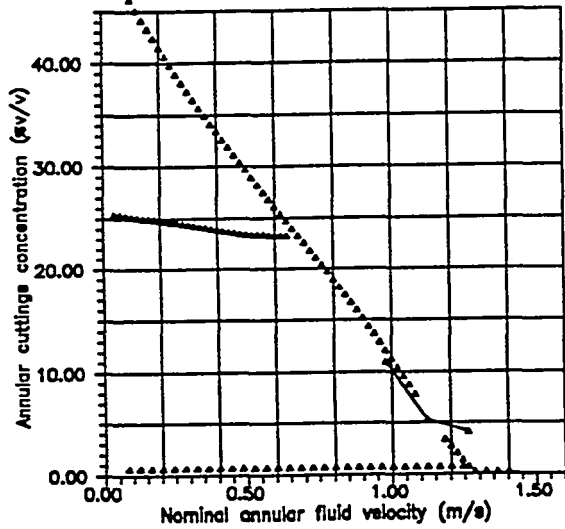
Annular inclination: 10 deg.



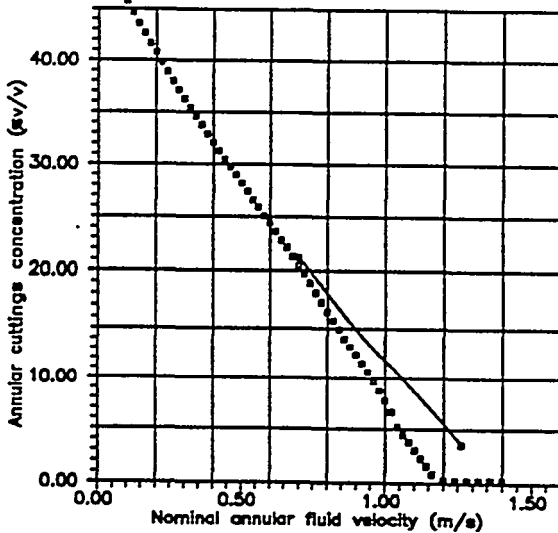
Annular inclination: 30 deg.



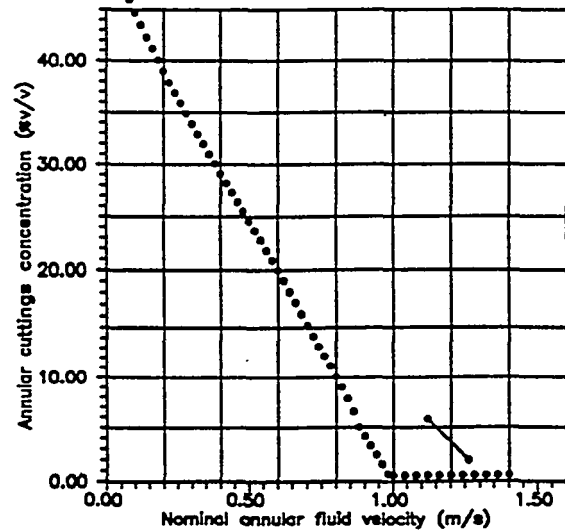
Annular inclination: 50 deg.



Annular inclination: 70 deg.



Annular inclination: 90 deg.



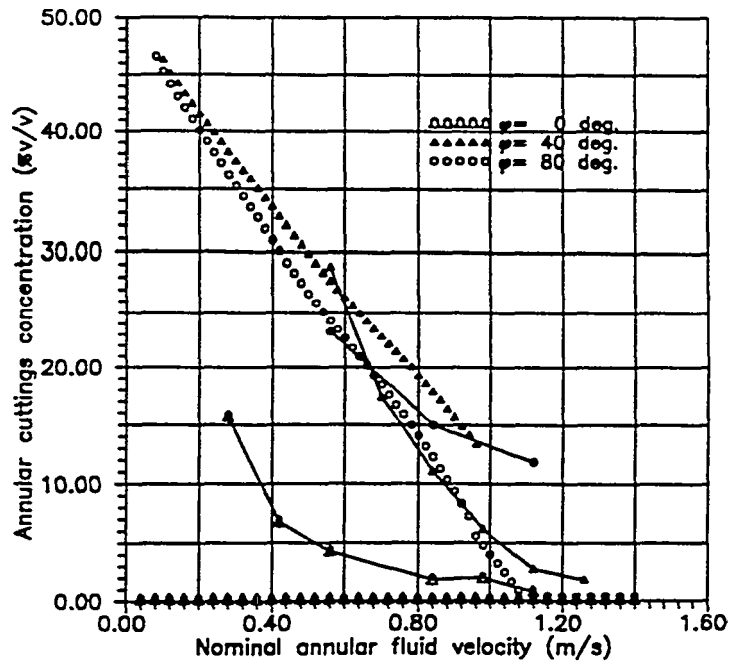


Fig. 5.2.2/4 Annular cuttings concentration vs. nominal fluid velocity for discrete inclinations. Fluid: Water. Flow regime: Turbulent. Unconnected data points: Predictions from the SCSB-model. Fully drawn curves: Experimental results by Iyoho²³.

$D=0.127$ m, $d=0.0482$ m, $\rho_c=2620$ kg/m³, $\rho_n=1000$ kg/m³, $d_c=0.00635$ m, $k=0.001$ Pa sec, $n=1.0$, ecc.=+50%, rot.=50 rpm, $\psi_t=36$ deg., $c_b=0.5$, $\eta_s=0.6$, $\eta_d=0.3$, $m_{feed}=0.15$ kg/sec.

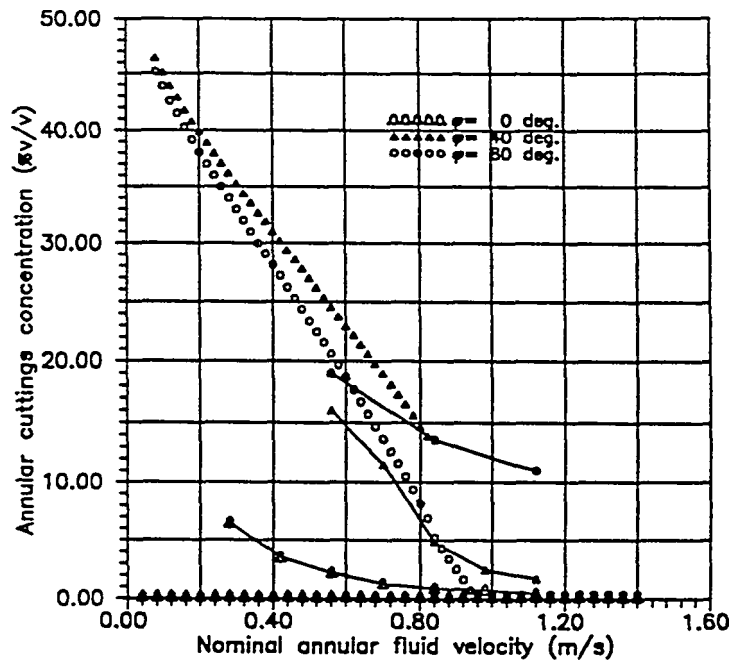


Fig. 5.2.2/5 Annular cuttings concentration vs. nominal fluid velocity for discrete inclinations. Fluid: Bentonite suspension. Flow regime: Turbulent. Unconnected data points: Predictions from the SCSB-model. Fully drawn curves: Experimental results by Iyoho²³.

$D=0.127$ m, $d=0.0482$ m, $\rho_c=2620$ kg/m³, $\rho_n=1000$ kg/m³, $d_c=0.00635$ m, $k=0.039$ Pa sec, $n=0.68$, ecc.=+50%, rot.=50 rpm, $\psi_t=36$ deg., $c_b=0.5$, $\eta_s=0.6$, $\eta_d=0.3$, $m_{feed}=0.15$ kg/sec.

Fig. 5.2.2/6

Annular particle concentration vs. nominal fluid velocity for discrete inclinations. Fluid: Newtonian. Flow regime: Turbulent. Unconnected data points: Predictions from the SCSB-model. Fully drawn curves: Experimental results by Grossmann 17.

$D=0.208$ m, $d=0.127$ m, $\rho_c=2600$ kg/m³, $\rho_a=1000$ kg/m³, $d_c=0.00074$ m, $k=0.008$ Pa sec, $n=1.0$, $ecc.=0\%$, $rot.=0$ rpm, $\psi_r=36$ deg., $c_b=0.5$, $\eta_s=0.6$, $\eta_d=0.3$, $m_{feed}=0.25$ kg/sec.

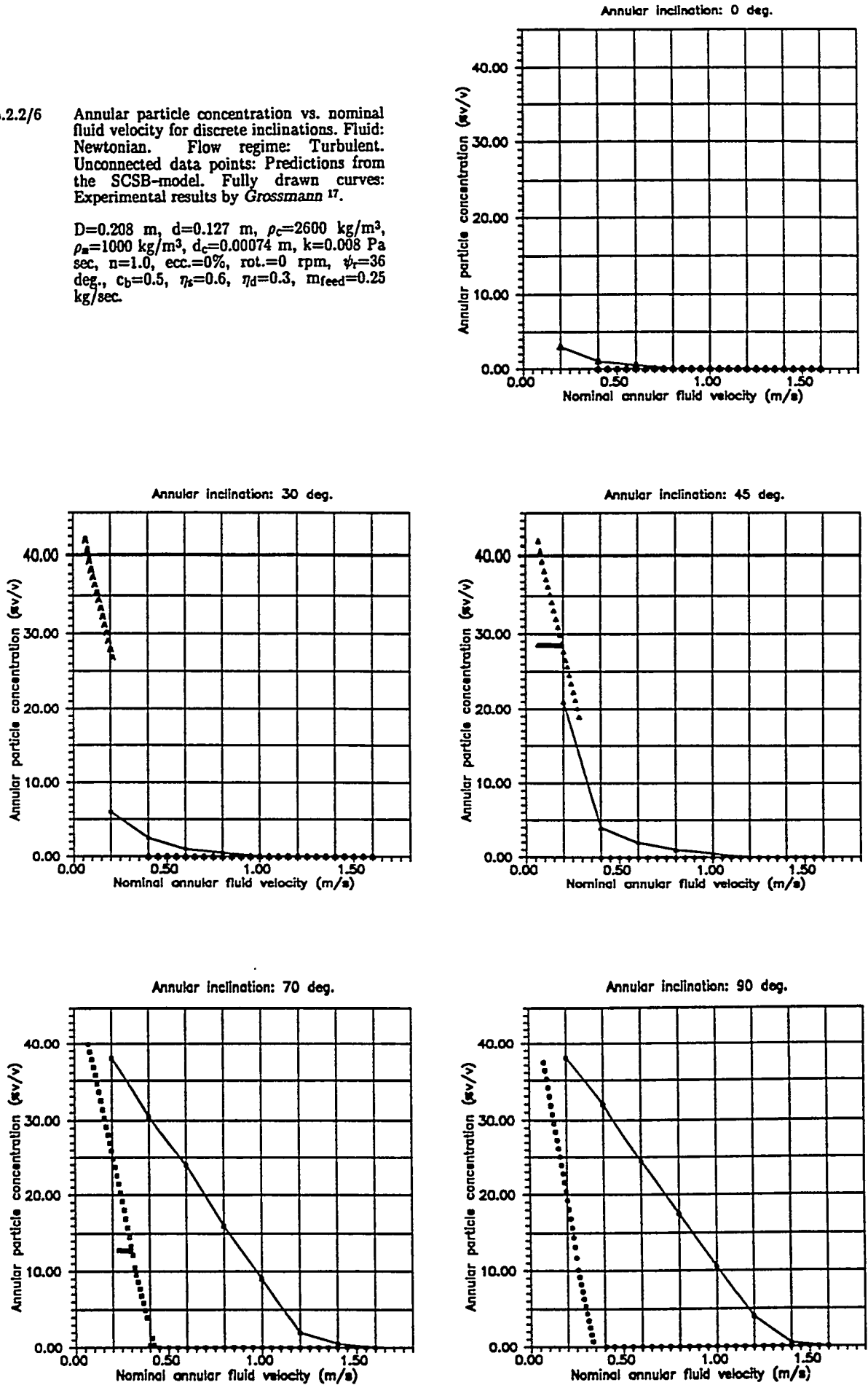


Fig. 5.2.2/7 Annular particle concentration vs. nominal fluid velocity for discrete inclinations. Fluid: Newtonian. Flow regime: Turbulent. Unconnected data points: Predictions from the SCSB-model. Fully drawn curves: Experimental results by Grossmann ¹⁷.

$D=0.208$ m, $d=0.127$ m, $\rho_c=2600$ kg/m³, $\rho_n=1000$ kg/m³, $d_c=0.00074$ m, $k=0.008$ Pa sec, $n=1.0$, $ecc.=+90\%$, $rot.=0$ rpm, $\psi_r=36$ deg., $c_b=0.5$, $\eta_s=0.6$, $\eta_d=0.3$, $m_{feed}=0.25$ kg/sec.

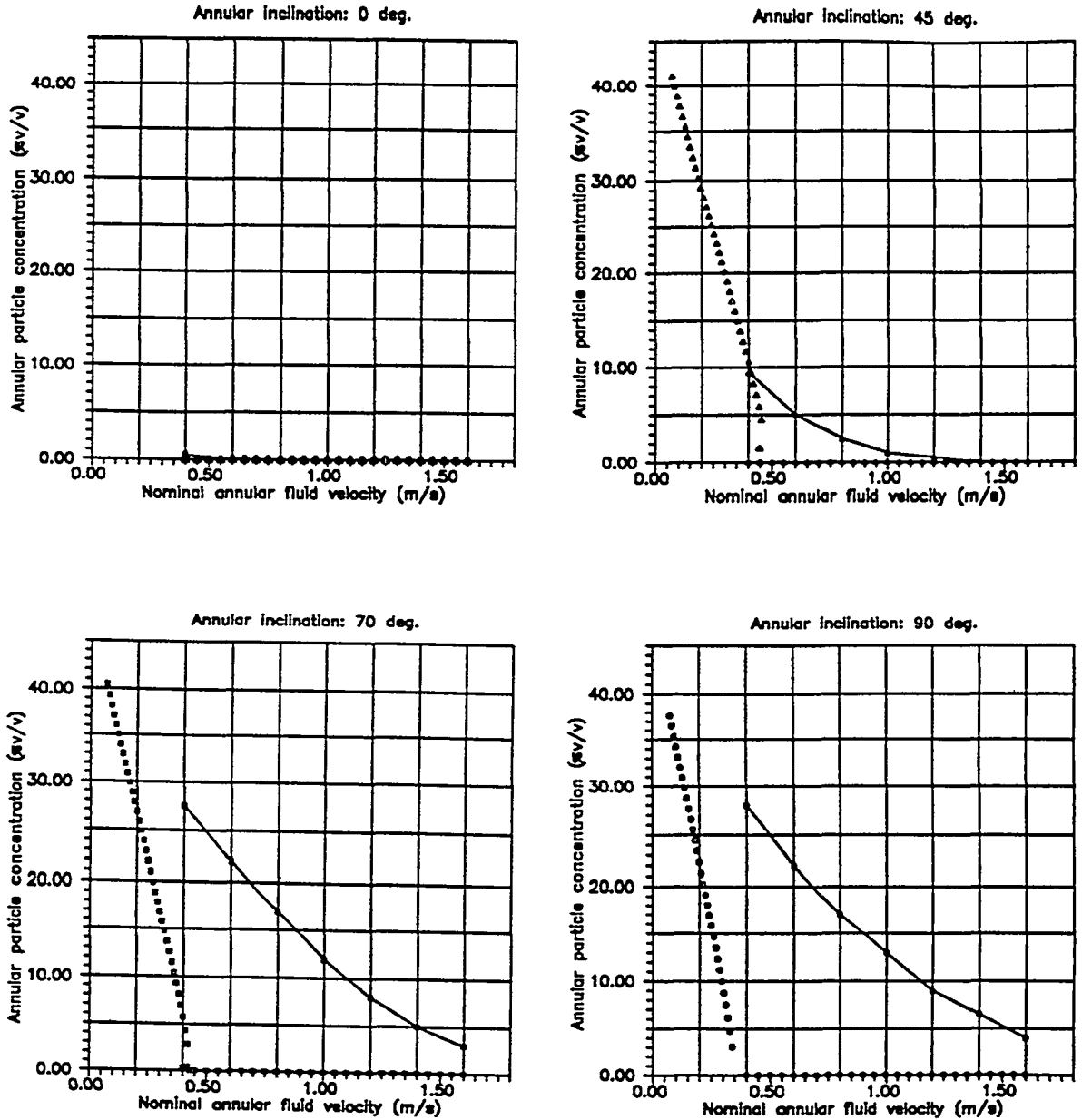


Fig. 5.2.2/8

Annular particle concentration vs. nominal fluid velocity for discrete inclinations. Fluid: Newtonian. Flow regime: Turbulent. Unconnected data points: Predictions from the SCSB-model. Fully drawn curves: Experimental results by Grossmann 17.

$D=0.208$ m, $d=0.127$ m, $\rho_c=2600$ kg/m³, $\rho_s=1000$ kg/m³, $d_p=0.004$ m, $k=0.008$ Pa sec, $n=1.0$, $ecc.=0\%$, $rot.=0$ rpm, $\psi_t=36$ deg., $c_b=0.5$, $\eta_s=0.6$, $\eta_d=0.3$, $m_{feed}=0.25$ kg/sec.

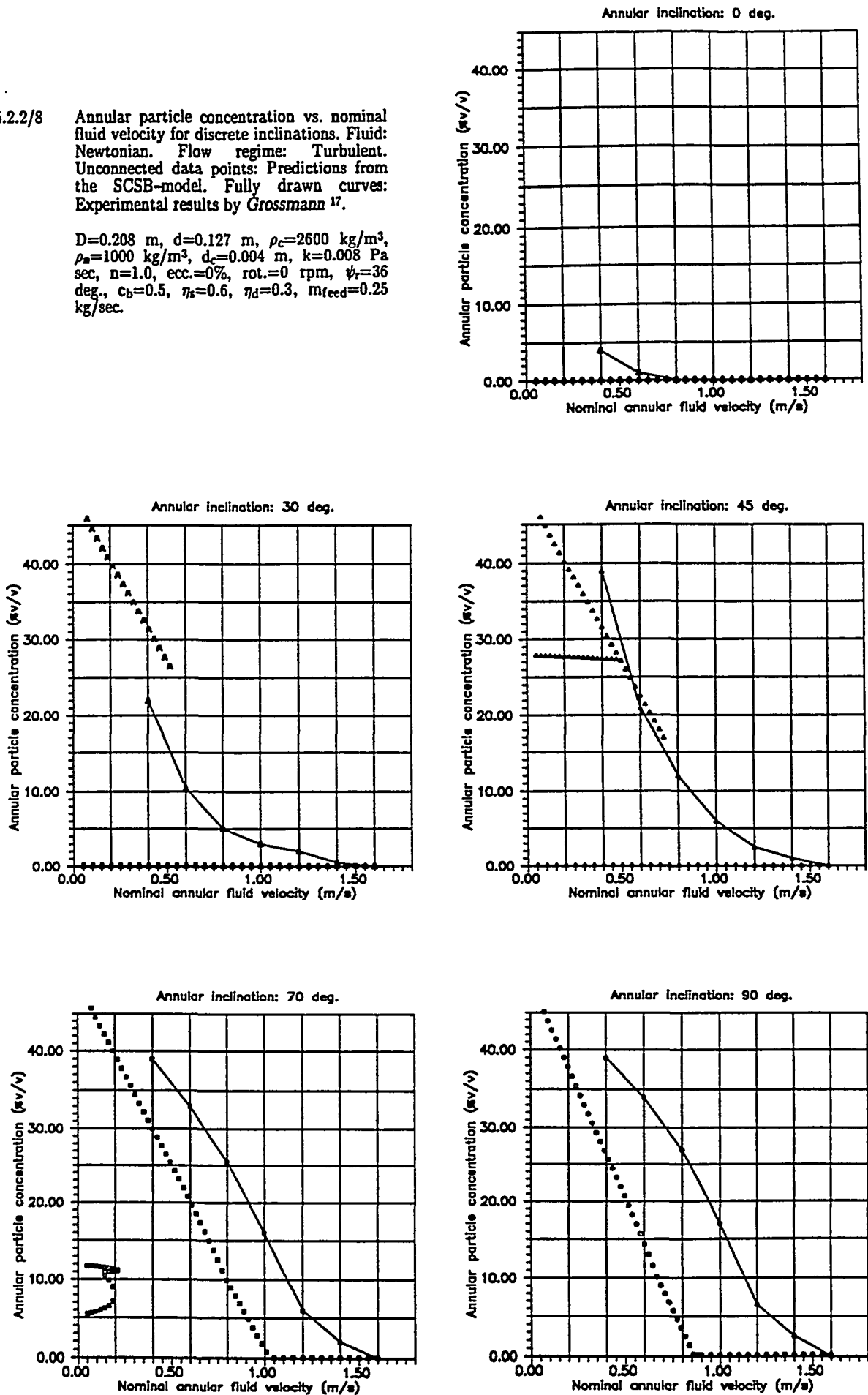
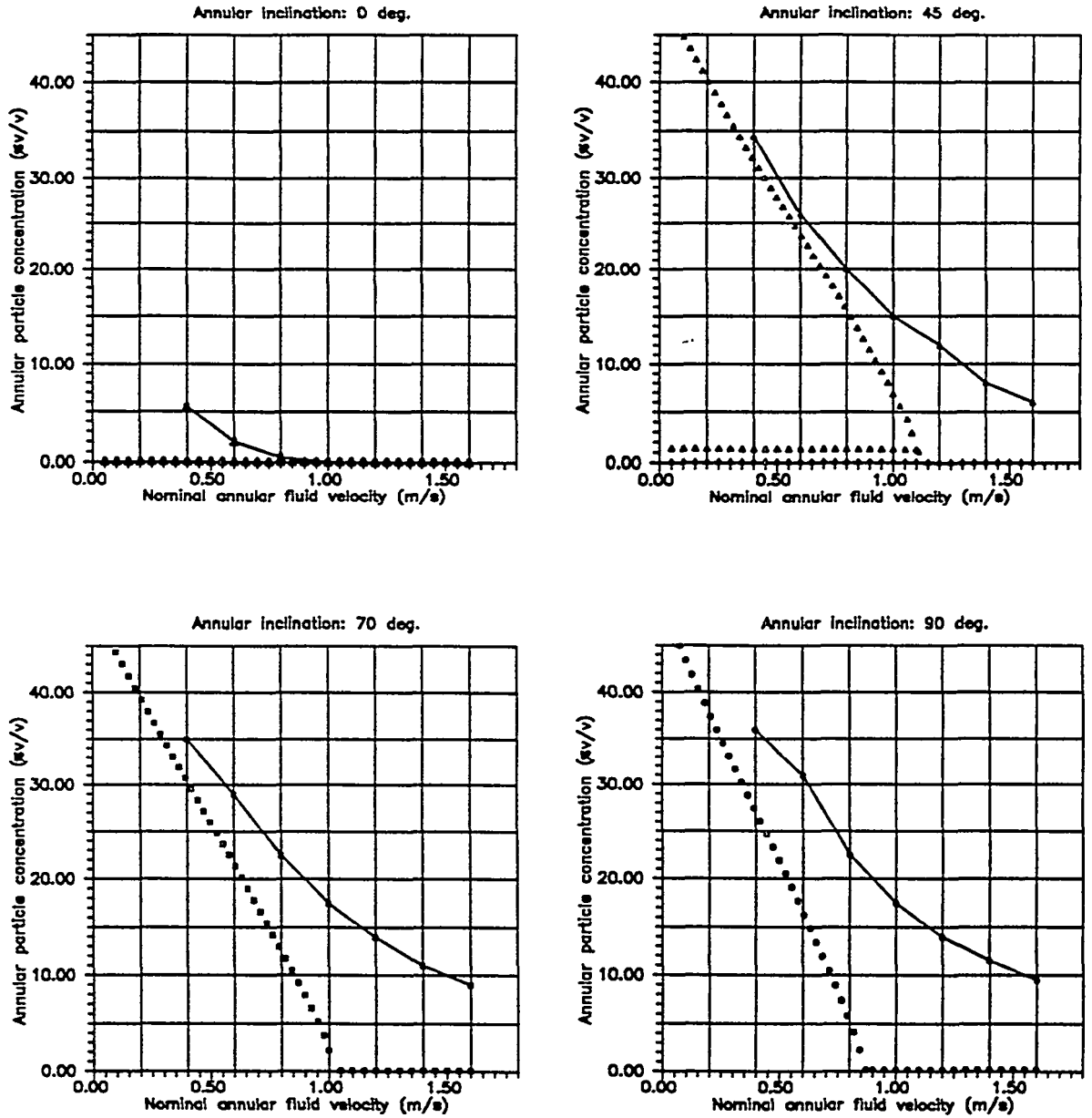


Fig. 5.2.2/9 Annular particle concentration vs. nominal fluid velocity for discrete inclinations. Fluid: Newtonian. Flow regime: Turbulent. Unconnected data points: Predictions from the SCSB-model. Fully drawn curves: Experimental results by Grossmann ¹⁷.

$D=0.208$ m, $d=0.127$ m, $\rho_c=2600$ kg/m³, $\rho_m=1000$ kg/m³, $d_c=0.004$ m, $k=0.008$ Pa sec, $n=1.0$, $ecc.=+90\%$, $rot.=0$ rpm, $\psi_t=36$ deg., $c_b=0.5$, $\eta_s=0.6$, $\eta_d=0.3$, $m_{feed}=0.25$ kg/sec.



5.3 $v(\varphi)$ -plots:

5.3.1 General remarks

Brown et al. ⁷ chose to present their experimental results as plots of the maximum annular fluid velocity allowing a specific annular cuttings concentration vs. annular inclination. The appearance of the general $v(\varphi)$ -plots is similar to the appearance of the general $c(\varphi)$ -plot outlined in fig. 5.1.1/1, except for the fact that the dependent variable is fluid velocity instead of annular cuttings concentration.

5.3.2 Specific remarks

Fig. 5.3.2/1 concerns cuttings behaviour in water in turbulent flow, and is based on experimental parameters and results reported by *Brown et al.* ⁷. The parameters varied are annular inclination and eccentricity. While the qualitative agreement with the SCSB-model is reasonable, the quantitative agreement varies with eccentricity and inclination. It ranges from very well for the eccentric annulus at relatively high annular inclinations to very poor for the concentric annulus in the range of lower inclinations.

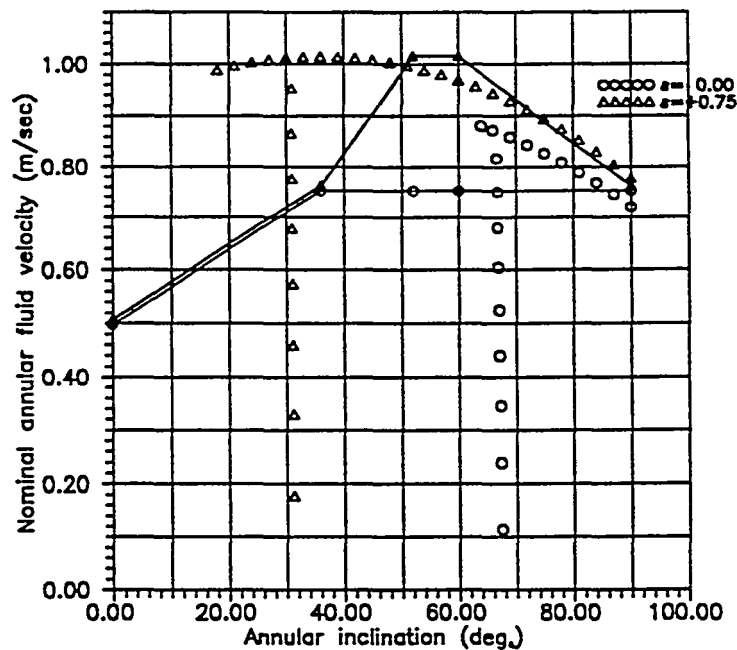


Fig. 5.3.2/1 Maximum nominal annular fluid velocity allowing a 15 %v/v cuttings concentration in an 8"/5" annulus vs. inclination and for discrete eccentricities. Fluid: Water. Flow regime: Turbulent. Unconnected data points: Predictions from the SCSB-model. Fully drawn lines: Experimental results by *Brown et al.* ⁷.

$D=0.208$ m, $d=0.127$ m, $\rho_c=2680$ kg/m³, $\rho_m=1000$ kg/m³, $d_c=0.00635$ m, $k=0.001$ Pa sec, $n=1.0$, $rot.=0$ rpm, $\psi_t=36$ deg., $c_b=0.5$, $\eta_s=0.6$, $\eta_d=0.3$.

Chapter 6

The flow loop.

In order to couple the theoretical work with experimental observations, an annular flow loop has been constructed. The design of the flow loop is sketched in fig. 6.3/1.

6.1 Specifications:

Dimensions (length/outer diameter/inner diameter)	6 m/0.127 m/0.0508 m
Inclinations	0 – 90 deg.
Inner pipe eccentricity	0 – ± 100%
Fluid flowrates	0 – 40 m ³ /hr
Inner pipe rotation	0 – 200 rpm
Particle feed rates	0 – 10.0 kg/min
Fluid reservoir volume	2500 l
Particle hopper volume	1 m ³

Note that the mentioned particle feed rate range has been obtained with 5 – 7 mm particles. It may be different for other particle sizes.

6.2 Equipment:

- Two 11.5 kW centrifugal pumps
- Flow meter
- Pneumatic pinch valve for flowrate control
- Tachometer for measurement of inner pipe rotational speed
- Temperature sensor at the outlet of the annular section
- Load cells for the determination of annular particle content
- Load cells for the determination of particle feed rate
- Heat exchanger for the maintenance of a constant fluid temperature
- Differential pressure transducers
- Computerized data logging
- Video equipment

6.3 A description of the loop.

When the flow loop is in operation, the fluid leaves the reservoir (1) due to the action of the centrifugal pump (5) and passes through the heat exchanger (3), the flow meter (7) and a pneumatic pinch valve (8) before it picks up particles from the hopper (12), fed by the auger (11) down into the fluid stream. After having passed the annular section, the particles are separated from the fluid on a perforated conveyor belt (29). The fluid is returned to the reservoir (1), while the particles are transferred to the temporary reservoir (31).

The fluid reservoir (1) is a 2500 l open cylindrical polyethylene vessel, equipped with a 0.22 kW stirrer (2).

The temperature of viscous fluids tends to increase by the action of the impeller blades in the centrifugal pump (5). In order to maintain a constant temperature, a 5 m² u-tube heat exchanger (3) has been installed. The fluid temperature measured at the exit of the annular section (27) is compared with a setpoint value, and a three band controller decides if the valve (4) is to be open or closed, i.e. whether cooling water is led to the heat exchanger or not. With this simple arrangement, it is possible to keep the temperature of the loop fluid within ± 0.5°C.

The flow loop is equipped with two 11.5 kW centrifugal pumps. However, for reasons which are described in chapter 6.4.2, normal operation of the flow loop only allows the use of one pump at the time. However, both pumps may be used in the process of mixing fluids with more than one component, if the mixture is recirculated to the reservoir (1) through the recirculation shunt (6).

The volumetric flowrate in the flow loop is determined by means of a magnetically inductive flow meter (7). The flowrate is controlled by a pneumatic pinch valve (8). A simple (PID) control algorithm operating in conjunction with the data logging program ensures that the annular flowrate is equal to a given setpoint value.

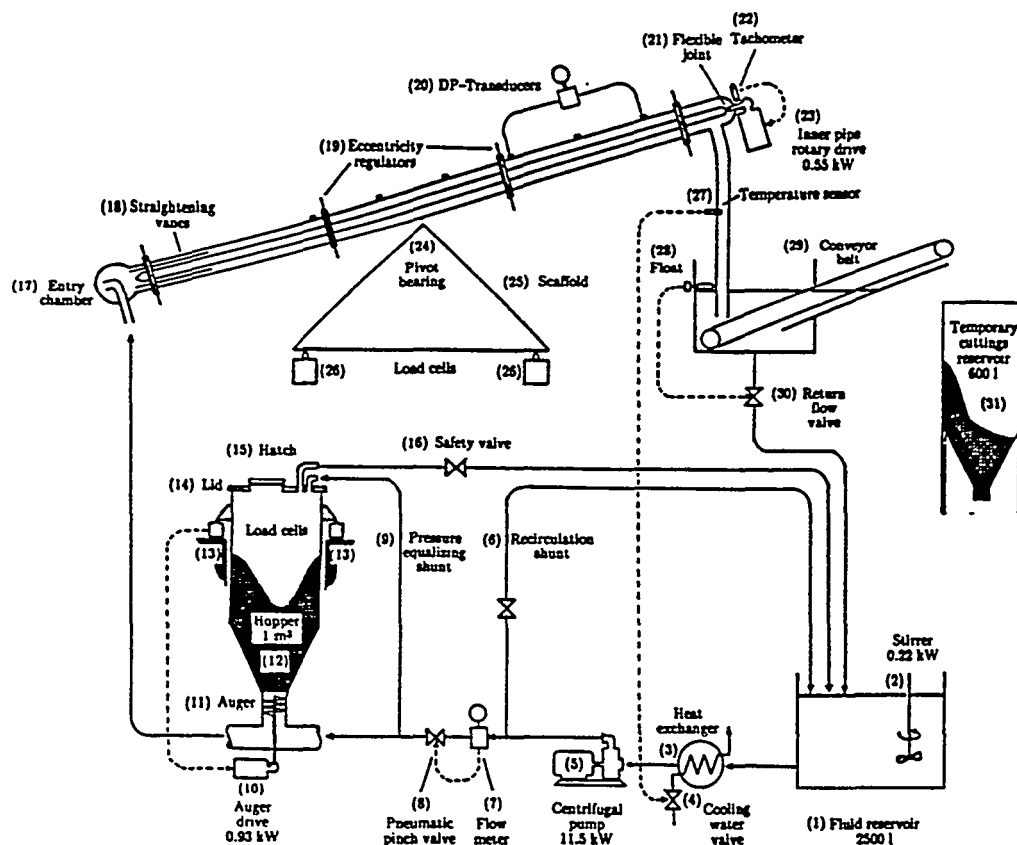


Fig. 6.3/1 Sketch of the flow loop. The fully drawn lines indicate the fluid flow while the dashed lines indicate control signals.

Under the influence of gravity, particles are fed vertically down into the fluid passing below the bottom outlet of the particle hopper (12). The rotational speed of the auger (11), which acts as a physical barrier to the particles leaving the hopper, controls the feed rate. The auger is driven by a 0.93 kW DC electromotor (10). The pressure equalizing shunt (9) prevents a countercurrent fluid flow through the auger, when particles are leaving the hopper.

The hopper is connected to the flow loop by flexible hoses and is suspended in load cells (13). This arrangement permits continuous measurement of the particle mass in the hopper and calculation of the change in the mass per unit time, i.e. the particle feed rate.

A simple control algorithm operating in conjunction with the data logging program adjusts the rotational speed of the auger (11), until the specified particle feed rate is attained. In order to prevent the escape of fluid, the hopper is equipped with a lid (14). Particles are conveyed to the hopper through a hatch (15). After the hatch has been closed, the air remaining in the hopper is expelled by the fluid through a vent in the lid. A safety valve (16) prevents the pressure inside the hopper to exceed some maximum limit.

The length of the annular section is 6 m. The outer pipe is made of Perspex and has an inner diameter of 0.127 m (5"), while the inner pipe is made of stainless steel and has an outer diameter of 0.0508 m (2"). The entire annular section may be rotated around a pivot bearing (24), making it possible to obtain any inclination between 0 and 90 degrees.

The annular section has been placed on a scaffold (25) resting on load cells (26) and connected to the other parts of the flow loop with flexible hoses. Apart from an instantaneous determination of annular particle content, the load cells make it possible to follow transient variations in the mass of particles in the annulus. Also the determination of when steady state conditions have been attained becomes simple.

In order to avoid that the fluid enters the annular section in the form of a long reaching jet, delaying the attainment of fully developed flow, the mixture of fluid and particles are led to the annular section through an entry chamber (17), where the mixture is forced to make a 180° turn. This creates a random whirl at the bottom of the annulus. In order to reduce the influence of this whirl on the attainment of fully developed flow, a couple of parallel straightening vanes (18) have been installed at the base of the annular section.

The inner pipe may be rotated at speeds between 0 and 200 rpm. The rotation is driven by a 0.55 kW DC electromotor (23) and the rotational speed is measured by means of a tachometer (22). A control algorithm operating in conjunction with the data logging program ensures that the inner pipe rotational speed is kept at a given setpoint value.

The outer- as well as the inner pipe is an assembly of three separate sections. At the assembly points, the inner pipe is led through flush mounted ball bearings, allowing it to rotate freely. Thin steel rods (19), inserted through the flanges of the outer pipe sections, are attached to the bearings. The displacement of these rods makes it possible to vary the annular eccentricity between 0 and 100%. A flexible joint (21) connects the inner pipe to the electromotor (23) at all eccentricities.

Along the annular section a number of taps has been fitted into the outer pipe wall. These taps may be connected to differential pressure sensors (20) in an arbitrary fashion, making it possible to determine the pressure drop along any part of the annular section covered. The location of the annular section above the fluid level in the conveyor belt casing produces a slight vacuum in the annular section. The DP-sensors are fitted with valves, making it possible to expell any air that may have been caught between the measuring points and the sensor. However, where a vacuum prevails, the valves may be used in an opposite fashion, i.e. to suck pure water into the tubes connecting the pressure sensors with the annular section. Water acts as an unbroken and unpolluted pressure transmitting media, which is quick responding to variations in the differential pressure. A highly viscous fluid would create a slow response, and a fluid displaying a yield point would form an immobile plug in the tubes. The amount of water being purged into the system is very little and is not considered to affect water based solutions to any significant extent.

After having left the annular section, the particles are separated from the fluid on a perforated conveyor belt (29). The separation takes place below the fluid surface, in order

to minimize the entrainment of air into the fluid. The entrainment of air may affect the rheological characteristics of the fluid, and it is attempted to keep the fluid in an unbroken "string" from the moment it leaves the reservoir (1) and until it returns back. The fluid level in the conveyor belt casing is controlled by a float (28) which acts on a pneumatic butterfly valve (30), that controls the flow from the casing to the fluid reservoir. After the fluid has drained away from the particles on the conveyor belt, the latter are transferred to a temporary reservoir (31).

The fluid flowrate, the weight of the annular section, the weight of the particle hopper, the inner pipe rotational speed, the fluid temperature and the differential pressure sensor indications are continuously logged into a computer and stored for later analysis.

6.3.1 A comment on the use of load cells in the flow loop.

A characteristic feature of the flow loop construction is the application of load cells in connection with the annular section and the particle hopper. In order to minimize the interaction with the surroundings, the annular section and the hopper are both connected to the rest of the construction with flexible hoses. The proper function of this type of arrangement has been tested.

In fig. 6.3.1/1 the indications of the load cells below the annular section are compared with the actual mass of particles present in the annular section for various annular inclinations and flowrates. The two quantities are generally in good agreement, and consequently the load cell arrangement appears to provide a correct indication of the particle content in the annular section.

In table 6.3.1/a the particle feed rate determined on the basis of the load cells, in which the particle hopper has been suspended, is compared with the feed rate calculated from the amount of particles leaving the annular section, under steady state conditions. It is seen that it is possible to obtain a given feed rate within a few percent.

6.4 Limitations

A number of limitations exist in the flow loop design. Some are of a general character and common for all laboratory scale flow loops, while other are specific for the design of the present flow loop.

6.4.1 General limitations

In a laboratory scale flow loop, the determination of annular particle concentration, calculated as the amount of particles present in the annular section divided by the total volume of the annulus, is bound to be encumbered with some error. The generation of fully developed flow cannot take place immediately when the dimensions and geometry of the conduit changes from the turbulence chamber to the annular section. Thus, steady state conditions with fully developed flow only exist in part of the annular section. How large this part is depends on the given operating conditions.

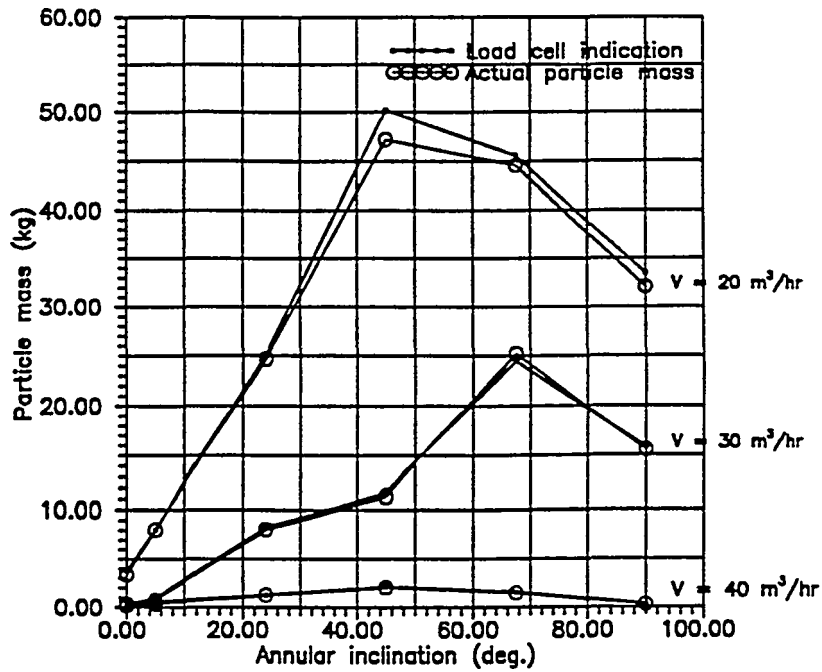


Fig. 6.3.1/1 Comparison of load cell indications with actual annular particle content for various annular inclinations and volumetric flowrates. For three discrete flowrates a deposit was allowed to form in the annular section of the flow loop. The indication of the load cells was recorded and circulation was stopped. The annular content of particles was emptied out through the entry chamber ((17) on fig. 6.3/1), dried and weighed. Note that no attempt was made to establish steady state conditions prior to the stop of circulation.

Setpoint value	Logged value	Measured value	Dev. between logged and measured value
1.00	1.00	1.00	0.0 %
1.50	1.55	1.51	2.6 %
2.00	2.03	1.98	2.5 %
2.50	2.45	2.51	- 2.5 %
3.00	3.09	2.99	3.2 %
3.50	3.49	3.46	0.9 %
4.00	4.11	4.02	2.2 %
4.50	4.53	4.47	1.3 %
5.00	5.07	5.03	0.8 %
5.50	5.38	5.30	1.5 %
6.00	6.01	5.86	2.5 %

Table 6.3.1/a Comparison of the logged and the actually measured particle feed rate from the hopper ((12) in fig. 6.3/1). The rotational speed of the auger ((11) in fig. 6.3/1) was adjusted until the logged feedrate, based on the indication of the load cells ((13) in fig. 6.3/1), was in accordance with the setpoint value. Particles were then collected at the end of the conveyor belt ((29) on fig. 6.3/1). The measured feedrate was calculated by dividing the dry weight of the particles with the collection time. The dimension for the figures in the table is kg/min.

In general, the conditions prevailing in a laboratory flow loop may deviate considerably from the conditions in a real wellbore. For example, the drill pipe rarely takes a fixed position in a wellbore, but moves around (*whipping*). Another example is that deposit sliding may occur under different conditions in a Perspex annulus and in a real wellbore. However, in order to perform systematic investigations, the experimental setup must be idealized.

6.4.2 Specific limitations

The flow loop has a number of specific limitations.

The hopper design has given rise to several problems. The hopper is a pressurized vessel with a large flat lid bolted on top (1 m², 5 mm thick). At a flowrate of approximately 40 m³/hr, the pressure on the inside of the lid is 1 bar above the outside pressure. This corresponds to a total load of approximately 10 tons, and a visible bulging of the lid makes the top packing leaky. A flowrate of 40 m³/hr is attained with just one of the two centrifugal pumps running, and consequently it is not possible to use them both at the same time. Among other things, this limits the ability to perform investigations based on the minimum transport velocity concept.

Another problem is the control of the particle feed rate from the hopper. The rotational speed of the auger is adjusted by a control algorithm that operates in conjunction with the data logging program. However, the analogue to digital conversion of the signal from the load cells, in which the hopper is suspended, puts a restriction on the resolution of the signal. Thus, even if the control algorithm works properly, a relatively long time interval has to pass, before the change in the weight of the hopper content is large enough to be used in the calculation of a correct feed rate. This makes the control of the feed rate a slow process.

Finally, there appears to be a lower limit for the dimension of the particles, if they are to be contained in the hopper. When the dimension is reduced, the particles tend to slip through the auger even if this is not in rotation.

Chapter 7

Conclusions.

A new model for the formation and behaviour of particle deposits in inclined annuli is proposed. The annular space is divided into two layers, separated by a plane boundary. The lower layer corresponds to the particle deposit, while the upper layer corresponds to the mixture of particles and fluid flowing above the deposit. The fluid shear stress at the deposit surface determines if particle deposition takes place or not. A force balance for the lower layer decides if it is stationary or it is sliding upwards or downwards. The model is denoted the SCSB-model.

The SCSB-model predictions are in good qualitative agreement with experimental results obtained by the author, and results published by others in the field. The quantitative agreement is varying with the conditions, presumably because the model is a somewhat simplified description of deposit behaviour in inclined annuli. The major simplifications are that the deposit surface always is plane, and that the flow in the upper layer is analogous to the flow in a pipe, with a diameter corresponding to the hydraulic diameter of the upper layer. The model is therefore not suited to situations, where a well defined deposit does not occur, i.e. at low inclinations with respect to vertical, and situations where the position of the inner pipe creates a very irregular shape of the upper layer cross section. However, even if further refinements of the model appear to be necessary in these situations, a sound physical description of deposit formation has been established.

In order to perform experimental investigations of cuttings transport and behaviour, a large scale flow loop has been constructed. The application of load cells allows the determination of the particle mass present in the annular section under steady state as well as transient conditions. Also the establishment and maintenance of a well defined particle feed rate to the annular section have been achieved by the use of load cells.

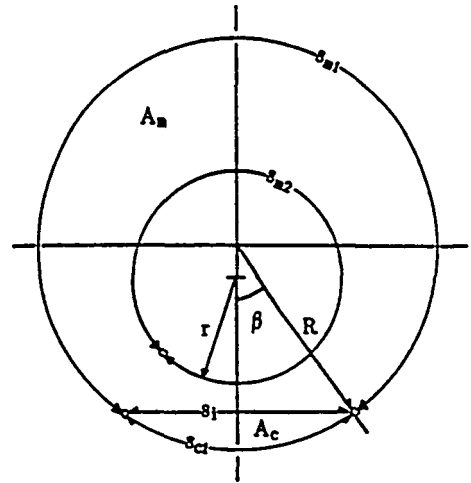
Appendix 1

**Geometrical relations
in the SCSB-model.**

This appendix contains the geometrical relations used in the SCSB-model. The geometrical quantities are all given in terms of the angle β , which is used as a measure for the position of the deposit surface.

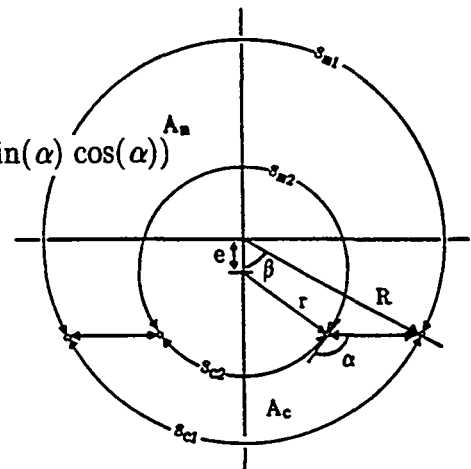
1) Inner pipe without contact to the deposit:

$$\begin{aligned} A_c &= R^2 (\beta - \sin(\beta) \cos(\beta)) \\ A_m &= A - A_c \\ s_{m1} &= 2 (\pi - \beta) R \\ s_{m2} &= 2 \pi r \\ s_{c1} &= 2 \beta R \\ s_{c2} &= 0 \\ s_i &= 2 R \sin(\beta) \end{aligned}$$



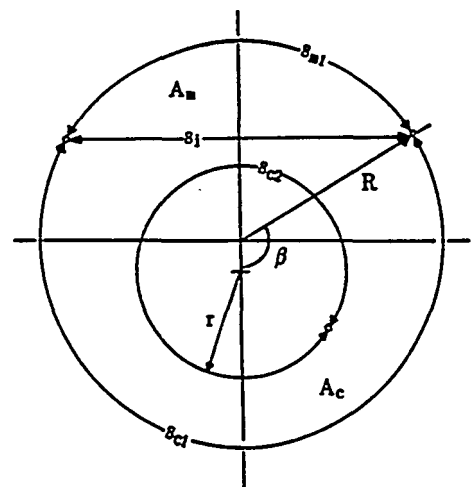
2) Inner pipe partly submerged in the deposit:

$$\begin{aligned} \alpha &= \arccos \left[\frac{e - R \cos(\beta)}{r} \right] \\ A_m &= R^2 ((\pi - \beta) + \sin(\beta) \cos(\beta)) - r^2 (\alpha - \sin(\alpha) \cos(\alpha)) \\ A_c &= A - A_m \\ s_{m1} &= 2 (\pi - \beta) R \\ s_{m2} &= 2 \alpha r \\ s_{c1} &= 2 \beta R \\ s_{c2} &= 2 (\pi - \alpha) r \\ s_i &= 2 (R \sin(\beta) - r \sin(\alpha)) \end{aligned}$$



3) Inner pipe totally submerged in the deposit:

$$\begin{aligned} A_m &= R^2 ((\pi - \beta) + \sin(\beta) \cos(\beta)) \\ A_c &= A - A_m \\ s_{m1} &= 2 (\pi - \beta) R \\ s_{m2} &= 0 \\ s_{c1} &= 2 \beta R \\ s_{c2} &= 2 \pi r \\ s_i &= 2 R \sin(\beta) \end{aligned}$$



Appendix 2

**Friction between the
deposit and the
annular walls.**

This appendix contains relations that quantifies the friction between the deposit and the annular walls. It is presumed that the grains are cohesionless and that there is no adhesion between the granular material and the annular walls.

The frictional stress, τ_c , between a stationary deposit and the annular walls is described by Coulombs law of friction:

$$\tau_c = \eta \tau_{n \text{ av}} \quad (\text{A2-1})$$

i.e. a linear relationship is presumed to exist between the frictional stress and the average normal stress, $\tau_{n \text{ av}}$, exerted by the deposit on the annular walls.

At the point of deposit sliding, relation (A2-1) defines the coefficient of static friction, η_s . If τ_c exceeds $\eta_s \tau_{n \text{ av}}$, the deposit slides, and the frictional stress is given by

$$\tau_c = \eta_d \tau_{n \text{ av}} \quad (\text{A2-2})$$

defining the coefficient of kinetic friction, η_d . The coefficient of static friction is larger than the coefficient of kinetic friction. It should be noted that Coulombs law indicates that the friction between a sliding deposit and the annular walls is independent of the sliding velocity.

The expressions quantifying the frictional forces between the deposit and the annular boundaries in the SCSB-model, are composed by two separate contributions:

- the friction between the deposit and the outer pipe wall, τ_{c1} .
- the friction between the deposit and the inner pipe wall, τ_{c2} .

The derivation of the expressions are performed in the rest of Appendix 2. Note that the expressions do not say anything about the direction of the frictional stresses.

I) The friction between a deposit and the outer pipe wall.

If the normal stress exerted by a deposit on a surface is presumed to be distributed in the same fashion as below a fluid continuum (Wilson⁴⁶), the normal stress on the outer pipe wall may be expressed as a function of the angle θ (see fig. A2/1):

$$\tau_n^0(\theta) = (\rho_c - \rho_m) (1 - \epsilon) g \sin(\varphi) R (\cos(\theta) - \cos(\beta)) \quad (\text{A2-3})$$

An average normal stress for the whole deposit is defined as:

$$\tau_n^0 \text{ av} = (\rho_c - \rho_m) (1 - \epsilon) g \sin(\varphi) \frac{2}{s_{c1}} \int_0^\beta R (\cos(\theta) - \cos(\beta)) R d\theta \quad (\text{A2-4})$$

and the frictional stress between the deposit and the outer pipe wall becomes:

$$\tau_{c1} = \eta \tau_n^0 \text{ av} = \eta (\rho_c - \rho_m) (1 - \epsilon) g \sin(\varphi) \frac{2}{s_{c1}} R^2 (\sin(\beta) - \beta \cos(\beta)) \quad (\text{A2-5})$$

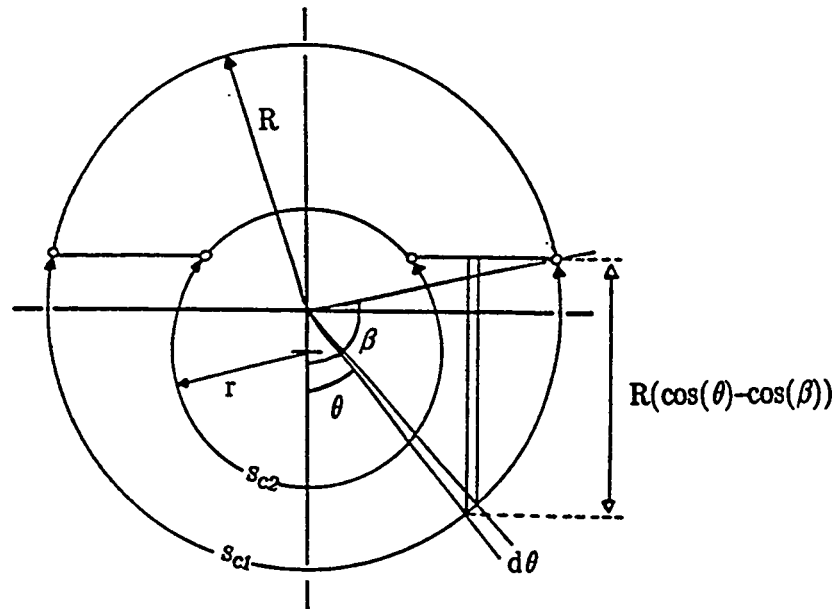


Fig. A2/1

II) The friction between a deposit and the inner pipe wall.

Again, the normal stress exerted by the deposit on the inner pipe is presumed to be distributed in the same way as below a fluid continuum. Three different situations are treated: 1) the drill string is without contact to the deposit, 2) the drill string is partly submerged in the deposit and 3) the drill string is totally submerged in the deposit.

ad. 1) There is no friction between the deposit and the inner pipe, i.e. $\tau_{c2} = 0$.

ad. 2) The normal stress on the inner pipe wall may be expressed as a function of the angle σ (see fig. A2/2):

$$\tau_n^i(\sigma) = (\rho_c - \rho_m) (1 - \epsilon) g \sin(\varphi) r (\cos(\sigma) - \cos(\pi - \alpha)) \quad (\text{A2-6})$$

An average normal stress for the deposit is defined as:

$$\tau_n^i \text{ av} = (\rho_c - \rho_m) (1 - \epsilon) g \sin(\varphi) \frac{2}{s_{c2}} \int_0^{\pi - \alpha} r (\cos(\sigma) - \cos(\pi - \alpha)) r d\sigma \quad (\text{A2-7})$$

and the frictional stress between the deposit and the inner pipe wall becomes:

$$\tau_{c2} = \eta \tau_n^i \text{ av} = \eta (\rho_c - \rho_m) (1 - \epsilon) g \sin(\varphi) \frac{2}{s_{c2}} r^2 (\sin(\pi - \alpha) - (\pi - \alpha) \cos(\pi - \alpha)) \quad (\text{A2-8})$$

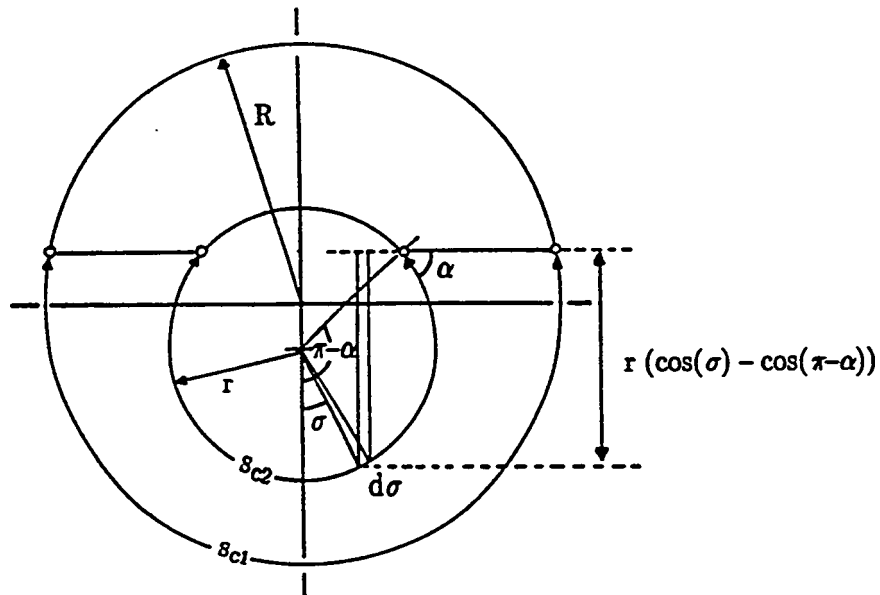


Fig. A2/2

ad.3) The normal stress on the inner pipe wall may be expressed as a function of the angle σ (see fig. A2/3):

$$\tau_n^i(\sigma) = (\rho_c - \rho_m) (1 - \epsilon) g \sin(\varphi) (e - R \cos(\beta) + r \cos(\sigma)) \quad (\text{A2-9})$$

An average normal stress for the deposit is defined as:

$$\tau_{n \text{ av}}^i = (\rho_c - \rho_m) (1 - \epsilon) g \sin(\varphi) \frac{2}{s_{c2}} \int_0^\pi (e - R \cos(\beta) + r \cos(\sigma)) r d\sigma \quad (\text{A2-10})$$

and the frictional stress between the deposit and the inner pipe wall becomes:

$$\tau_{c2} = \eta \tau_{n \text{ av}}^i = \eta (\rho_c - \rho_m) (1 - \epsilon) g \sin(\varphi) (e - R \cos(\beta)) \quad (\text{A2-11})$$

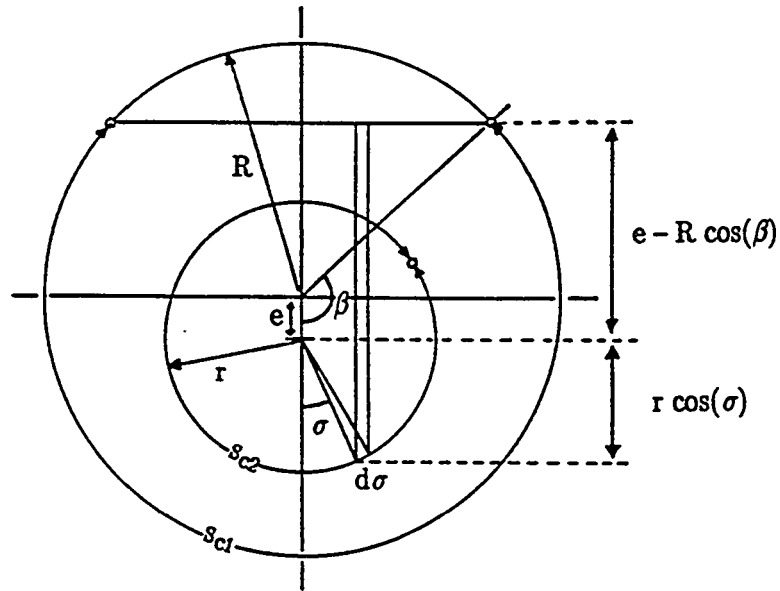


Fig. A2/3

Appendix 3

**The Shields concept
for inclined deposits.**

This appendix concerns a criterion for the incipient motion of a particle resting on an inclined deposit surface. The resulting expression is an adaptation of a criterion, derived by *Shields*³⁷, for the incipient motion of a particle resting on a plane horizontal deposit surface. In order to make the deposit inclination equivalent to the annular inclination in the SCSB-model, the former is measured relative to vertical. However, due to convention, the angle of repose, ψ_r , is still given relative to horizontal.

The inclined surface on which the particle is resting is taken to be plane and the particle is presumed to be influenced by gravity, buoyancy, fluid drag and friction. Fluid dynamic forces in other directions than the one parallel to the deposit surface are ignored. At the point of incipient motion, the axial components of the forces acting on the particle are:

Net gravity:

$$F_{gax} = (\rho_p - \rho) g \pi \frac{1}{6} d_p^3 \cos(\varphi) \quad (A3-1)$$

Fluid drag:

$$F_{fd} = C_d (\xi \pi d_p^2) \frac{1}{2} \rho u_0^2 \quad (A3-2)$$

Friction between the particle and the deposit surface:

$$F_f = \eta_p (\rho_p - \rho) g \pi \frac{1}{6} d_p^3 \sin(\varphi) \quad (A3-3)$$

ρ_p is the particle density, ρ the fluid density, g the gravitational acceleration, d_p the particle diameter and φ the deposit inclination. In eq. (A3-2) u_0 is some unknown fluid velocity characteristic for the interaction between the fluid and the particle. C_d is the drag coefficient at the particle Reynolds number corresponding to the velocity u_0 . ξ is a factor determining a characteristic surface area in the interaction between the particle and the fluid. In eq. (A3-3) η_p is the coefficient of friction for the interaction between the particle and the deposit surface.

At the point of incipient particle motion, the following force balance is posed:

$$F_{gax} \pm F_f = F_{fd}$$

The sign in front of the second term may either be positive or negative, depending on whether the particle is on the verge of being pulled along by the fluid or it is barely kept from sliding downwards the sloping surface.

If the expressions (A3-1), (A3-2) and (A3-3) are inserted it follows that:

$$\left[(\rho_p - \rho) g \pi \frac{1}{6} d_p^3 \cos(\varphi) \right] \pm \left[\eta_p (\rho_p - \rho) g \pi \frac{1}{6} d_p^3 \sin(\varphi) \right] = \left[C_d (\xi \pi d_p^2) \frac{1}{2} \rho u_0^2 \right]$$

or:

$$(\rho_p - \rho) g d_p \left[\cos(\varphi) \pm \eta_p \sin(\varphi) \right] = C_d \xi \frac{1}{2} \rho u_0^2 \quad (A3-4)$$

The characteristic fluid velocity, u_o , and the drag coefficient, C_d , may be given as functions of a Reynolds number Re_o^* based on the friction velocity u_o^* :

$$Re_o^* = \frac{\rho u_o^* d_p}{\mu} \quad ; \quad u_o^* = \sqrt{\frac{\tau_o}{\rho}}$$

where μ is the fluid viscosity and τ_o the fluid shear stress at the deposit surface at the point of incipient motion.

Now, it may be shown (see for example *Garde & Ranga Raju* ¹⁴ p.55) that

$$C_d u_o^2 = (u_o^*)^2 F(Re_o^*) \quad (A3-5)$$

where $F(Re_o^*)$ is some unspecified function.

If eq. (A3-5) is inserted in eq. (A3-4), it follows that:

$$\frac{\tau_o}{(\rho_p - \rho) g d_p} = \left[\frac{1}{\eta_p} \cos(\varphi) \pm \sin(\varphi) \right] \left[\frac{2 \eta_p}{\xi F(Re_o^*)} \right] \quad (A3-6)$$

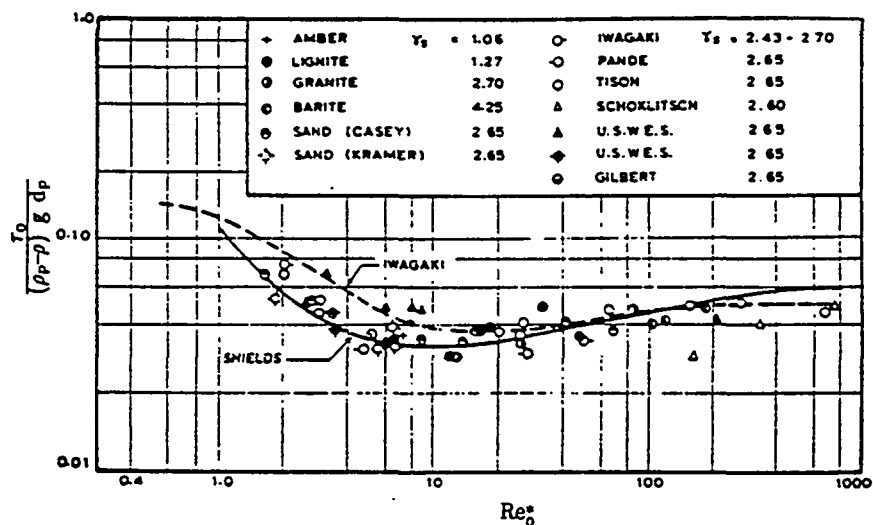


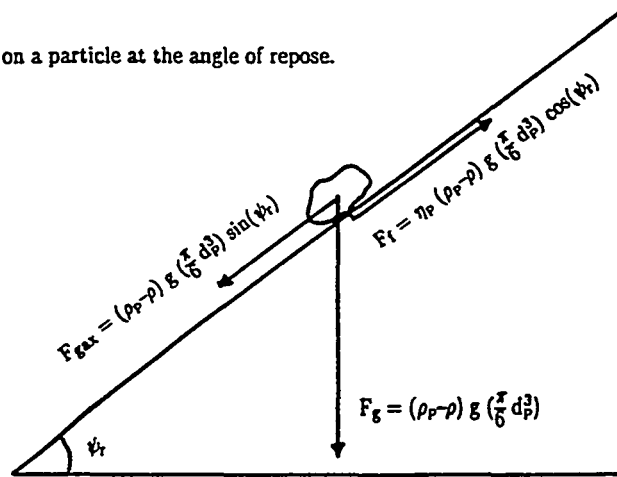
Fig. A3/1 A Shields plot (from *Garde & Ranga Raju* ¹⁴ p. 56).

While the last quantity in brackets on the R.H.S of eq. (A3-6) is identical to the R.H.S. of eq. (3.18) in *Garde & Ranga Raju* ¹⁴ and similar to the function f_a in eq. 5 in *Shields* ³⁷, the first quantity in brackets is new and represents a modification of the original Shields criterion derived for a horizontal deposit.

From experiments with horizontal deposits *Shields*³⁷ found that the quantity between the last brackets of eq. (A3-6) depended on Re^*_o as shown in fig. A3/1 (taken from *Garde & Ranga Raju*¹⁴). The shape of the curve reflects a transition from hydraulically smooth to completely rough flow, similar to the transition observed in rough pipe flow (see fig. 4.2.4/1). It is seen that the value of the quantity varies between 0.03 and 0.06. However, due to the relative modest variation, the largely constant value attained for completely rough flow is used throughout this work. The Shields criterion for the incipient motion of a particle resting on an inclined surface then becomes:

$$\frac{\tau_o}{(\rho_p - \rho) g d_p} = \left[\frac{1}{\eta_p} \cos(\varphi) \pm \sin(\varphi) \right] 0.06 \quad (A3-7)$$

Fig. A3/2 Forces acting on a particle at the angle of repose.



When the inclination of a rough deposit surface with respect to horizontal becomes larger than the angle of repose, ψ_r , a particle is unable to remain at rest. The angle of repose for granular materials typically lies between 30 and 40 degrees (see for example *Brown & Richards*⁸ p.29). The angle of repose may be used to calculate the frictional coefficient for the interaction between a particle and the deposit surface (see fig. A3/2). A force balance for a particle at the angle of repose is given by:

$$(\rho_p - \rho) g \frac{\pi}{6} d_p^3 \sin(\psi_r) = \eta_p (\rho_p - \rho) g \frac{\pi}{6} d_p^3 \cos(\psi_r)$$

i.e.

$$\eta_p = \tan(\psi_r) \quad (A3-8)$$

If this expression for η_p is inserted in equation (A3-7) the criterion for incipient motion of a particle on an inclined deposit surface becomes:

$$\frac{\tau_o}{(\rho_p - \rho) g d_p} = \left[\frac{\cos(\varphi)}{\tan(\psi_r)} \pm \sin(\varphi) \right] 0.06 \quad (A3-9)$$

Recall that ψ_r is given relative to horizontal, while φ is measured relative to vertical. The term in brackets on the right hand side of equation (A3-9) describes how much the surface shear stress at the point of incipient particle motion changes with the inclination of the deposit.

In fig. A3/3 the value of the right hand side of equation (A3-9) is plotted as function of inclination φ . Values located on the upper curve (I) correspond to a situation where the particle is on the verge of being pulled along by the fluid. Points located on the lower curve (II) correspond to a situation where the fluid drag is just able to keep the particle from sliding down the sloping surface under the influence of the net axial gravity. In the region between the two curves particles may remain at rest on the deposit surface, i.e. deposition takes place.

It is noted that the right hand side of eq. (A3-9) may take positive as well as negative values. At surface inclinations larger than $(90^\circ - \psi_r)$, the particle cannot slide down the sloping surface, even if there should be no fluid drag in the upwards direction. At these inclinations a negative shear stress (i.e. fluid flow in the downhill direction) is required, in order to make the particle move in the downhill direction.

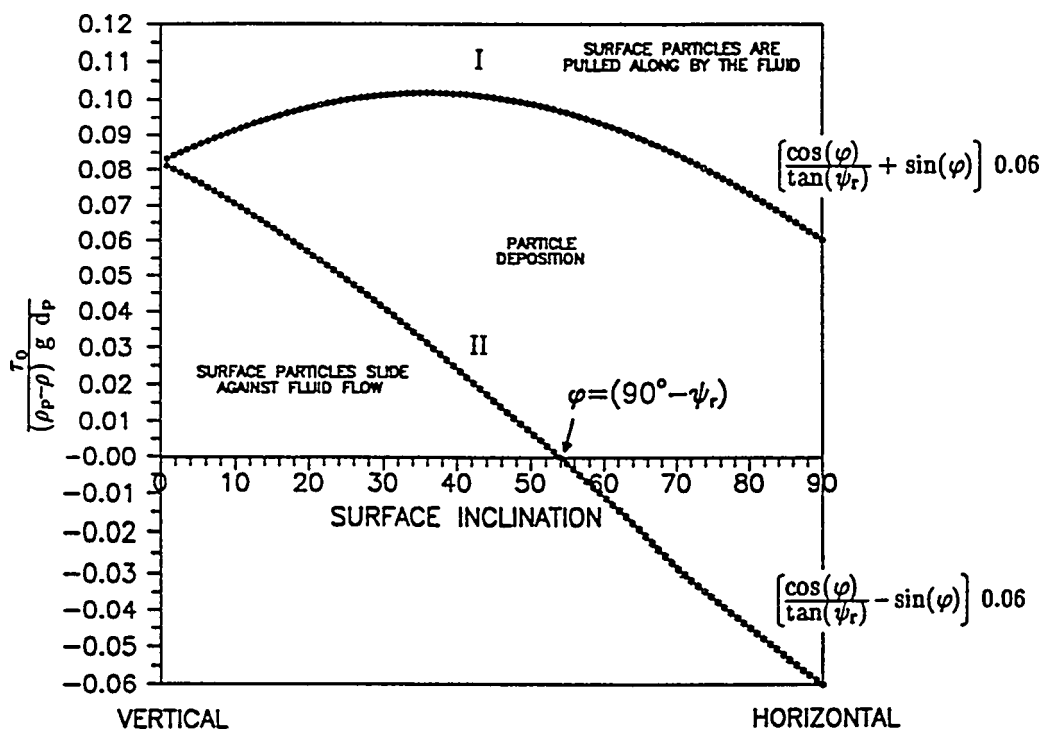


Fig. A3/3 The value of the non-dimensional Shields ratio plotted against surface inclination.

Appendix 4

**The Artyushkov et al.
theory for the flow of
non-Newtonian fluids in
smooth and rough pipes.**

This appendix contains a semiempirical model for the turbulent flow of Power Law fluids through smooth and rough pipes, originally presented by *Artyushkov et al.*^{1 2}.

The pipe flow is considered axisymmetrical, and a coordinate system with origin at the pipe wall is introduced (see fig. A4/1).

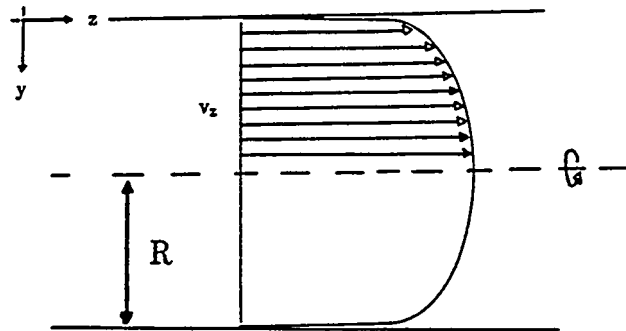


Fig. A4/1 The geometry in the *Artyushkov et al.* theory.

In turbulent flow, the fluid shear stress at a given position in the fluid is considered to consist of a laminar and a turbulent contribution, i.e.:

$$\tau = \tau_{\text{lam}} + \tau_{\text{turb}} \quad (\text{A4-1})$$

For an incompressible fluid flowing in the z -direction, the laminar contribution is given by the well known Power Law expression:

$$\tau_{\text{lam}} = k \left| \frac{dv_z}{dy} \right|^n \quad (\text{A4-2})$$

Due to the axisymmetry, it is necessary to consider only half the cross section outlined in fig. A4/1. With the chosen coordinate system, the velocity gradient will always be positive and it is not necessary to operate with the numerical value sign.

The turbulent contribution is described by an expression suggested by *Prandtl*⁶:

$$\tau_{\text{turb}} = \rho l^2 \left[\frac{dv_z}{dy} \right]^2 \quad (\text{A4-3})$$

where ρ is the fluid density and l the so called *mixing length*. The mixing length depends

on the distance from the pipe wall, the roughness of the wall and the rheology of the fluid. The relationship between the mixing length and radial position, y , is given by:

$$l = \varphi_a \kappa_0 Q(\eta_a, n, h^*) y \quad (\text{A4-4})$$

where

$$\varphi_a = \left[\frac{n+1}{2n} \right]^{\frac{1}{2}}$$

κ_0 is the *von Karman constant* (equal to 0.4) and Q a non-dimensional "damping" factor. Q depends on the non-dimensional radial coordinate $\eta_a = y u^*/\nu$, the Power Law flow behaviour index, n , and a non-dimensional roughness parameter, $h^* = h u^*/\nu$, where ν is the kinematic viscosity and u^* the friction velocity of the fluid.

In hydraulically smooth turbulent pipe flow, a cross section of the pipe may be divided into three regions, described in terms of the non-dimensional distance from the pipe wall:

- 1) A thin layer close to the wall, $0 \leq \eta_a < \eta_v$, denoted the viscous sublayer, where the laminar contribution, τ_{lam} , to the overall shear stress, τ , dominates over the turbulent contribution, τ_{turb} .
- 2) A transition layer, $\eta_v \leq \eta_a < \eta_t$, where the laminar- and turbulent contributions are both of significance.
- 3) A (large) central core area, $\eta_a \geq \eta_t$, with fully developed turbulence, where the turbulent contribution, τ_{turb} , to the overall shear stress, τ , dominates over the laminar contribution, τ_{lam} .

When the height of the roughness protrusions is less than the thickness of the viscous sublayer i.e. $0 \leq h^* < \eta_v$, the flow remains hydraulically smooth. However, when the roughness protrusions enter the transition layer, i.e. $\eta_v \leq h^* < \eta_t$, the viscous sublayer is disturbed by vortex formation. *Rotta*³³ pointed out that the thickness of the viscous sublayer gradually decreases when the size of the protrusions are increased, and that it disappears completely when the protrusions enter the fully turbulent core area, i.e. when $h^* \geq \eta_t$. The flow is then said to be completely rough.

For hydraulically smooth flow, *van Driest*⁴¹ suggested the following expression for the damping factor Q in equation (A4-4):

$$0 \leq h^* < \eta_v \quad Q = \left[1 - \exp \left[-\frac{\eta_a}{A(n)} \right] \right] \quad (\text{A4-5})$$

$A(n)$ is an empirical function of the Power Law flow behavior index, determined on the basis of experimental data. For Newtonian fluids, i.e. $n = 1.0$, $A(n) = 27$. As would be expected in hydraulically smooth flow, the expression is independent of wall roughness.

In the transitional regime, *Artyushkov et al.* suggested the expression:

$$\eta_v \leq h^* < \eta_t \quad Q = \left[1 - \exp \left[-\frac{\eta_a}{A(n) \log_{10} \left[\frac{\eta_t}{h^*} \right]} \right] \right] \quad (\text{A4-6})$$

The logarithmic term in the denominator reflects the gradual breakdown of the viscous sublayer with the increasing size of the roughness protrusions. For $h^* = \eta_v$ the term is set equal to 1.0, i.e. the flow is still hydraulically smooth. For $h^* \rightarrow \eta_t$ the term goes towards zero, and Q approaches 1.0, i.e. the damping gradually disappears when the roughness protrusions pass through the transition layer.

In completely rough flow *Rotta* ³³ suggested the form:

$$\eta_t \leq h^* \quad Q = \left[1 + \frac{0.014}{\kappa_0 \eta_a} (h^* - \eta_t) \right] \quad (\text{A4-7})$$

It should be noted that eq. (A4-7) leads to a non-zero value of the mixing length at the pipe wall.

The size of η_v and η_t depends on the rheology of the fluid. For a Power Law fluid *Artyushkov et al.* made the assumptions:

$$\eta_v = \frac{A(1.0)}{A(n)} \eta_{v(n=1.0)} \quad (\text{A4-8})$$

and

$$\eta_t = \frac{A(1.0)}{A(n)} \eta_{t(n=1.0)} \quad (\text{A4-9})$$

Where $\eta_{v(n=1.0)} = 5.4$ and $\eta_{t(n=1.0)} = 54$ (The former value is in accordance with *Schlichting* ³⁵ (p.579), while the latter presumably is taken from the work by *Rotta* ³³).

Insertion of eqs. (A4-2) and (A4-3) into eq. (A4-1) gives:

$$\tau = k \left[\frac{dv_z}{dy} \right]^n + \rho l^2 \left[\frac{dv_z}{dy} \right]^2 \quad (\text{A4-10})$$

The fluid shear stress, τ , is now presumed to be independent of position and equal to the wall shear stress, τ_w . (This is obviously an incorrect assumption (see *Bird et al.* p.158). Among other things, it leads to a non-zero velocity gradient at the pipe centre. Nevertheless it is often used in the theory of turbulent pipe flow (e.g. *Bird et al.* ⁶ p.162 or *Schlichting* ³⁵ p.555)).

Introduction of the friction velocity $u^* = \sqrt{\frac{\tau_w}{\rho}}$ and rearrangement yields:

$$(u^*)^2 = \frac{k}{\rho} \left[\frac{dv_z}{dy} \right]^n + l^2 \left[\frac{dv_z}{dy} \right]^2 \quad (\text{A4-11})$$

The introduction of non-dimensional variables and a number of rearrangements transform eq. (A4-11) into the non-dimensional differential equation:

$$\varphi_a^2 \kappa_0^2 \bar{y}^2 Q^2 R^{*n} \left[\frac{d\psi}{d\bar{y}} \right]^2 + \left[\frac{d\psi}{d\bar{y}} \right]^n - (R^*)^n = 0 \quad (\text{A4-12})$$

where:

$$\bar{y} = y/R$$

$$R^* = \frac{R (u^*)^{2-n}}{(k/\rho)^{1/n}}$$

$$\psi = \psi(\bar{y}) = \frac{v_z}{u^*}$$

For hydraulically smooth flow and for flow in the transitional regime, the boundary conditions to eq. (A4-12) are:

- 1) $\psi(0) = 0$
- 2) $\left[\frac{d\psi}{d\bar{y}} \right]_{\bar{y}=0} = R^*$

While the boundary condition 1) is valid also for completely rough flow, boundary condition 2) is not. Instead the value of the velocity gradient at the wall is determined by considering eq. (A4-12) as an algebraic equation, i.e.:

$$\alpha_1 \left[\frac{d\psi}{d\bar{y}} \right]_{\bar{y}=0}^2 + \alpha_2 \left[\frac{d\psi}{d\bar{y}} \right]_{\bar{y}=0}^n - \alpha_3 = 0 \quad (\text{A4-13})$$

where $\alpha_1 = \varphi_a^2 \kappa_0^2 (\bar{y} Q)_{\bar{y}=0}^2 R^{*n}$; $\alpha_2 = 1$; $\alpha_3 = (R^*)^n$

and this non-linear equation is solved iteratively.

The non-linear ordinary differential equation (A4-12) requires a numerical solution technique. The interval:

$$\bar{y} \in [0;1]$$

is divided into a suitable number of subintervals N. On each subinterval:

$$\Delta \bar{y}_{i-1} = [\bar{y}_{i-1} ; \bar{y}_i] \quad i = 2, 3, \dots, N+1$$

the solution ψ to eq. (A4-12) is approximated with a second order polynomial:

$$\psi = A_i \bar{y}^2 + B_i \bar{y} + C_i \quad (\text{A4-14})$$

whereafter the overall velocity profile ψ is pieced together by the N second order polynomials. Consequently, the solution of eq. (A4-12) has become a problem of determining the coefficients A_i , B_i and C_i , $i=2,3,\dots,N+1$.

From eq. (A4-14) it follows that:

$$\psi_{i-1} = A_i \bar{y}_{i-1}^2 + B_i \bar{y}_{i-1} + C_i \quad (\text{A4-15})$$

$$\dot{\psi}_{i-1} = 2 A_i \bar{y}_{i-1} + B_i \quad (\text{A4-16})$$

$$\dot{\psi}_i = 2 A_i \bar{y}_i + B_i \quad (\text{A4-17})$$

If the values of \bar{y}_{i-1} , \bar{y}_i , ψ_{i-1} , $\dot{\psi}_{i-1}$ and $\dot{\psi}_i$ are known, the eqs. (A4-15), (A4-16) and (A4-17) form a simple set of linear equations, which may be solved with respect to A_i , B_i and C_i . The solution is:

$$A_i = \frac{\dot{\psi}_i - \dot{\psi}_{i-1}}{2(\bar{y}_i - \bar{y}_{i-1})} \quad (\text{A4-18})$$

$$B_i = \dot{\psi}_{i-1} - 2 A_i \bar{y}_{i-1} \quad (\text{A4-19})$$

$$C_i = \psi_{i-1} - A_i (\bar{y}_{i-1})^2 - B_i \bar{y}_{i-1} \quad (\text{A4-20})$$

$i=2,3,4,\dots,N+1$.

The determination of the approximated velocity profile is performed stepwise, starting at the wall and moving towards the pipe centre, sequentially determining the polynomial coefficients for each subinterval.

The distribution of \bar{y}_i , $i=1,2,3, \dots, N+1$ should ensure a suitable resolution of the velocity profile ψ everywhere within the interval $[0;1]$. However, because the velocity gradient is expected to be large at the pipe wall, while it approaches zero close to the pipe centre, an equidistant division of the interval is not calculatory efficient. Instead, the division should be small at the pipe wall and large at the pipe centre. *Artyushkov et al.* suggested the following method of division:

$$\bar{y}_i = \bar{y}_{i-1} + \Delta \bar{y}_i$$

where $\bar{y}_1 = 0$ and $\Delta \bar{y}_i = \min \left[\frac{1}{\dot{\psi}_{i-1}} ; 0.002 \right]$, $i=2,3,4,\dots,N+1$

The values of $\dot{\psi}_i$, $i=2,3,4\dots N+1$ in eqs. (A4-18)–(A4-20) are determined by again considering eq. (A4-12) as an algebraic equation, i.e.:

$$\alpha_1 (\dot{\psi}_i)^2 + \alpha_2 (\dot{\psi}_i)^n - \alpha_3 = 0 \quad (\text{A4-21})$$

where $\alpha_1 = \varphi_a^2 \kappa_0^2 (\bar{y}_i)^2 Q^2 R^{*n}$; $\alpha_2 = 1$; $\alpha_3 = (R^*)^n$

This non-linear equation is solved iteratively. The value of $\dot{\psi}_1$ is available from the boundary conditions to eq. (A4-12).

From the boundary conditions to eq. (A4-12) it is known that $\psi_1=0$. Using this fact, the values of ψ_i , $i=2,3,4\dots N+1$ are easily found in the stepwise solution procedure. The polynomial coefficients A_i , B_i and C_i are calculated on the basis of ψ_{i-1} , whereupon ψ_i is calculated by insertion in the polynomial (A4-14) for interval $(i-1)$, i.e.:

$$\psi_i = A_i \bar{y}_i^2 + B_i \bar{y}_i + C_i$$

The connection between the velocity profile $\psi(\bar{y})$ and the friction factor, f , in pipe flow is the relationship:

$$f = 2 \left[\frac{u^*}{u} \right]^2 \quad (\text{A4-22})$$

where it can be deduced that:

$$\frac{u}{u^*} = 2 \int_{\bar{y}=0}^{\bar{y}=1} (1 - \bar{y}) \psi \, d\bar{y} \quad (\text{A4-23})$$

Using the approximation for ψ based on eq. (A4-14), eq. (A4-23) may be reformulated as:

$$\frac{u}{u^*} = 2 \sum_{i=2}^{N+1} \int_{\bar{y}_{i-1}}^{\bar{y}_i} (A_i \bar{y}^2 + B_i \bar{y} + C_i)(1 - \bar{y}) \, d\bar{y} \quad (\text{A4-24})$$

Whereafter the determination of f is straightforward according to equation (A4-22).

The *Artyushkov et al.* theory has been implemented in the program FRICFAC, described in Appendix 5. For a given fluid rheology and wall roughness, the program provides the

user with corresponding values of the friction factor and Reynolds number:

$$\text{Re}' = \frac{\rho D^n u^{2-n}}{\left[\frac{3n+1}{4n}\right]^n k g^{n-1}}$$

In fig. A4/2, experimental results for water in rough pipes, obtained by *Nikuradse*²⁶, are plotted together with the predictions from the *Artyushkov et al.*^{1 2} theory, for discrete values of the relative wall roughness. The agreement is good, except for the smallest roughness values and for the Reynolds numbers in the transition from laminar to turbulent flow, i.e. $\text{Re}'=2-4000$. (Note that *Nikuradse*²⁶ does not list results for the region below $\text{Re}'=4000$, but these are shown in *Schlichting*³⁵ (see fig. 4.2.4/1))

In fig. A4/3 the predictions from the *Artyushkov et al.* model is compared with the predictions from a theoretical relation derived by *Dodge & Metzner*¹⁰. The latter is based on experimental measurements of Power Law fluids in hydraulically smooth pipes and reads:

$$f = \left[4.0 n^{-0.75} \log_{10} \left[\text{Re}' (f)^{1-\frac{n}{2}} \right] - 0.40 n^{-1.2} \right]^{-2} \quad (\text{A4-26})$$

Also here there is a reasonable agreement, except for a range of Reynolds numbers where the shift from laminar to hydraulically smooth flow takes place ($\text{Re}'=2-10000$).

It should be noted that the experimental verification of the *Artyushkov et al.* model is missing for the completely rough flow of Power Law fluids, where $n \neq 1$. No experimental data appear to exist for this situation yet.

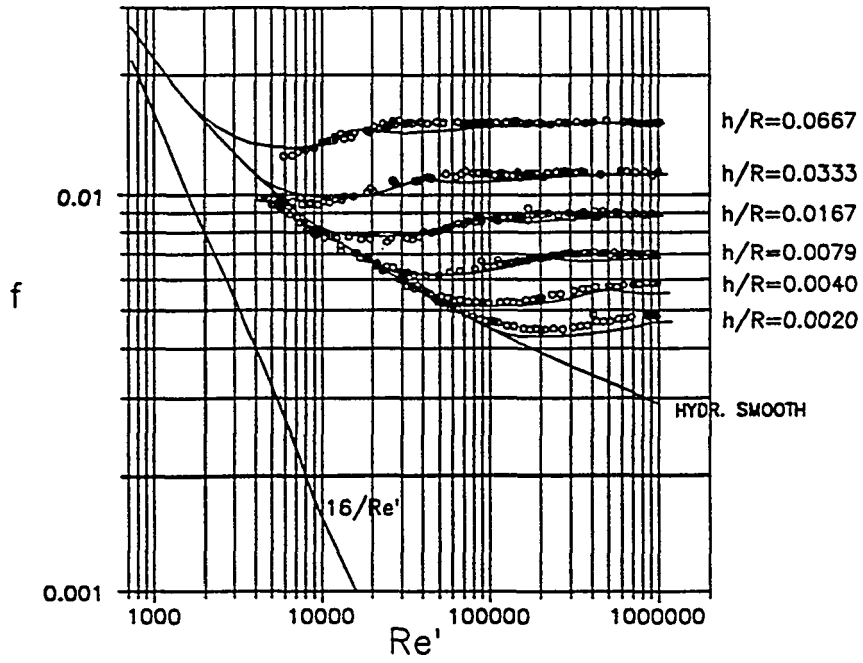


Fig. A4/2 Comparison of the predictions from the Artyushkov et al.^{1,2} theory (fully drawn curves) with the experimental measurements of Nikuradse²⁶ (single data points) for water flowing through pipes of different roughness. The discrete variable is the relative roughness h/R .

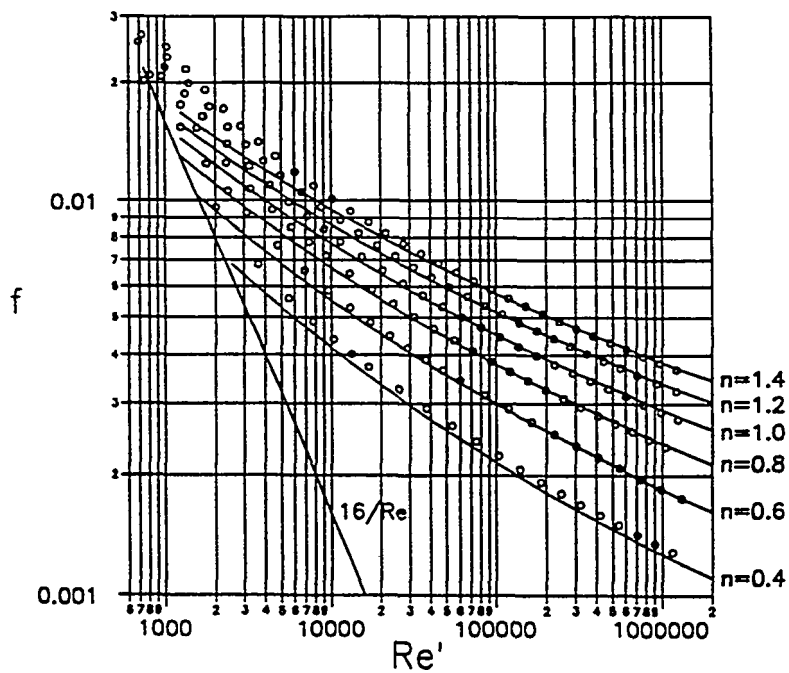


Fig. A4/3 Comparison of the predictions from the Artyushkov et al.^{1,2} theory (single data points) with the predictions from relations developed by Dodge & Metzner¹⁰ (fully drawn curves) for Power Law fluids in hydraulically smooth pipe flow. The discrete variable is the Power Law flow behaviour index n .

Appendix 5

Computer programs.

This Appendix contains documentation of the Fortran programs applied in the theoretical work. Four programs form the basis for the theoretical results outlined in chapters 4 and 5 and Appendix 4:

SCSB-CT
 SCSB-CV
 SCSB-VT
 FRICFAC

I) SCSB-CT, SCSB-CV & SCSB-VT.

The programs SCSB-CT, SCSB-CV and SCSB-VT, which are used to obtain the theoretical predictions in chapter 5, are very similar in structure. In SCSB-CT the dependent variable is annular cuttings Concentration and the upper layer flow is Turbulent. In SCSB-CV the dependent variable is annular cuttings Concentration and the upper layer flow is taking place in the Viscous flow regime. In SCSB-VT the dependent variable is the nominal annular fluid Velocity producing a specific annular cuttings concentration and the flow is presumed to be Turbulent.

The diagrams in figs. A5/1, A5/2 and A5/3 describe the structure of SCSB-CT, SCSB-CV and SCSB-VT respectively. The names of the subroutines should be noted. If a given name occurs in more than one program, it indicates that the subroutine is completely identical in the programs considered. The names of two subroutines occurring in two different programs may also differ only by the addition of a number or one or two letters. This indicates that the difference between the two subroutines is only marginal (e.g. SECALC-F, SECALC-V and SECALC-T).

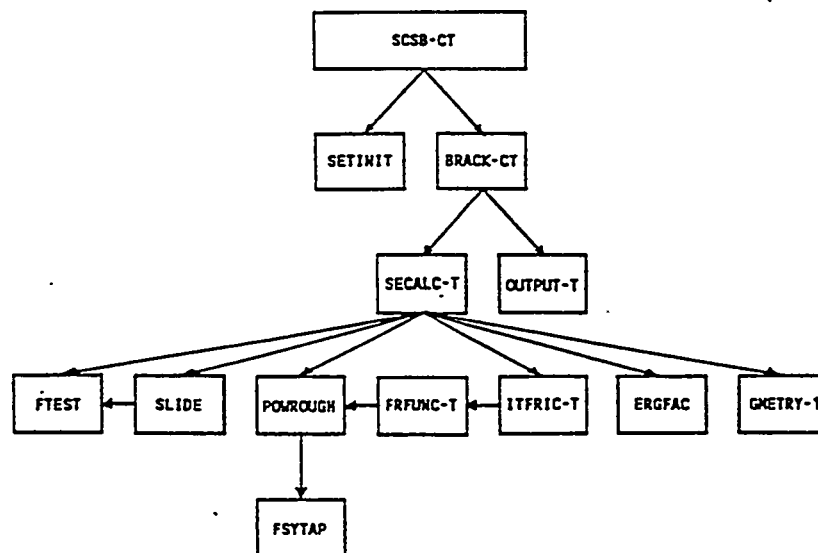


Fig. A5/1 The structure of program SCSB-CT

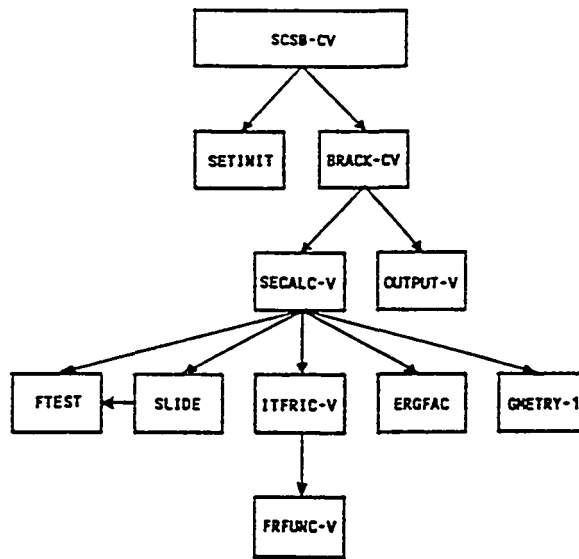


Fig. A5/2 The structure of program SCSB-CV

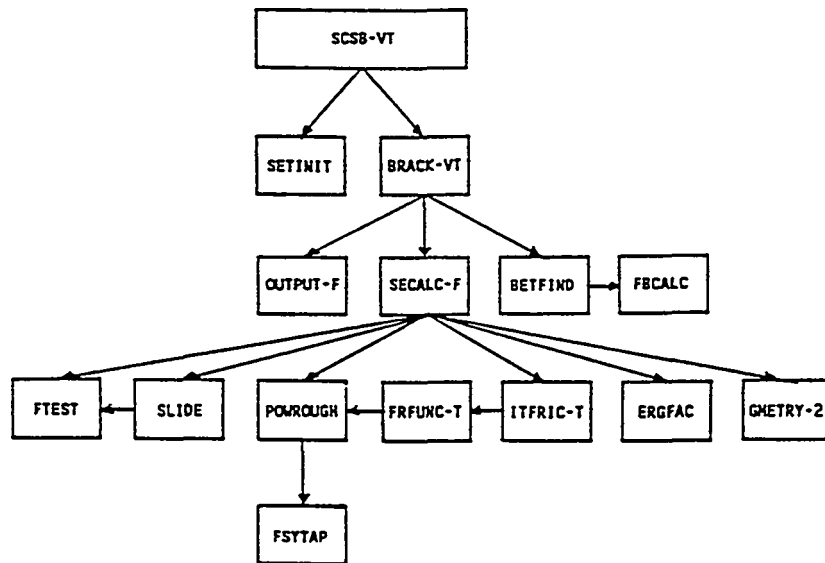


Fig. A5/3 The structure of program SCSB-VT

The input to programs SCSB-CT, -CV and -VT is entered interactively. Each computer code contains a default list of the variables required to perform the calculations. These are:

- 1) Outer pipe radius
- 2) Inner pipe radius
- 3) Fluid density
- 4) Cuttings density
- 5) Coefficient of kinetic friction (deposit/outer pipe wall)
- 6) Coefficient of kinetic friction (deposit/inner pipe wall)
- 7) Cuttings diameter
- 8) Annular eccentricity
- 9) Annular inclination
- 10) Cuttings concentration in the deposit
- 11) Coefficient of static friction (deposit/outer pipe wall)
- 12) Coefficient of static friction (deposit/inner pipe wall)
- 13) Angle of repose
- 14) Number of steps in independent variable
- 15) Volumetric flowrate (-CT & -CV)/ Annular cuttings concentration (-VT)
- 16) Power Law consistency index
- 17) Power Law flow behaviour index
- 18) Number of steps in iterative solution procedure (-VT only)

When the codes are executed, the user is allowed to change the values in the default list. When the list is accepted, the programs will request which of the listed variables that is to be the independent, how large an interval of the independent variable that is to be considered and how many discrete values the interval is to contain.

The output from SCSB-CT, -CV and -VT may in principle be designed according to the wishes of the user. However it may require a modification of the output subroutine and in some cases its calling arguments. In the documented versions of SCSB-CT, SCSB-CV and SCSB-VT given in the present appendix, the default output is:

- 1) The value of the independent variable
- 2) Annular cuttings concentration (-CT & -CV)/ nominal annular fluid velocity (-VT)
- 3) The upper layer fluid velocity, u_m
- 4) The nominal lower layer fluid velocity, u_c
- 5) The deposit sliding velocity, u_b
- 6) The upper layer Reynolds number relative to the annular walls
- 7) The upper layer Reynolds number relative to the deposit surface

The $c(\varphi)$ - and $c(v)$ -plots in chapter 5 were generated with the programs SCSB-CT and SCSB-CV. Note that the nominal annular fluid velocity does not appear anywhere in the SCSB-model, and if this quantity is desired in the output, the volumetric flowrate must be divided by the cross sectional area of the annular space. For the $c(v)$ plots in chapter 5 this slight change in the codes SCSB-CT and SCSB-CV is performed directly in the output routine, and no separate documentation of this modification has been performed.

II) FRICFAC.

FRICFAC is written on the basis of the *Artyushkov et al.*^{1 2} model (see App. 4) and generates the friction factor vs. Reynolds number plots of the type outlined in figs. 4.3.3/1 - 4.3.3/4. The diagram in fig. A5/4 shows the structure of the program.

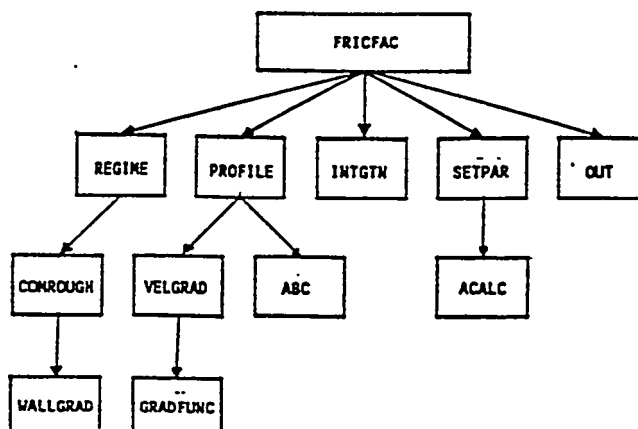


Fig. A5/4 The structure of program FRICFAC

The input to FRICFAC is entered interactively. The computer code contains a default list of the parameters required to perform the calculations. These are:

- 1) The Power Law flow behaviour index
- 2) The Power Law consistency index
- 3) The smallest size of the roughness protrusions
- 4) The pipe radius
- 5) The fluid density
- 6) Initial wall shear stress value.

When the code is executed, the user is allowed to change the default list. The program generates friction factor vs. Reynolds number plots for multipla of the smallest roughness size given in the input. The wall shear stress specified in the input corresponds to a Reynolds number in the output. The program secures that the friction factors corresponding to Reynolds numbers between 10^2 and 10^7 are calculated. (Consequently the value of the initial shear stress may be given an arbitrary value. However, the given value may affect the time before useful output is produced).

Default output from the program is:

- 1) The Reynolds number
- 2) The friction factor
- 3) The relative roughness of the pipe
- 4) The Power Law flow behaviour index
- 5) A flag describing if the data has been obtained in completely rough flow, hydraulically smooth flow or in the transition between.
- 6) The wall shear stress

Program SCSB-CT

Program SCSB-CV

Program SCSB-VT

```

PROGRAM SCSS.VT
IMPLICIT DOUBLEPRECISION (A-N,O-Z)
DIMENSION Z(20)
C
C
C THIS CODE CALCULATES THE NOMINAL ANNUAL FLUID VELOCITY REQUIRED
C TO ACHIEVE A GIVEN ANNUAL CUTTINGS CONCENTRATION. THE FLOW IS
C PRESUMED TO BE TURBULENT
C
CALL SETINIT(Z,P1,G,XSE1,XSE2,MUM,NST,NVS)
C
DO 100 J=1,NST+1
  MUM(J) = XSE1*(J-1)*XSE2/NST
  FAF = DCOS(90)/(71451122)
  CALL BRACK_VT(Z,P1,G,MUM,XIT1,NVS)
100 CONTINUE
C
CLOSE(UNIT=2)
END
C
-----
SUBROUTINE SETINIT(P1,G,XSE1,XSE2,MUM,NST,NVS)
IMPLICIT DOUBLEPRECISION (A-N,O-Z)
DIMENSION Z(20)
CHARACTER*80 OUTFIL
C
C THIS SUBROUTINE INITIALIZES THE VARIABLES OF THE SCSS-MODEL
C
P1 = 4.00*DATAK(1,DO)
G = 9.81DO
C
Z(1) = 10.16D-2
Z(2) = 1.00D-2
Z(3) = 1.00D-3
Z(4) = 0.30D-3
Z(5) = 0.30D-3
Z(6) = 0.30D-2
Z(7) = 0.00
Z(8) = 0.00
Z(9) = 0.25D0
Z(10) = 0.20D0
Z(11) = 0.20D0
Z(12) = 0.20D0
Z(13) = 0.175D0
Z(14) = 0.00
Z(15) = 0.00
Z(16) = 0.00
C
WRITE(6,201) Z(1)
201 FORMAT(1X,10I10)
WRITE(6,202) Z(2)
202 FORMAT(1X,10I10)
WRITE(6,203) Z(3)
203 FORMAT(1X,10I10)
WRITE(6,204) Z(4)
204 FORMAT(1X,10I10)
WRITE(6,205) Z(5)
205 FORMAT(1X,10I10)
WRITE(6,206) Z(6)
206 FORMAT(1X,10I10)
WRITE(6,207) Z(7)
207 FORMAT(1X,10I10)
WRITE(6,208) Z(8)
208 FORMAT(1X,10I10)
WRITE(6,209) Z(9)
209 FORMAT(1X,10I10)
WRITE(6,210) Z(10)
210 FORMAT(1X,10I10)
WRITE(6,211) Z(11)
211 FORMAT(1X,10I10)
WRITE(6,212) Z(12)
212 FORMAT(1X,10I10)
WRITE(6,213) Z(13)
213 FORMAT(1X,10I10)
WRITE(6,214) Z(14)
214 FORMAT(1X,10I10)
WRITE(6,215) Z(15)
215 FORMAT(1X,10I10)
C
201 FORMAT(1X,10I10)
202 FORMAT(1X,10I10)
203 FORMAT(1X,10I10)
204 FORMAT(1X,10I10)
205 FORMAT(1X,10I10)
206 FORMAT(1X,10I10)
207 FORMAT(1X,10I10)
208 FORMAT(1X,10I10)
209 FORMAT(1X,10I10)
210 FORMAT(1X,10I10)
211 FORMAT(1X,10I10)
212 FORMAT(1X,10I10)
213 FORMAT(1X,10I10)
214 FORMAT(1X,10I10)
215 FORMAT(1X,10I10)
C
WRITE(6,230)
230 FORMAT(1X,10I10)
C
IF 'NO: ' ENTER 0)
C
READ(5,*) MUM
IF (MUM.EQ.0) GO TO 250
240 FORMAT(1X,10I10)
READ(5,*) Z(MUM)
GO TO 200
C
250 WRITE(6,260)
260 FORMAT(1X,10I10)
READ(5,*) MUM
XSE1 = Z(MUM)
IF (MUM.EQ.9) XSE1=XSE1*2.00*PI/360.00
C
270 WRITE(6,270)
270 FORMAT(1X,10I10)
READ(5,*) XSE2
IF (MUM.EQ.9) XSE2=XSE2*2.00*PI/360.00
C
WRITE(6,*) 'OUTPUT FILE?'
280 FORMAT(1X,10I10)
OPEN(UNIT=2,FILE=OUTFIL)
C
Z(9) = Z(9)*PI/180.00
NST = Z(14)
NVS = Z(18)
C
RETURN
END

```

```

SUBROUTINE BRACK_VT(Z,P1,G,MUM,XIT1,NVS)
IMPLICIT DOUBLEPRECISION (A-N,O-Z)
DIMENSION Z(20)
C
C THIS SUBROUTINE DETERMINES SOLUTIONS TO THE SYSTEM EQUATION (4.2.2-3)
C BY USE OF AN ENCLOSURE TECHNIQUE.
C
CALL BETFIND(P1,Z,BETO,AR,E,A1,A2,A4)
C
VOL1 = 1.0D-10
CALL SECALC_F(VOL1,BETO,Z,P1,G,F1,A1,A2,A4,AC,XIT1,
  UM,UC,UB,AEA,AEF)
C
DO 320 I=1,NVS
  VOL2 = 1.0D0/NVS
  CALL SECALC_F(VOL2,BETO,Z,P1,G,F2,A1,A2,A4,AC,XIT1,
  UM,UC,UB,AEA,AEF)
  IF (F1*F2.GT.0.00) GO TO 310
  KBR = 0
  FOLD = F1
  300 VOL0 = (F1*VOL2-F2*VOL1)/(F1-F2)
  CALL SECALC_F(VOL0,BETO,Z,P1,G,F0,A1,A2,A4,AC,XIT1,
  UM,UC,UB,AEA,AEF)
  IF (F0*F1.GT.0.00) THENA
    VOL1 = VOL0
    F1 = F0
  ELSE
    VOL2 = VOL0
    F2 = F0
  ENDIF
  IF ((DABS(F0).LT.1.D-10).AND.(DABS(VOL2-VOL1).LT.1.D-10)) THEN
    GO TO 310
  ENDIF
  IF (F0*FOLD.GT.0.00) THEN
    SCL = FOLD/F0
    IF (F0*F1.GT.0.00) THEN
      F1 = SCL*F1
    ELSE
      F2 = SCL*F2
    ENDIF
    FOLD = F0
    KBR = KBR+1
    IF (KBR.LT.25) GO TO 300
  310 VOL1 =VOL2
  F1 = F2
  320 CONTINUE
  RETURN
  END
C
-----
SUBROUTINE BETFIND(P1,Z,BETO,AR,E,A1,A2,A4)
IMPLICIT DOUBLEPRECISION (A-N,O-Z)
DIMENSION Z(20)
C
C THIS SUBROUTINE DETERMINES THE POSITION OF THE DEPOSIT SURFACE
C CORRESPONDING TO A GIVEN ANNUAL CUTTINGS CONCENTRATION
C
BET1 = D.DD
BET2 = D1
CALL FRCALC(FB1,Z,A1,A2,A4,P1,BET1,ACT,AR,E)
IF (FB1.EQ.0) THEN
  WRITE(6,*) 'NO CHANGE OF SIGN IN SUBROUTINE BETFIND'
  STOP
  ENDF
C
BET = 0
BETO = FB1*BET2-FB2*BET1/(FB1-FB2)
CALL FRCALC(FB2,Z,A1,A2,A4,P1,BETO,ACT,AR,E)
IF (FB2*FB1.GT.0.00) THEN
  BET1 = FB2
  ELSE
    BET2 = FB2
  ENDF
C
IF (DABS(FB2).GT.1.D-10) THEN
  BET = FBET1
  IF (FB2.LT.0) THEN
    WRITE(6,*) 'DIVERGENCE IN SUBROUTINE BETFIND'
    STOP
  ENDF
  IF (FB2*FB0.GT.0.00) THEN
    SCL = FB0/FB2
    IF (FB0*FB1.GT.0.00) THEN
      FB1 = SCL*FB1
    ELSE
      FB2 = FB0
    ENDIF
  400
  ENDF
  RETURN
  END
C
-----
SUBROUTINE FRCALC(Z,A1,A2,A4,P1,BET,ACT,AR,E)
IMPLICIT DOUBLEPRECISION (A-N,O-Z)
DIMENSION Z(20)
C
C THIS SUBROUTINE CALCULATES THE DIFFERENCE BETWEEN THE CROSS SECTIONAL AREA
C OF A DEPOSIT OCCUPYING THE GIVEN PERCENTAGE OF THE ANNUAL VOLUME AND THE
C AREA CORRESPONDING TO THE DEPOSIT SURFACE POSITION IN THE ITERATION SCHEME
C
AR = D1*(Z(1)**2)-(Z(2)**2)
E = Z(9)*(Z(1)-Z(2))
A1 = E-Z(2)
A2 = E-Z(1)
ACT = Z(15)*AR/(100.00*Z(10))
C
IF (A1.LE.A2) THEN
  ACT=AR*(Z(1)+Z(2))*((P1-BET)*DSIN(BET)*DCOS(BET))
  ENDF
C
IF (A4.GT.A1) AND (A4.LT.A2) THEN
  ALFA = D1*DCOS(BET)*DCOS(BET)
  F = ACT-AR*(Z(1)+Z(2))*((P1-BET)*DSIN(BET)*DCOS(BET))
  -Z(2)**2)*(ALFA*DSIN(ALFA)*DCOS(ALFA))
  ENDF
C
IF (A4.GE.A2) THEN
  F = ACT-((Z(1)+Z(2))*((BET-DSIN(BET)*DCOS(BET)))
  ENDF
C
RETURN
END

```


Program FRICFAC

```

PROGRAM PRICFAC
  IMPLICIT DOUBLEPRECISION (A-H,O-Z)
  DIMENSION PSI(2000),DELPSI(2000),YBAR(2000),A(2000),B(2000),
    C(2000)
  C
  CALL SETPAR(POM,POK,ROUGHO,R,RNO,TALM,YKAR,PHI,AINT,ETAV,ETAT)
  DO 30 I=1,10
    REOLD = 10.00
    RE1 = 0.00
    N = 1+ROUGHO
  C
  DO 20 J=1,1000
    TALM = J*(FIRST*DEXP(/0.100))
    RE1CY = DSORT(TALM/RNO)
    RSTAR = (R*RE1CY**((2.0-POM)/POM))/((POK/RNO)**(1.00/POM))
    NSTAR = N*RSTAR/R
  C
  CALL REGIME(ETAV,ETAT,PHI,POM,NSTAR,RSTAR,AINT,DELPSI,ALFR,
    JFLAG)
  C
  CALL PROFILE(YBAR,JFLAG,NSTAR,ETAT,YKAR,RSTAR,ALFR,AINT,
    POM,PHI,N,DELPSI,STEP,A,B,C,K,PSI)
  C
  CALL INTGN(A,B,C,YBAR,SUMTERM,K)
  RE = (2.00**POM)**((2.00**SUMTERM)**(2.00-POM))/RSTAR**POM
  RE1 = RE*(1.00**POM)**(1.00/POM)/(1.00**POM**2.00)**POM
  RESCOF = 1.00/(2.00**SUMTERM**2)
  C
  IF ((JFLAG.EQ.0).AND.(RE1.GT.1.02)) THEN
    FIRST = FIRST/2.00
    GO TO 10
  ELSE
    JFLAG = 1
  ENDIF
  C
  IF (DABS(DLOG10(RE1)-DLOG10(REOLD)).LT.0.100) GO TO 20
  REOLD = RE1
  IF (RE1.GT.1.07) GO TO 30
  CALL OUT(RE1,RESCOF,N,R,POM,JFLAG,TALM)
  C
  CONTINUE
  CLOSE(UNIT=3)
  STOP
  END
  C
  SUBROUTINE SETPAR(POM,POK,ROUGHO,R,RNO,TALM,YKAR,PHI,
    AINT,ETAV,ETAT)
  IMPLICIT DOUBLEPRECISION (A-H,O-Z)
  DIMENSION U(6)
  C
  THIS SUBROUTINE INITIALIZES THE INPUT PARAMETERS TO THE ARTYUSHKOV
  ET AL. MODEL. A SIMPLE LOOP STRUCTURE ALLOWS CHANGES TO BE PERFORMED.
  CHARACTER*60 OUTFIL
  C
  U(1) = 1.00
  U(2) = 1.00
  U(3) = 1.00
  U(4) = 1.00
  U(5) = 1.00
  U(6) = 1.00
  C
  WRITE(6,101) U(1)
  WRITE(6,102) U(2)
  WRITE(6,103) U(3)
  WRITE(6,104) U(4)
  WRITE(6,105) U(5)
  WRITE(6,106) U(6)
  C
  101 FORMAT(1X,1) POWER LAW FLOW BEHAVIOR INDEX      /E12.5)
  102 FORMAT(1X,1) POWER LAW CONSISTENCY INDEX      /E12.5)
  103 FORMAT(1X,1) HEIGHT OF ROUGHNESS, LOWER BOUNDARY /E12.5)
  104 FORMAT(1X,1) RADIUS OF ROUGHNESS              /E12.5)
  105 FORMAT(1X,1) FLUID DENSITY                    /E12.5)
  106 FORMAT(1X,1) INITIAL WALL SHEAR STRESS VALUE  /E12.5,/)
  C
  WRITE(6,110)
  110 FORMAT(1X,'CHANGE OF PARAMETER ?',/, 'IF YES: ENTER THE INDEX',/,
    'IF NO: ENTER 0')
  C
  READ(5,*) NUM
  IF (NUM.EQ.0) GO TO 130
  WRITE(6,120)
  120 FORMAT(1X,'ENTER NEW VALUE')
  READ(5,*) U(NUM)
  GO TO 100
  C
  130 WRITE(6,*) 'OUTPUT FILE?'
  READ(1,120) OUTFIL
  140 FORMAT(1X,60)
  OPEN(UNIT=3,FILE=OUTFIL)
  C
  POM = U(1)
  POK = U(2)
  ROUGHO = U(3)
  R = U(4)
  RNO = U(5)
  TALM = U(6)
  YKAR = 0.200
  PHI = DSORT((POM+1.00)/(2.00**POM))
  C
  CALL ACALC(POM,AINT)
  C
  ETAV = 3.400**27.00/AINT
  ETAT = 34.00**27.00/AINT
  C
  RETURN
  END
  C
  SUBROUTINE ACALC(POM,AINT)
  IMPLICIT DOUBLEPRECISION (A-H,O-Z)
  DIMENSION AA(30),BB(30),CC(30),P(30)
  C
  THIS SUBROUTINE GENERATES A FORSYTHE POLYNOMIAL APPROXIMATION TO
  THE FUNCTION A(n) WHICH IS GIVEN IN THE MODEL OF ARTYUSHKOV ET AL.
  CHARACTER*60 INFIL
  INFIL = 'ACALC.DAT'
  INFIL = CHARACTER(TRANSFER('erough.dat'))
  OPEN(UNIT=2,FILE=INFIL)
  C
  READ(2,*) NTP,NPOL
  DO 200 K=1,NTP
    READ(2,*) AA(KK),BB(KK),CC(KK)
    P(K) = 1.00
    AINT = 0.4**NPOL**2
    IF (K.EQ.2) THEN
      P(K) = POM-AA(K-1)
    ELSE
      P(K) = (POM-AA(K-1))**P(K-1)-BB(K-1)**P(K-2)
    ENDIF
  210 AINT = AINT+CC(K)**P(K-1)
  C
  CLOSE(UNIT=2)
  RETURN
  END

```

```

  C
  SUBROUTINE REGIME(ETAV,ETAT,PHI,POM,NSTAR,RSTAR,AINT,DELPSI,
    ALFR)
  IMPLICIT DOUBLEPRECISION (A-H,O-Z)
  DIMENSION DELPSI(2000)
  C
  THIS SUBROUTINE DETERMINES IF THE FLOW IS HYDRAULICALLY SMOOTH,
  IN THE TRANSITIONAL- OR THE COMPLETELY ROUGH FLOW REGIME.
  C
  IF (NSTAR.GT.ETAV) THEN
    JFLAG = 1
    CALL CORRUGH(NSTAR,ETAT,PHI,RSTAR,POM,DELPSI)
    GO TO 300
  ENDIF
  C
  IF (NSTAR.LT.ETAV) THEN
    JFLAG = 0
    DELPSI(1) = RSTAR
    ALFR = 1.00
    GO TO 300
  ENDIF
  C
  IF ((NSTAR.GT.ETAV).AND.(NSTAR.LT.ETAV)) THEN
    JFLAG = 1
    DELPSI(1) = RSTAR
    ALFR = DLOG10(1.58.00/(AINT**NSTAR))
  ENDIF
  C
  300 RETURN
  END
  C
  SUBROUTINE CORRUGH(NSTAR,ETAT,PHI,RSTAR,POM,DELPSI)
  IMPLICIT DOUBLEPRECISION (A-H,O-Z)
  DIMENSION DELPSI(2000)
  C
  CALCULATES THE VELOCITY GRADIENT AT THE PIPE WALL IF THE FLOW IS
  COMPLETELY ROUGH
  C
  X1 = 0.00
  X2 = 0.00
  WFAC = (10.01400**((NSTAR-ETAT)**PHI)**2)**(RSTAR**POM-2.00)
  WGR1 = WALLGRAD(WFAC,POM,RSTAR,X1)
  WGR2 = WALLGRAD(WFAC,POM,RSTAR,X2)
  C
  IF (WGR1**WGR2-GE.0.00) THEN
    WRITE(6,400)
    400 FORMAT(1X,'NO SHIFT OF SIGN IN SUBROUTINE CORRUGH')
    STOP
    ENDOF
  C
  KCO = 0
  WGR0 = WGR1
  C
  410 X0 = (WGR1**WGR2-WGR2**X1)/(WGR1-WGR2)
  WGR0 = WALLGRAD(WFAC,POM,RSTAR,X0)
  IF (WGR0**WGR1-GE.0.00) THEN
    WGR1 = WGR0
  ELSE
    X0 = X0
    WGR2 = WGR0
  ENDIF
  C
  IF (DABS(WGR0).GT.1.0-5) THEN
    KCO = KCO+1
    IF (KCO.GE.100) THEN
      STOP
      WRITE(6,*) 'DIVERGENCE IN SUBROUTINE CORRUGH'
    ENDIF
  C
  IF (WGR0**WGR0-GE.0.00) THEN
    SCL = WGR0/(WGR0**WGR0)
    IF (WGR0**WGR1-GE.0.00) THEN
      WGR1 = SCL*WGR2
    ELSE
      WGR1 = SCL*WGR1
    ENDIF
    WGR0 = WGR0
    GO TO 410
  ENDIF
  C
  DELPSI(1) = X0
  RETURN
  END
  C
  FUNCTION WALLGRAD(WFAC,POM,RSTAR,X)
  IMPLICIT DOUBLEPRECISION (A-H,O-Z)
  C
  THIS FUNCTION CALCULATES THE VALUE OF THE L.N.S. OF THE ALGEBRAIC
  EQUATION THAT GOVERNS IF THE VELOCITY GRADIENT IS CONSIDERED TO BE
  AN INDEPENDENT VARIABLE IN EQ.(A-12) AND THE RADIAL POSITION IS ZERO
  WALLGRAD = WFAC**(X**2)+(X**POM)-RSTAR**POM
  END
  C
  SUBROUTINE PROFILE(YBAR,JFLAG,NSTAR,ETAT,YKAR,RSTAR,ALFR,AINT,
    POM,PHI,N,DELPSI,STEP,A,B,C,K,PSI)
  IMPLICIT DOUBLEPRECISION (A-H,O-Z)
  DIMENSION YBAR(2000),PSI(2000),DELPSI(2000),A(2000),B(2000),
    C(2000)
  C
  THIS SUBROUTINE APPROXIMATES THE VELOCITY PROFILE WITH A NUMBER OF
  SECOND ORDER POLYNOMIALS, EACH VALID ON A SUBINTERVAL OF THE RADIUS.
  C
  DO 500 K=1,2000
    YBAR(K) = 0.00
    PSI(1) = 0.00
  510 STEP = DABS(DELPSI(K))*0.00200
    IF (STEP.GE.1.00) THEN
      NT = DABS(1.00/DELPSI(K))
    ELSE
      NT = 0.00200
    ENDIF
    K = K+1
    YBAR(K) = YBAR(K-1)+NT
    IF (YBAR(K).GT.1.00) YBAR(K) = 1.00
    C
    IF (JFLAG.EQ.1) THEN
      O = 1.00-0.01400**((NSTAR-ETAT)/(YKAR**YBAR(K)**RSTAR))
    ELSE
      O = 1.00-DEXP(-(YBAR(K)**RSTAR)/(ALFR**AINT))
    ENDIF
    C
    ALPHA = (RSTAR**POM)**(PHI**YKAR**YBAR(K)**O)**2
    CALL VELGRAD(ALPHA,RSTAR,POM,DELPSI,R)
    C
    CALL ABC(PSI,DELPSI,YBAR,A,B,C,K)
    C
    IF (YBAR(K).LT.1.00) GO TO 510
  500 RETURN
  END

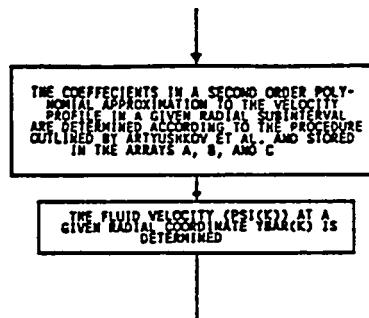
```


Appendix 6

**Subroutine
descriptions**

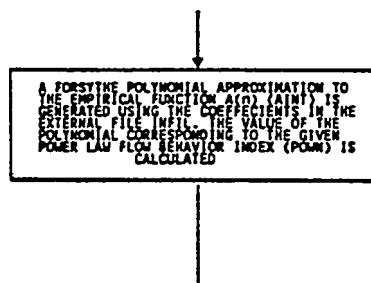
Subroutine ABC

ABC determines the coefficients A_k , B_k and C_k in the second order polynomial approximation to the fluid velocity profile in the radial subinterval $(\bar{y}_{k-1} ; \bar{y}_k)$. The polynomial coefficients are calculated as outlined in Appendix 4, eqs. (A4-18), (A4-19) and (A4-20).



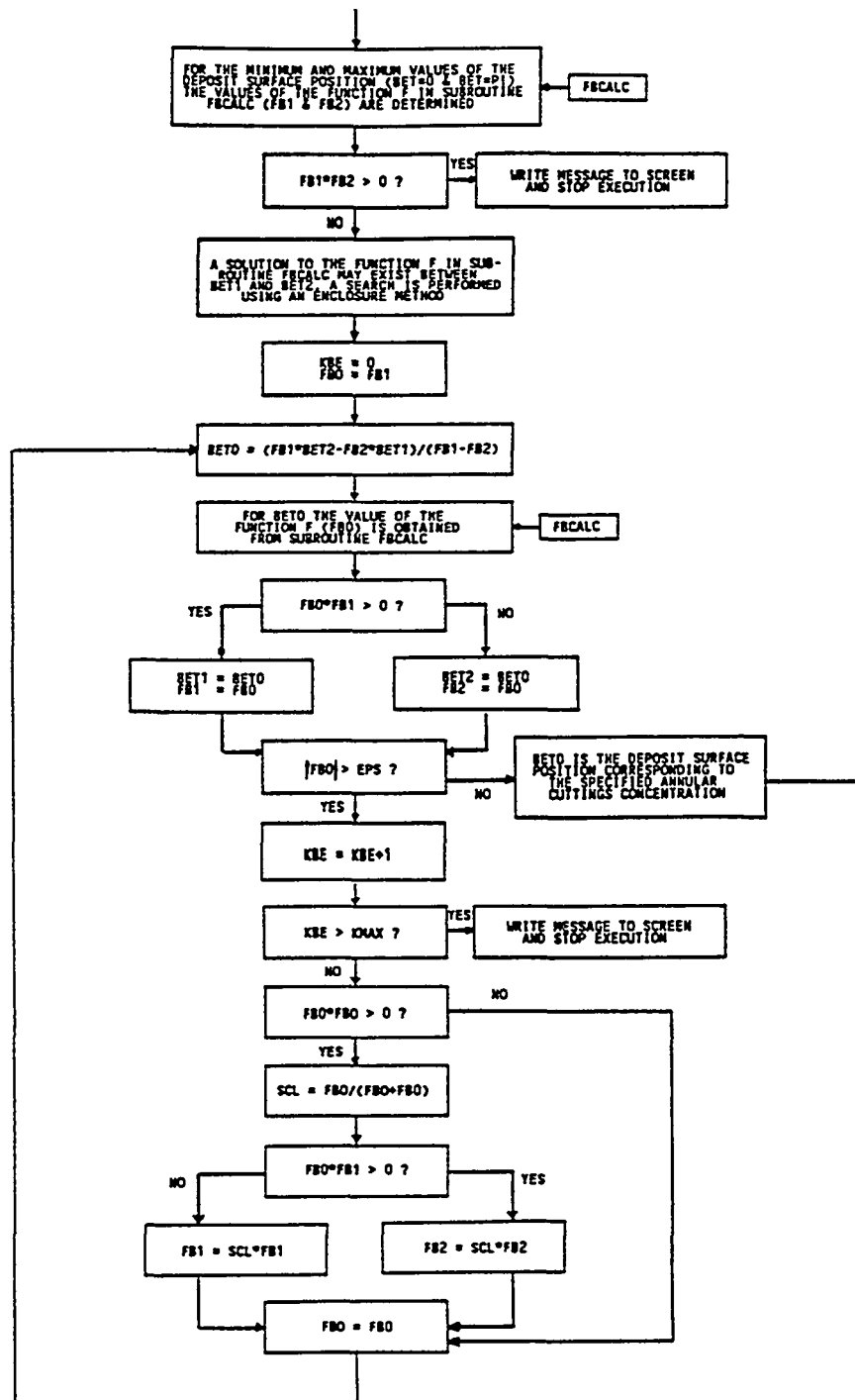
Subroutine ACALC

ACALC generates a Forsythe polynomial approximation to the empirical function $A(n)$ given by Artyushkov *et al.* The polynomial coefficients are imported from an external data file. The value of the polynomial corresponding to the given Power Law flow behavior index, n , is determined.

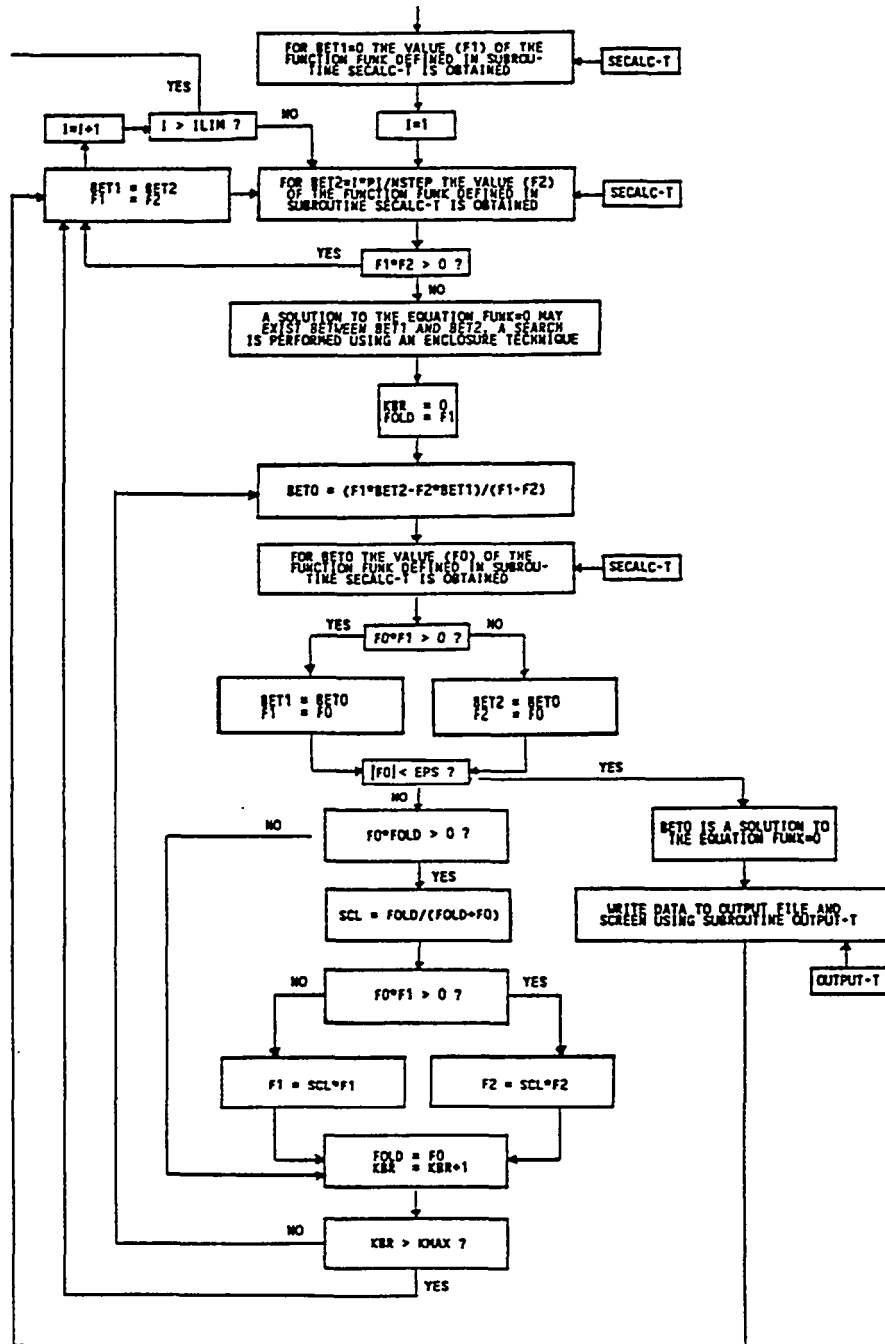


Subroutine BETFIND

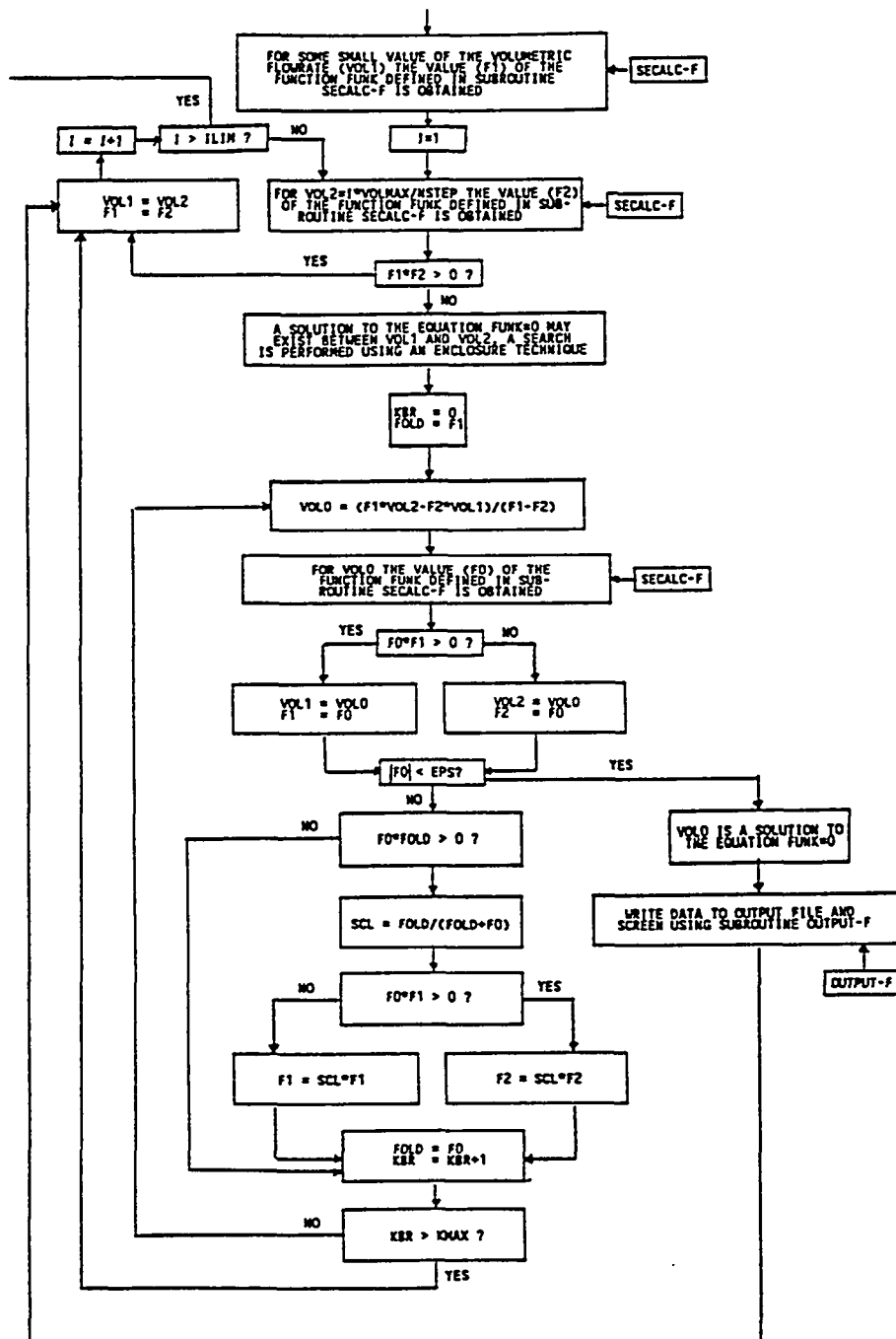
BETFIND determines the angle β that corresponds to a given annular cuttings concentration. The given concentration corresponds to a deposit which occupies a well defined part of the annular cross section. BETFIND performs an iterative search for the β -value which makes the difference between the specified and the calculated area equal to zero.



BRACK-CT performs a systematic search for the annular cuttings concentration, in terms of the angle β , which satisfies the system equation (4.2.2-3) under given physical conditions. The angle β may take a value between 0 radians (no bed) and π radians (the bed occupies the whole of the annular space). The interval between 0 and π radians is divided into a suitable number of subintervals, and an iterative search for solutions to the system equation is performed in each interval, using an enclosure technique. If a solution is found, relevant data is directed to the output file specified in SETINIT.

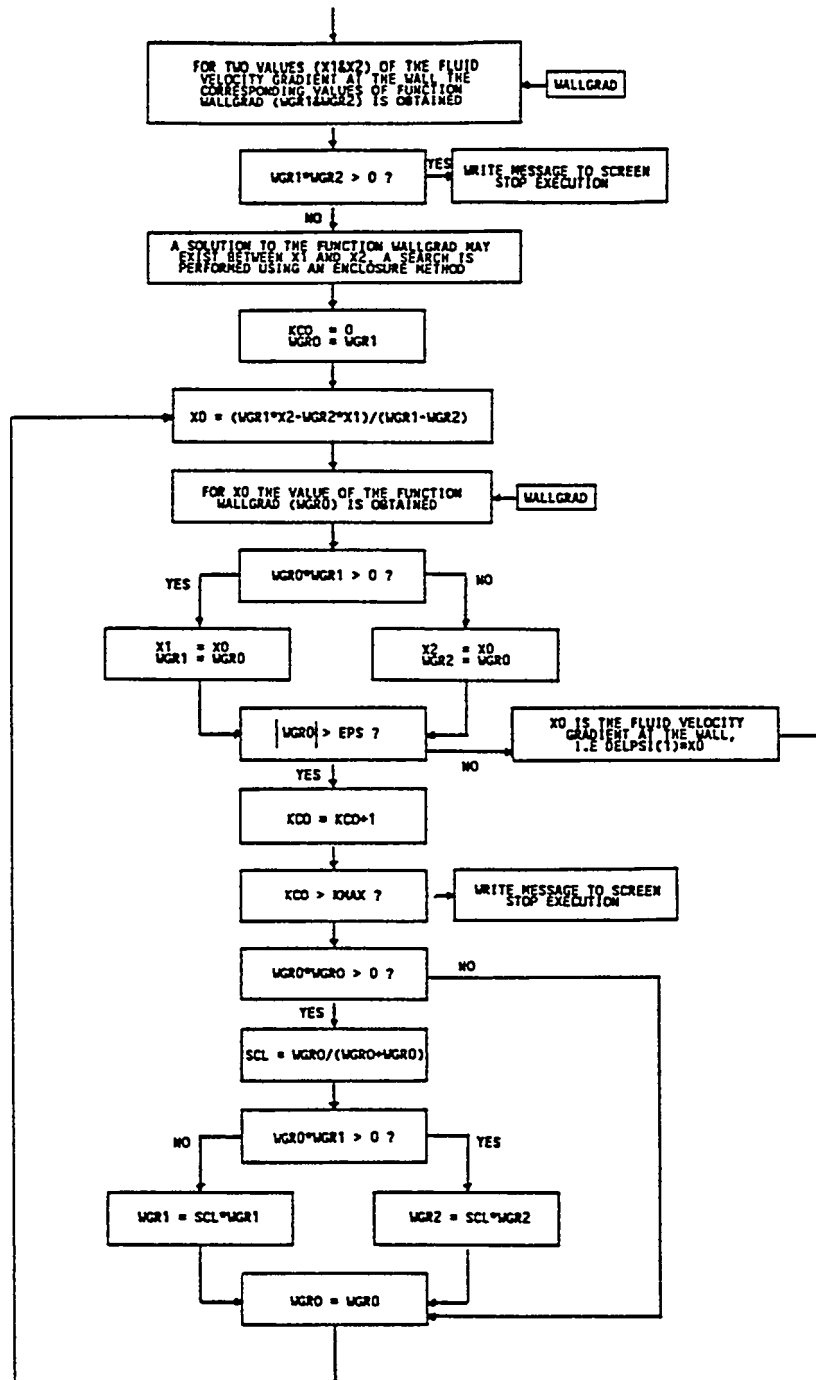


BRACK-VT performs a systematic search for the volumetric flowrate that satisfies the system equation (4.2.2-3) for a given annular cuttings concentration. BRACK-VT is very similar to BRACK-CT and BRACK-CV, but where the deposit surface position is restricted to a limited interval (β between 0 and π), there is not a well defined upper bound for the volumetric flowrate, and the value must depend on experience from previous program executions. The interval between the upper- and lower bound for the volumetric flowrate is divided into a suitable number of subintervals, and an iterative search for solutions to the system equation is performed in each interval, using an enclosure technique. If a solution is found, relevant data is directed to the output file specified in SETINIT. BRACK-VT calls its own version of OUTPUT, denoted OUTPUT-F.



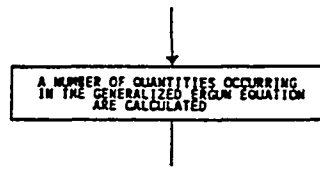
Subroutine COMROUGH

COMROUGH determines the fluid velocity gradient at the wall when the flow is completely rough. The non-dimensional differential equation (A4-12) is considered to be an algebraic equation, where the velocity gradient is the independent variable and where $\bar{y} = 0$. An iterative enclosure method is used in the search for a solution.



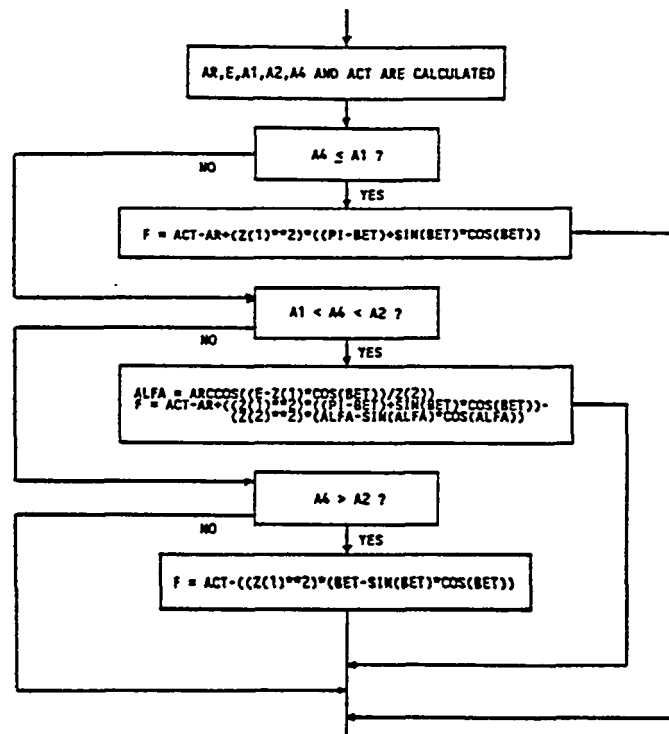
Subroutine ERGFAC

ERGFAC calculates a number of quantities appearing in the generalized Ergun Equation proposed by *Kemblowski & Mertl*.



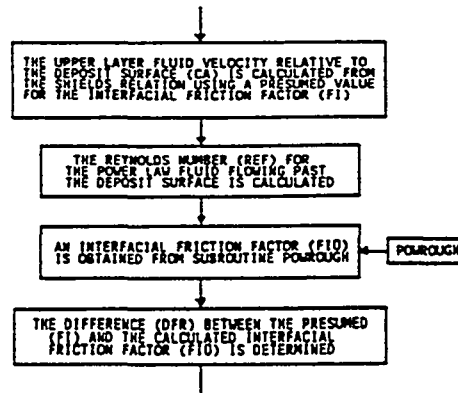
Subroutine FBCALC

FBCALC calculates the difference between the part of the annular cross sectional area occupied by deposit of specific size and the cross sectional area corresponding to some predicted deposit surface position.



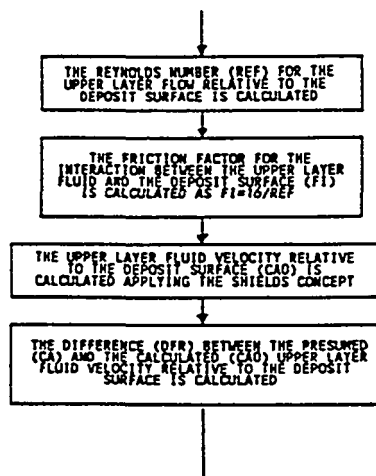
Subroutine FRFUNC-T

FRFUNC-T calculates the difference between a predicted and a calculated value of the interfacial friction factor. The calculated value is obtained by inserting the predicted value of the friction factor in eq. (4.2.8-2), whereupon the resulting value for the upper layer fluid velocity is used in the *Artyushkov et al.* model (see App. 4).



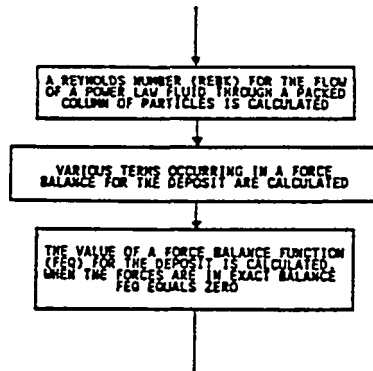
Subroutine FRFUNC-V

FRFUNC-V calculates the difference between a predicted and a calculated value for the upper layer fluid velocity. The calculated upper layer fluid velocity is determined from eq. (4.2.8-2), using $f_1=16/Re$ in the denominator.



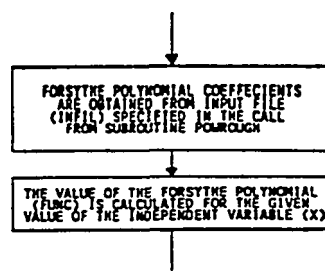
Subroutine FTEST

FTEST defines a function, which is a sum of the forces acting on the lower annular layer. Under equilibrium conditions the function should be equal to zero.

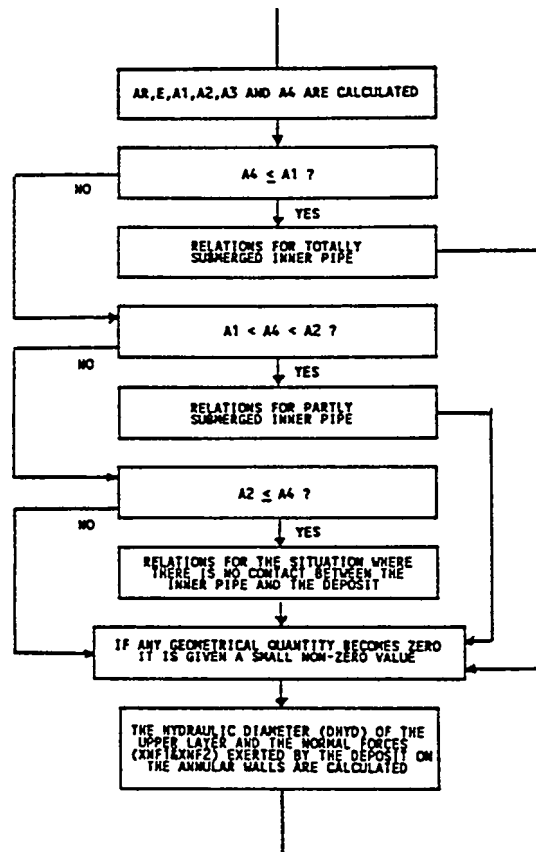


Subroutine FSYTAP

FSYTAP reads the coefficients in the input file specified in the call from subroutine POWROUGH. The coefficients are characteristic for a Forsythe polynomial, which is an approximation to either a friction factor vs. roughness plot or a logarithmic friction factor vs. Reynolds number plot. FSYTAP returns either the friction factor corresponding to a given roughness or the logarithm to the friction factor corresponding to a given Reynolds number.

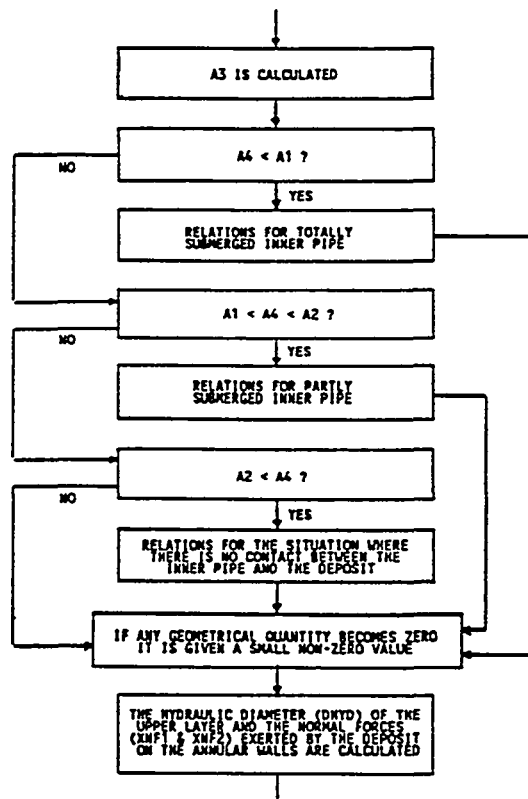


GMETRY-1 calculates the various geometrical quantities characterizing the annular cross section corresponding to a given value of β . According to the relations outlined in Appendix 1, it is necessary to distinguish between three types of annular configuration: The situation where the inner pipe is totally submerged in the deposit, the situation where it is partly submerged, and the situation where the inner pipe not is in contact with the deposit. Each type of configuration leads a given set of geometrical relations. If a geometrical quantity is zero, it may create problems in subsequent calculations and it is given a small non-zero value instead.



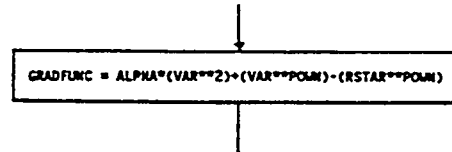
GMETRY-2 calculates the various geometrical quantities characterizing the annular cross section corresponding to a given value of β . According to the relations outlined in Appendix 1, it is necessary to distinguish between three types of annular configuration: The situation where the inner pipe is totally submerged in the deposit, the situation where it is partly submerged, and the situation where the inner pipe not is in contact with the deposit. Each type of configuration leads a given set of geometrical relations. If a geometrical quantity is zero, it may create problems in subsequent calculations and it is given a small non-zero value instead.

GMETRY-2 is used in connection with SCSB-VT and is identical to GMETRY-1 except for that the quantities AR, E, A1, A2 and A4 has been omitted because they already have been calculated in subroutine FBCALC.



Function GRADFUNC

GRADFUNC calculates the value of the L.H.S. of the algebraic equation that forms if the velocity gradient is considered to be the independent variable in equation (A4-12).



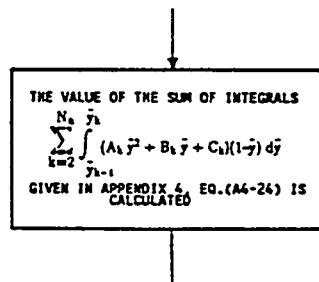
A flowchart consisting of a single rectangular box with a downward arrow above it and a downward arrow below it. The box contains the mathematical expression: $GRADFUNC = ALPHA*(VAR**2) + (VAR**POW) - (RSTAR**POW)$

Subroutine INTGTN

INTGTN calculates the value of the integral:

$$\sum_{k=2}^{N_a} \int_{\bar{y}_{k-1}}^{\bar{y}_k} (A_k \bar{y}^2 + B_k \bar{y} + C_k)(1-\bar{y}) d\bar{y}$$

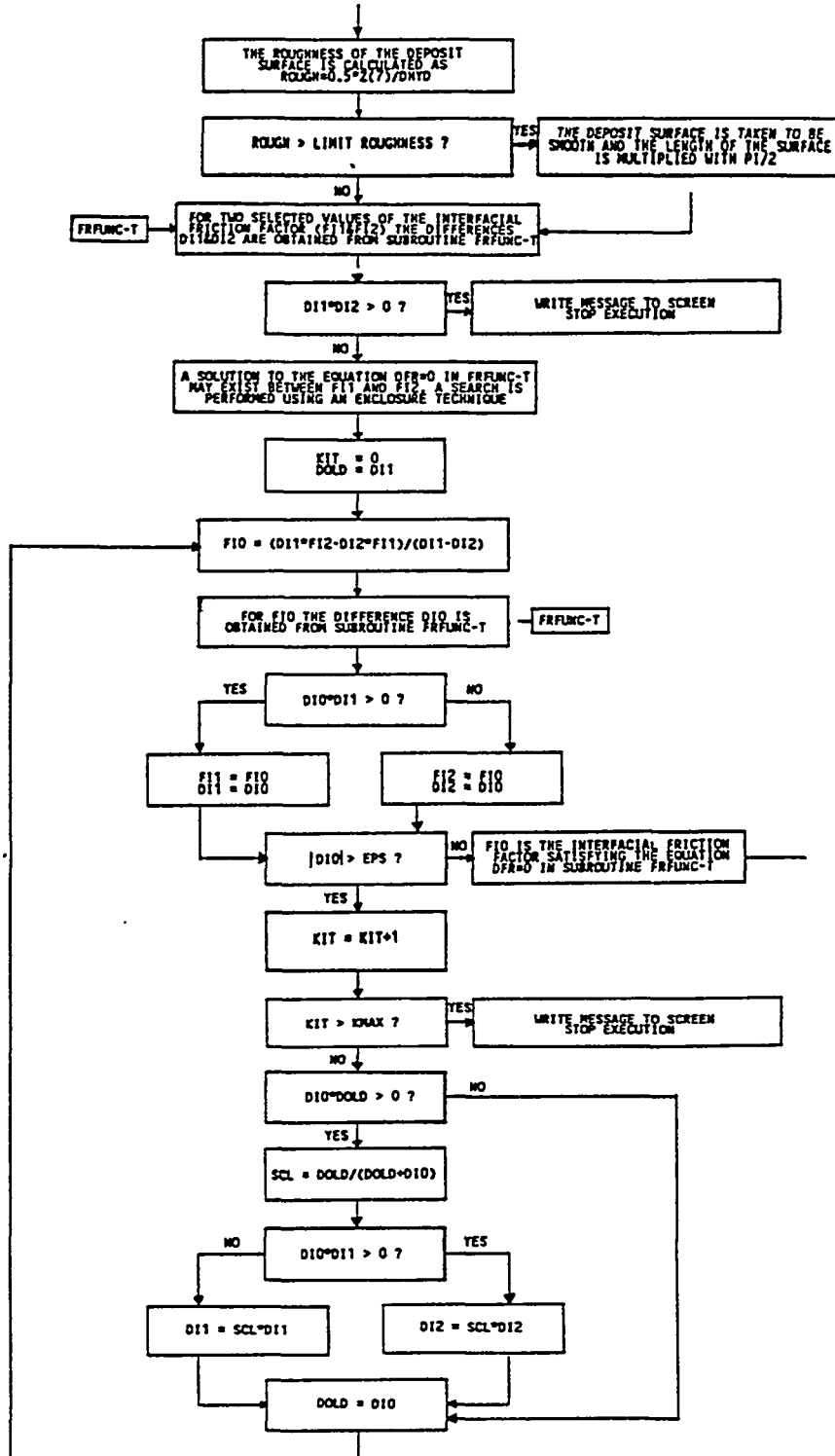
given in Appendix 4, equation (A4-24). The integral forms the basis for the calculation of the friction factor f in equation (A4-22).



A flowchart consisting of a single rectangular box with a downward arrow above it and a downward arrow below it. The box contains the text: "THE VALUE OF THE SUM OF INTEGRALS" followed by the mathematical expression $\sum_{k=2}^{N_a} \int_{\bar{y}_{k-1}}^{\bar{y}_k} (A_k \bar{y}^2 + B_k \bar{y} + C_k)(1-\bar{y}) d\bar{y}$ and the text "GIVEN IN APPENDIX 4, EQ.(A4-24) IS CALCULATED".

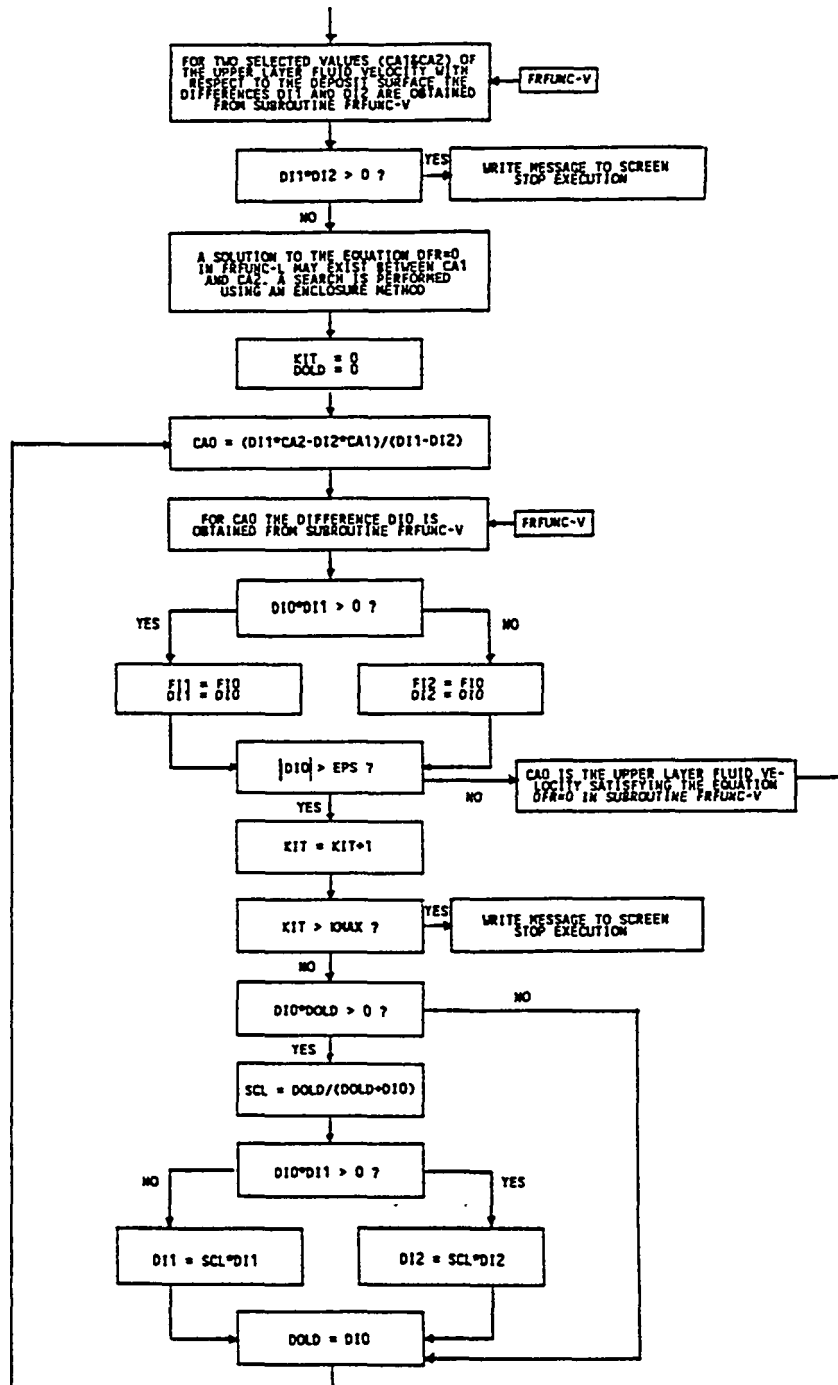
Subroutine ITFRIC-T

The friction factor at the deposit surface and the average fluid velocity above the surface are coupled, and consequently the expression (4.2.8-2) is not an explicit expression for the upper layer fluid velocity. ITFRIC-T determines corresponding values of the upper layer fluid velocity and the interfacial friction factor, applying an enclosure method. The difference between a predicted and a calculated value for the interfacial friction factor is determined. The predicted value is inserted in eq. (4.2.8-2), and the resulting upper layer fluid velocity is used in the calculation of a new interfacial friction factor, using the Artyushkov *et al.* theory (App. 4). When the difference between the predicted and calculated value becomes (close to) zero, a correct set of upper layer fluid velocity and interfacial friction factor has been obtained.



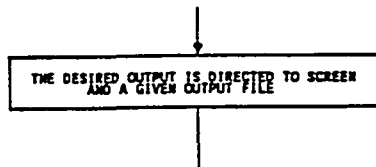
Subroutine ITFRIC-V

The friction factor at the deposit surface and the average fluid velocity above the surface are coupled, and consequently the expression (4.2.8-2) is not an explicit expression for the upper layer fluid velocity. ITFRIC-V determines corresponding values of the upper layer fluid velocity and the interfacial friction factor, applying an enclosure method. The difference between a predicted and a calculated value for the upper layer fluid velocity is determined. The calculated value is obtained by inserting $f_i=16/Re$ in eq. (4.2.8-2). When the difference between the predicted and calculated value becomes (close to) zero, a correct set of the upper layer fluid velocity and interfacial friction factor has been obtained.



Subroutine OUT

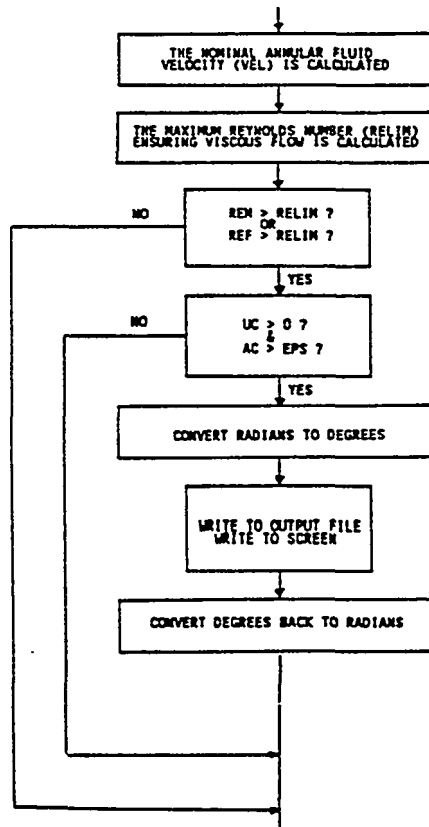
OUT directs selected data to the screen and to the output file specified in subroutine SETPAR.



Subroutine OUTPUT-F

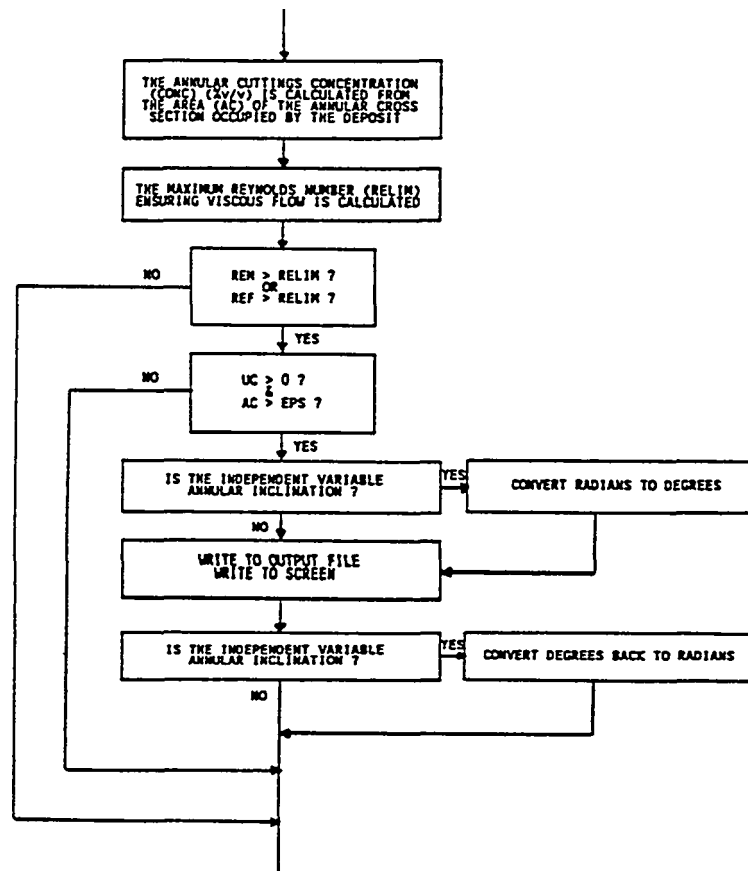
When a solution to the expression (4.2.2-3) has been determined, relevant data is directed to the output file specified in subroutine SETINIT and to the computer screen. The output from the listed version of SCSB-VT is:

- 1) the value of the independent variable
- 2) the nominal annular fluid velocity
- 3) the upper layer fluid velocity relative to the annular walls
- 4) the nominal lower fluid velocity
- 5) the deposit sliding velocity
- 6) the upper layer Reynolds number relative to the annular walls
- 7) the upper layer Reynolds number relative to the deposit surface



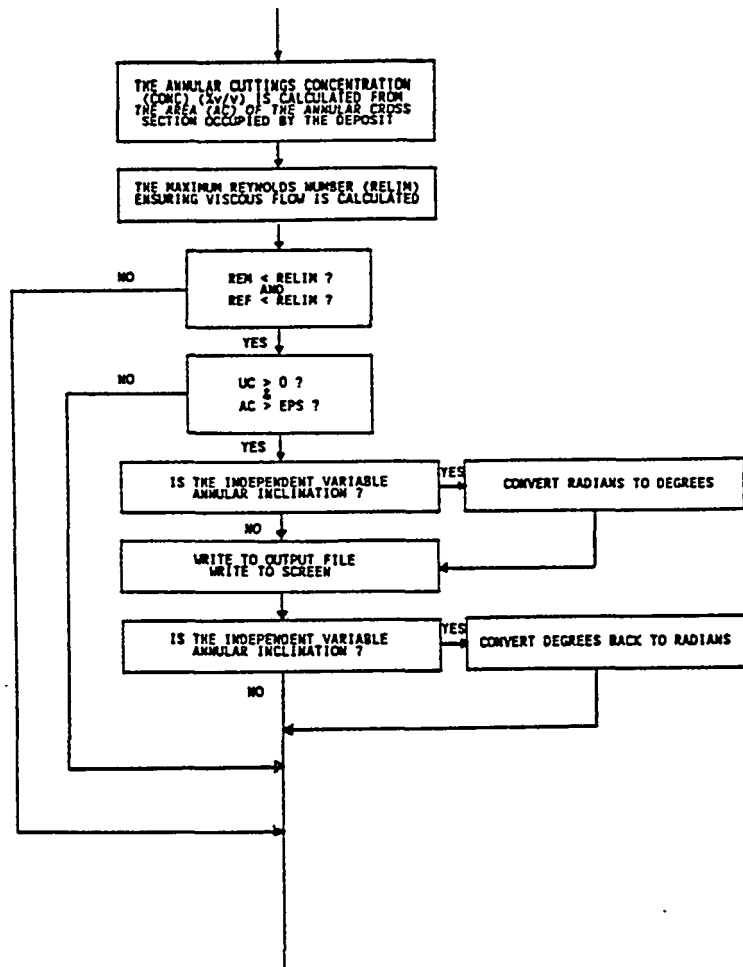
When a solution to the expression (4.2.2-3) has been determined, relevant data is directed to the output file specified in subroutine SETINIT and to the computer screen. The output from the listed version of SCSB-CT is:

- 1) the value of the independent variable
- 2) the annular cuttings concentration
- 3) the upper layer fluid velocity relative to the annular walls
- 4) the nominal lower layer fluid velocity
- 5) the deposit sliding velocity
- 6) the upper layer Reynolds number relative to the annular walls
- 7) the upper layer Reynolds number relative to the deposit surface



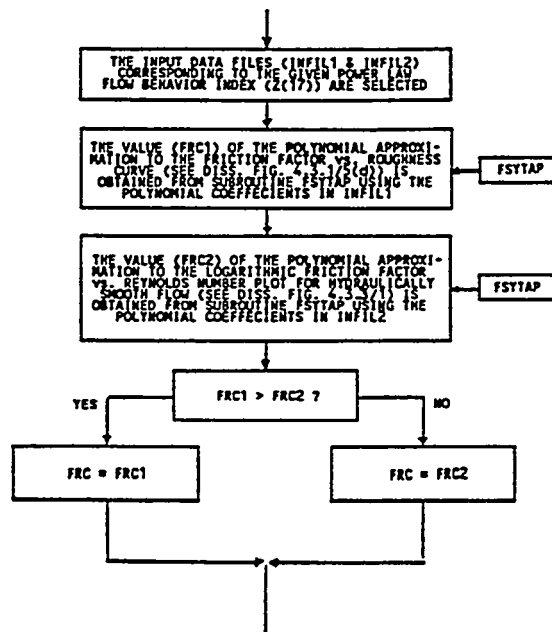
When a solution to the expression (4.2.2-3) has been determined, relevant data is directed to the output file specified in subroutine SETINIT and to the computer screen. The output from the listed version of SCSB-CV is:

- 1) the value of the independent variable
- 2) the annular cuttings concentration
- 3) the upper layer fluid velocity relative to the annular walls
- 4) the nominal lower layer fluid velocity
- 5) the deposit sliding velocity
- 6) the upper layer Reynolds number relative to the annular walls
- 7) the upper layer Reynolds number relative to the deposit surface

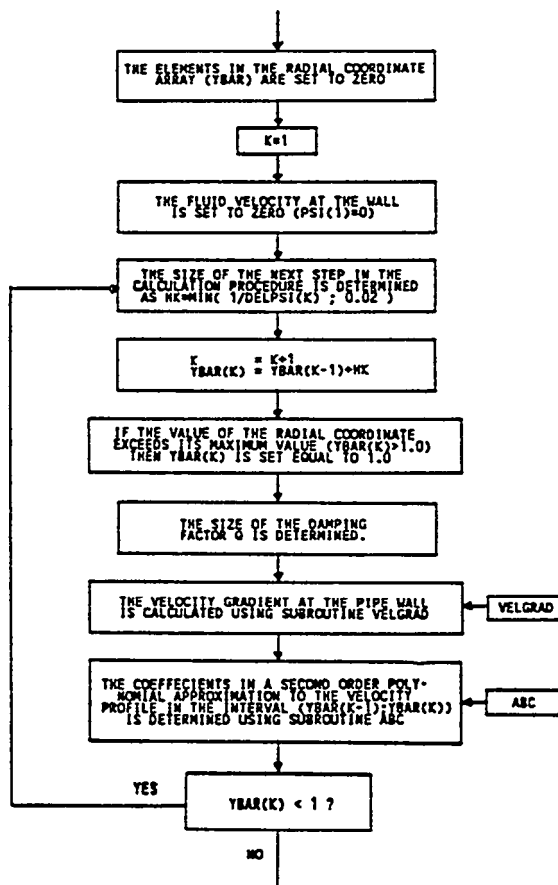


Subroutine POWROUGH

POWROUGH considers the value of the Power Law flow behavior index and selects the data files which contains the polynomial coefficients used in the polynomial approximation to the friction factor vs. roughness plot and the logarithmic friction factor vs. Reynolds number plot respectively (see section 4.3.3). The subroutine then decides which of the curves that is to be applied under the given conditions, i.e. whether the smooth flow curve or the rough/transitional approximation curve is to be used.

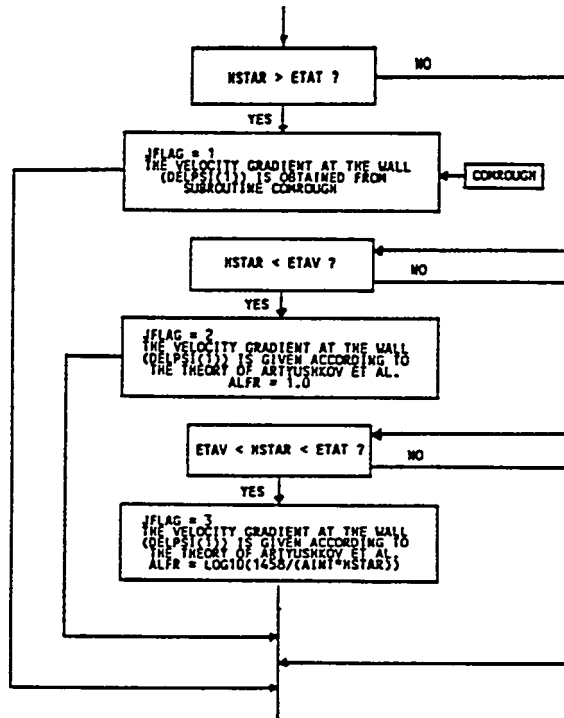


PROFILE divides the pipe radius into a suitable number of subintervals, according to the guidelines given by *Artyushkov et al.* On each subinterval the fluid velocity profile is approximated with a second order polynomial, according to the procedure outlined in Appendix 4, eq.(A4-14)-(A4-20).

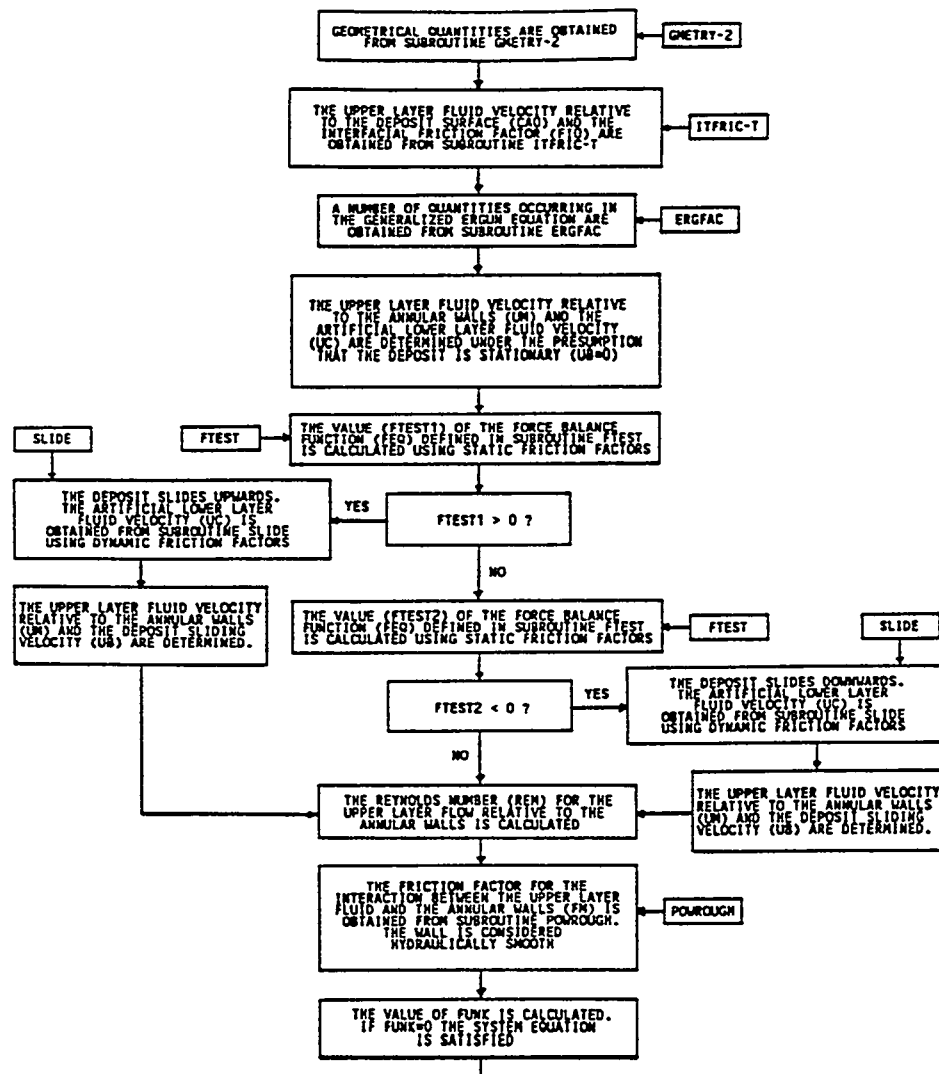


Subroutine REGIME

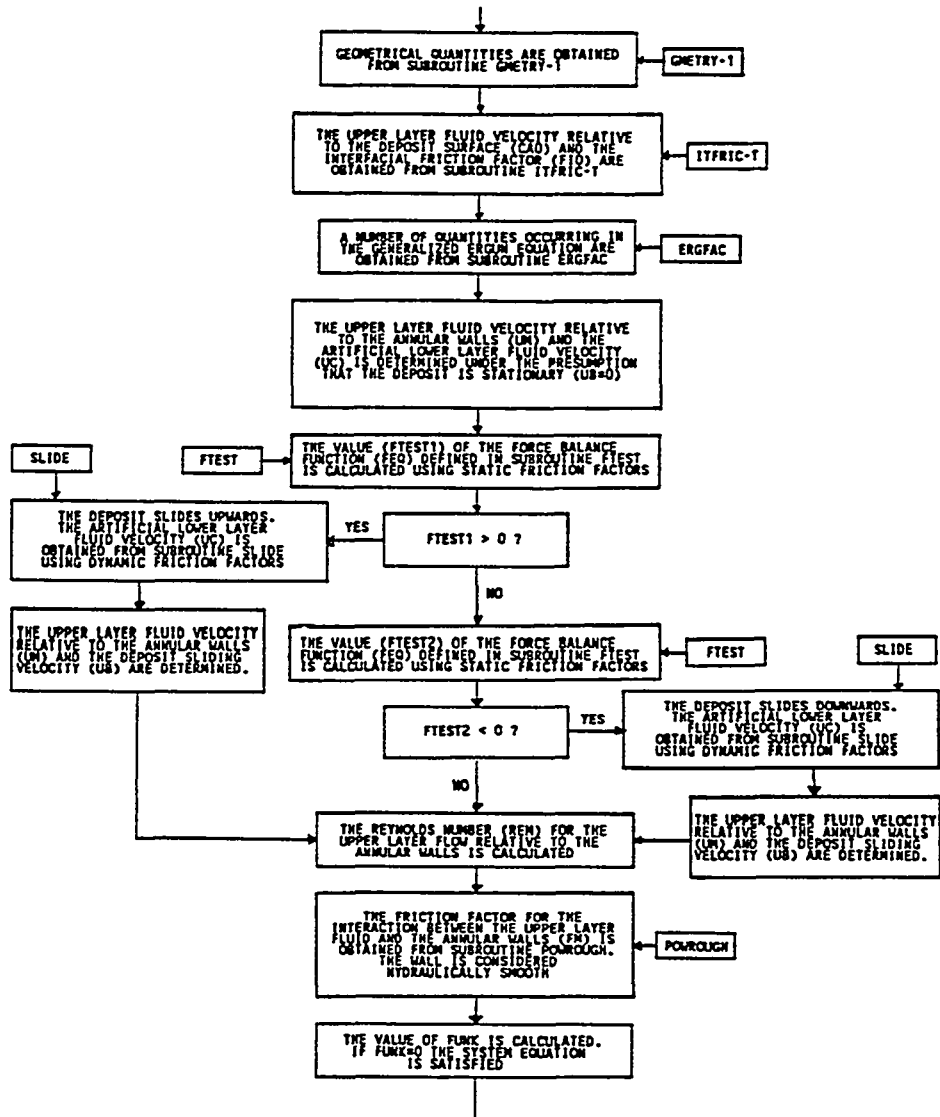
REGIME compares the height of the roughness protrusions with the thickness of the sublayer structure in hydraulically smooth flow and determines whether the flow is to be considered hydraulically smooth, in the transitional regime or completely rough. The regime affects the velocity gradient at the pipe wall and (through the variable ALFR) the damping factor Q described in the *Artyushkov et al.* model.



SECALC-F calculates and combines the various terms in equation (4.2.2-3). A value of β that satisfies this equation specifies a deposit size which makes the pressure gradient in the upper annular layer equal to the one in the lower layer. SECALC-F differs only slightly from SECALC-T: The call to GMETRY-2 replaces the call to GMETRY-1.

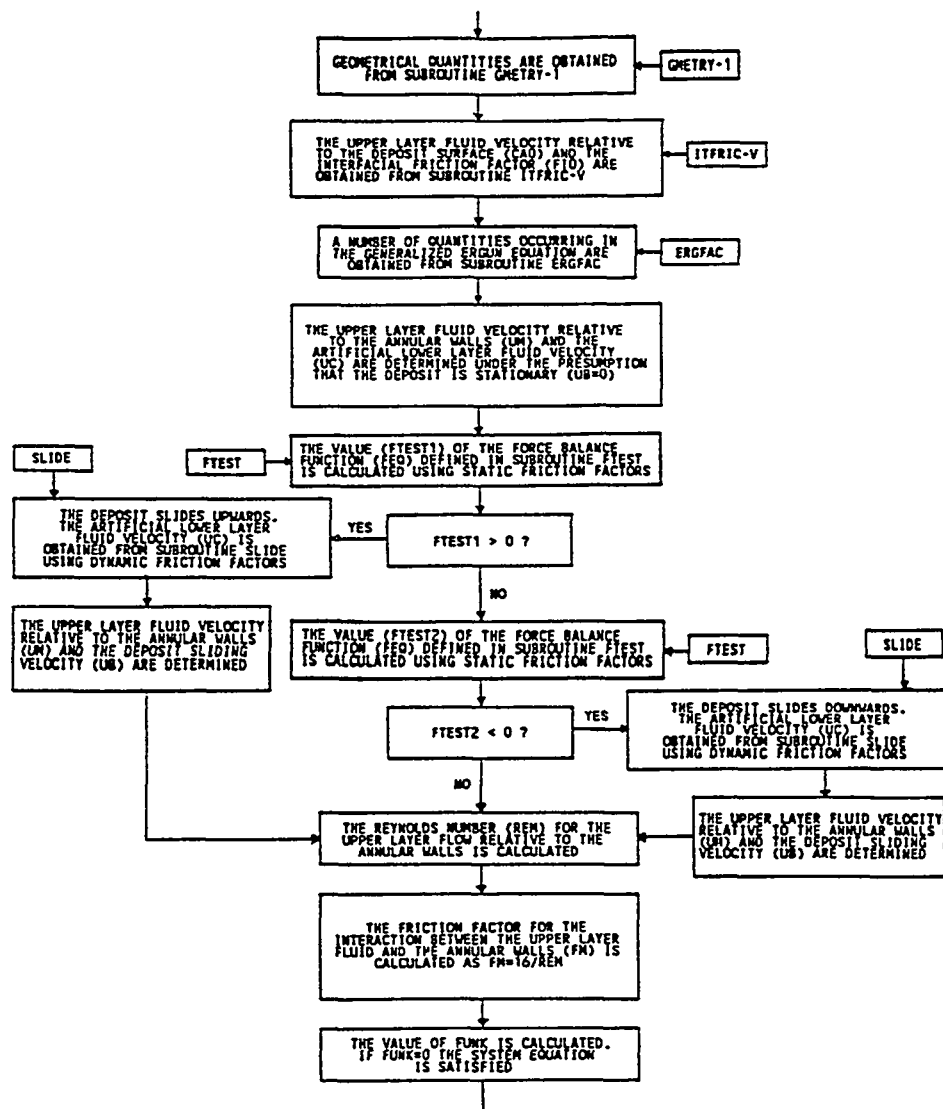


SECALC-T calculates and combines the various terms in equation (4.2.2-3). A value of β that satisfies this equation specifies a deposit size which makes the pressure gradient in the upper annular layer equal to the one in the lower layer.



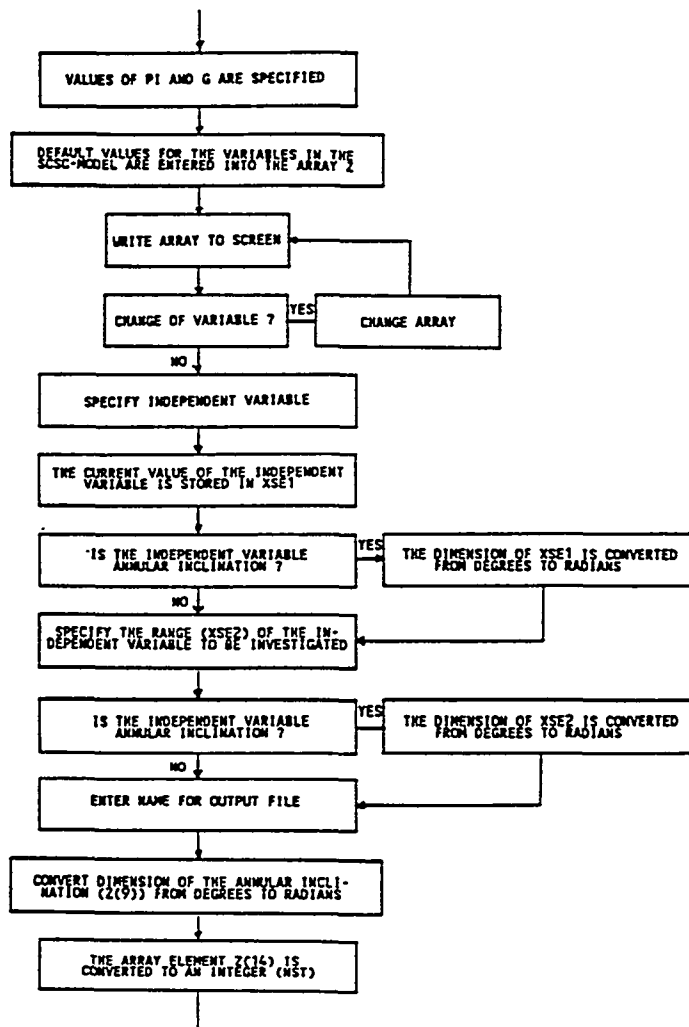
SECALC-V calculates and combines the various terms in equation (4.2.2-3). A value of β that satisfies this equation specifies a deposit size which makes the pressure gradient in the upper annular layer equal to the one in the lower layer.

SECALC-V differs only slightly from SECALC-T. The call to ITFRIC-V replaces the call to ITFRIC-T and the use of the laminar pipe flow relation ($f_m = 16/Re_m$) in the calculation of the friction factor at the upper layer annular walls replaces the use of subroutine POWROUGH.



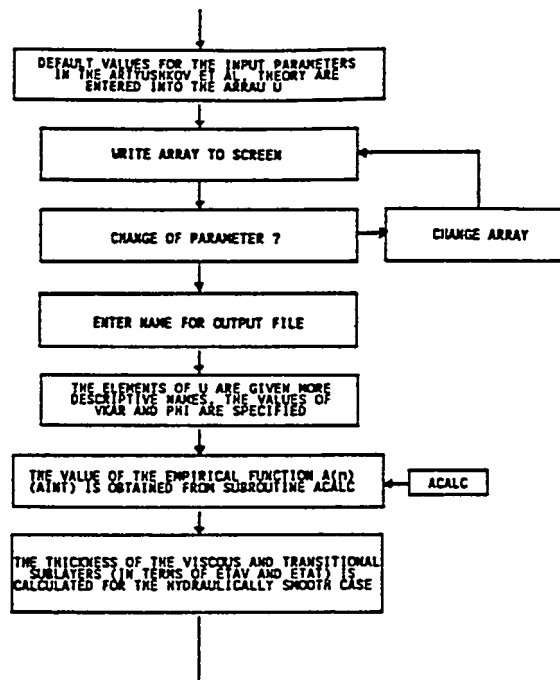
SETINIT present a default list of the physical variables which are required in the SCSB-model. A simple loop allows the user to change the value of any variable in the list. When the appearance of the list is accepted, the independent variable and the range inside which it is to be varied is requested. Finally a name must be given the file to which the programme directs the results.

It should be noted that while the annular inclination is listed in degrees, the computer code operates with radians, and consequently the dimension of this variable is transformed into radians before the return to the main programme.



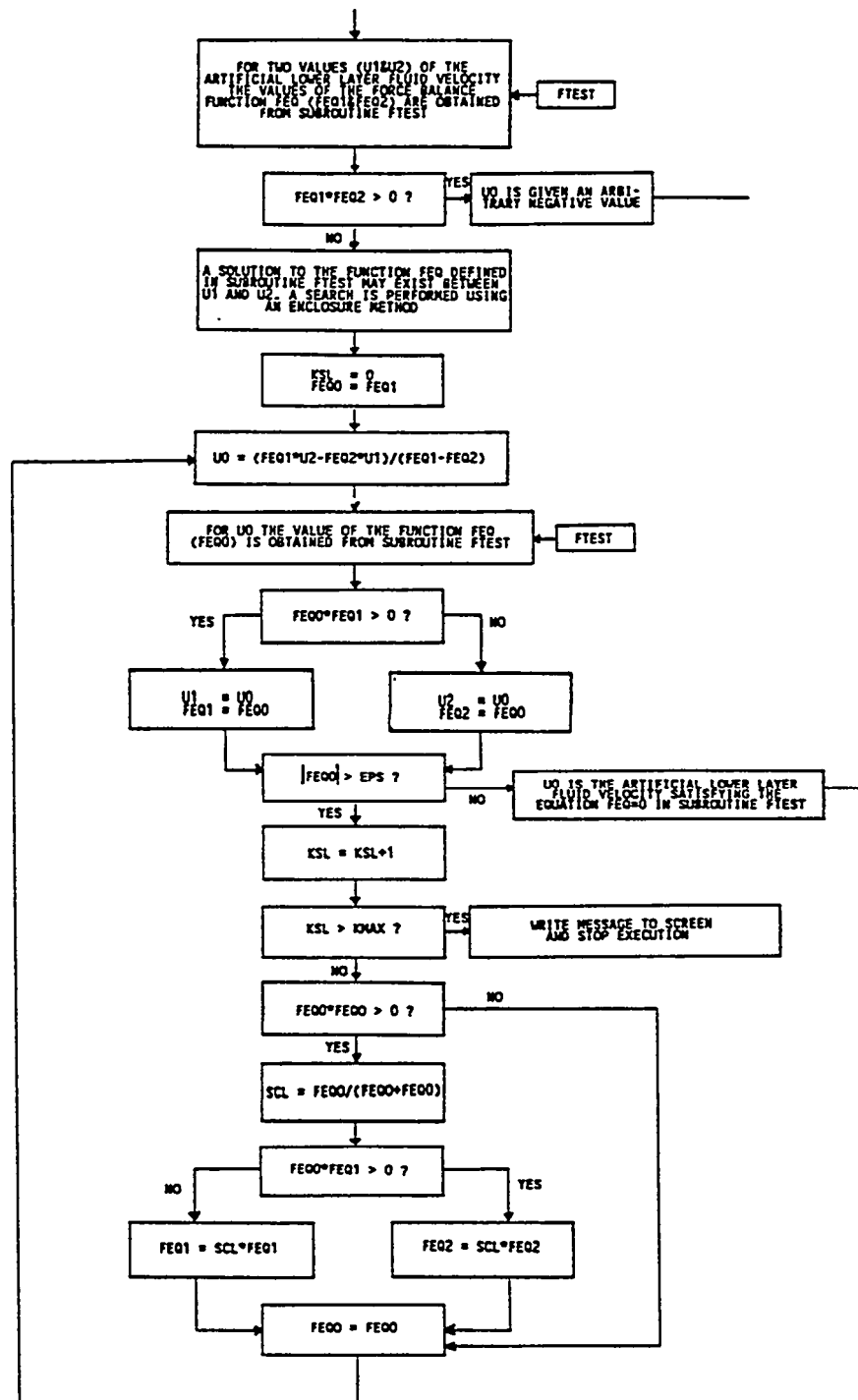
Subroutine SETPAR

SETPAR present a default list of the physical parameters occurring in the model outlined by *Artyushkov et al.* A simple loop allows the user to change the value of any parameter in the list. When the appearance of the list is accepted, a name of the file to which output data is to be directed, must be specified. Finally the value of the empirical function $A(n)$ given by *Artyushkov et al.* is determined.

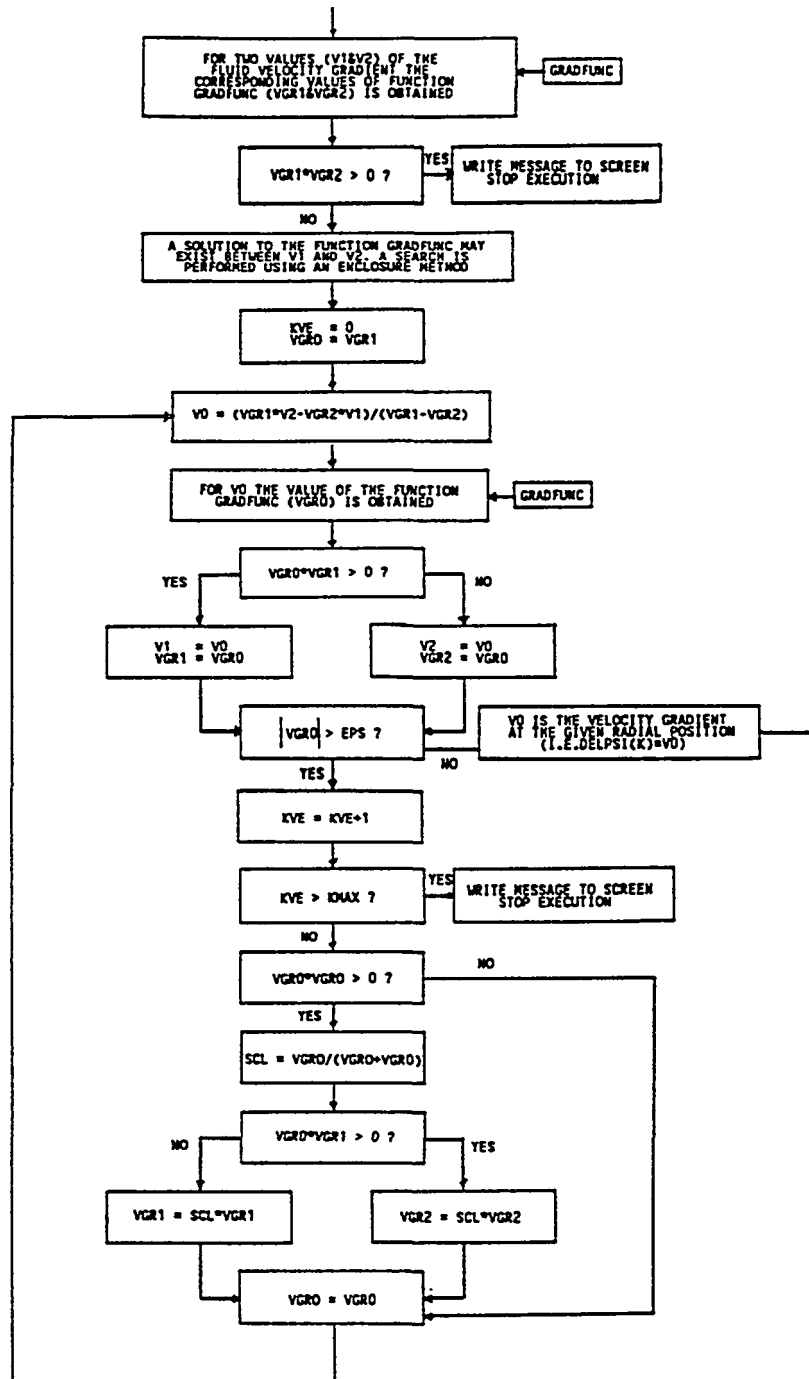


Subroutine SLIDE

When the deposit is stationary, the deposit sliding velocity is zero, and the upper- and lower layer fluid velocity are determined from relation (4.2.8-2) and the volumetric balance (4.2.5-1). If deposit sliding occurs, the nominal lower layer fluid velocity is determined by using the functions f_1 and f_2 defined in eqs. (4.2.7-1) and (4.2.7-2). Subroutine **SLIDE** performs an iterative solution of the equation $f_1=0$ (upwards sliding) or $f_2=0$ (downwards sliding).

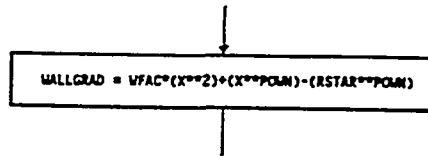


VELGRAD determines the fluid velocity gradient at a given radial position. The non-dimensional differential equation (A4-12) is considered to be an algebraic equation, where the velocity gradient is the independent variable. An iterative enclosure method is used in the search for a solution.



Function WALLGRAD

WALLGRAD calculates the value of the L.H.S. of the algebraic equation that forms if the velocity gradient is considered to be the independent variable in equation (A4-12) and $\bar{y} = 0$.


$$\text{WALLGRAD} = \text{VFAC} \cdot (\text{X}^2) + (\text{X}^{\text{POW}}) - (\text{RSTAR}^{\text{POW}})$$

Reference list

- 1) Artyushkov L. S., Khodorkovskiy Ya. S.: A Mathematical Model of Turbulent Flow of Power-Law, Purely-Viscous Non-Newtonian Fluids in Smooth and Rough Pipes. Fluid Mechanics - Soviet Research, 17 no.4, pp.61-67, 1988.
- 2) Artyushkov L. S., Narvskiy A. S.: Mathematical Modelling of Turbulent Flow of Power-Law Purely Viscous Non-Newtonian Fluids in Circular Cylindrical Pipes. Fluid Mechanics and Theory of Ships, pp.25-34, Leningrad Shipbuilding Institute, 1980. (In russian).
- 3) Becker T. E.: The Effects of Mud Weight and Hole Geometry Variations on Cuttings Transport in Directional Well Drilling. M.Sc. thesis, The University of Tulsa, 1982.
- 4) Becker T. E.: Mud-Weight and Hole Geometry Effects on Cuttings Transport While Drilling Directionally. SPE-paper 14711, 1985.
- 5) Becker T. E., Azar J. J., Okrajni S. S.: Correlations of Mud Rheological Properties With Cuttings Transport Performance in Directional Drilling. SPE-paper 19535, 1989. (Also in SPE Drilling Engineering, March 1991, pp.16-24)
- 6) Bird R. B., Stewart W. E., Lightfoot E. N.: Transport Phenomena. John Wiley & Sons, New York, 1960.
- 7) Brown N. P., Bern P. A., Weaver A.: Cleaning Deviated Holes: New Experimental and Theoretical Studies. SPE-paper 18636, 1989.
- 8) Brown R. L. & Richards J. C.: Principles of Powder Mechanics. 1. ed. Pergamon Press, Oxford, 1970.
- 9) Chien S-F: Annular Velocity for Rotary Drilling Operations. Int. J. Rock Mech. Min. Sci., 9, pp.403-416, 1972.
- 10) Dodge D. W., Metzner A. B.: Turbulent Flow of Non-Newtonian Systems. AIChE Journal, 5 no.2, pp.189-204, 1959.
- 11) Doron P., Granica D., Barnea D.: Slurry Flow in Horizontal Pipes - Experimental and Modelling. International Journal of Multiphase Flow, 13 no.4, pp.535-547, 1987.
- 12) Dowell Schlumberger: Cementing Technology. Nova Communications, London, 1984.
- 13) Fayed M. E., Otten L.: Handbook of Powder Science and Technology. Van Nostrand Reinhold Company, New York, 1984.
- 14) Garde R. J., Ranga Raju K. G.: Mechanics of Sediment Transportation and Alluvial Stream Problems. 1. reprint, Wiley Eastern Ltd., New Delhi, 1978.
- 15) Gavignet A. A., Sobey I. J.: A Model for the Transport of Cuttings in Highly Deviated Wells. SPE-paper 15417, 1986. (Also in Journal of Petroleum Technology, September 1989, pp.916-921).
- 16) Gonzalez G. S. P.: Part-Full Flow in Pipes with a Sediment Bed. Report Series A:17, Department of Hydraulics, Chalmers University of Technology, Goteborg, Sweden, 1988.

- 17) Grossmann U.: Hydraulischer Feststofftransport in Geneigten und Horizontalen Ringraumen Wahrend des Bohrprocesses. Ph.D. dissertation, Institut fur Tiefbohrtechnik, Erdol- und Erdgasgewinnung der Technischen Universitat Claustahl, Januar 1988. (In german). (Also in Erdol Erdgas Kohle, 106 no.2, Februar 1990)
- 18) Hall H. N., Thompson H., Nuss F.: Ability of Drilling Mud to Lift Bit Cuttings. Petroleum Transactions, AIME, 189, pp.35-46, 1950.
- 19) Heiss J. F., Coull J.: The effect of Orientation and Shape on the Settling Velocity of Non-Isometric Particles in a Viscous Medium.
- 20) Hemphill T.: Tests Determine Oil-Mud Properties to Watch in High-Angle Wells. Oil & Gas Journal, November 1990, pp.64-70.
- 21) Hopkin E. A.: Factors Affecting Cuttings Removal During Rotary Drilling. Journal of Petroleum Technology, 19, pp.807-814, 1967.
- 22) Hussaini R. S., Azar J. J.: Experimental Study of Drilled Cuttings Transport Using Common Drilling Muds. Society of Petroleum Engineers Journal, February 1983, pp.11-20.
- 23) Iyoho A. W.: Drilled-Cuttings Transport by Non-Newtonian Drilling Fluids Through Inclined, Eccentric Annuli. Ph.D. dissertation, The University of Tulsa, 1980.
- 24) Kemblowski Z., Mertl J.: Pressure Drop During the Flow of Stokesian Fluids Through Granular Beds. Chemical Engineering Science, 29, pp.213-223, 1974.
- 25) Martin M., Georges C., Bisson P., Kornisch O.: Transport of Cuttings in Directional Wells. SPE-paper 16083, 1987.
- 26) Nikuradse J.: Stromungsgesetze in rauhen Rohren. Forschungsheft 361, VDI-Verlag GmbH, Berlin, 1933. (In german).
- 27) Nikuradse J.: Gesetzmassigkeiten der turbulenten Stromung in glatten Rohren. Forschungsheft 356, VDI-Verlag GmbH, Berlin, 1932. (In german).
- 28) Okrajni S. S., Azar J. J.: Mud Cuttings Transport in Directional Well Drilling. SPE-paper 14178, 1985. (Also in SPE Drilling Engineering, August 1986, pp.297-308).
- 29) Peden J. M., Ford J. T., Oyenyin M. B.: Comprehensive Experimental Investigation of Drilled Cuttings Transport in Inclined Wells Including the Effects of Rotation and Eccentricity. SPE-paper 20925, 1990.
- 30) Peden J. M., Luo Y.: Settling Velocity of Variously Shaped Particles in Drilling and Fracturing Fluids. SPE Drilling Engineering, December 1987, pp.337-343.
- 31) Pettyjohn E. S., Christiansen E. B.: Effect of Particle Shape on Free Settling Rates of Isometric Particles. Chemical Engineering Progress, 44 no.2, pp.157-172, 1948.

- 32) Piggot R. J. S.: Mud Flow in Drilling. The Oil and Gas Journal, May 1941, pp.62-64 and p.146.
- 33) Rotta J.: Das in Wandnahe Gultige Geschwindigkeitgesetz Turbulenter Stromungen. Ingenieur Archiv, 18 no.4, pp.277-280, 1950. (In german).
- 34) Sample K. J., Bourgoyne A. T.: An Experimental Evaluation of Correlations Used for Predicting Cutting Slip Velocity. SPE-paper 6645, 1977.
- 35) Schlichting H.: Boundary Layer Theory. 6. Edition, McGraw-Hill Book Company, New York, 1968.
- 36) Seeberger M. H., Matlock R. W., Hanson P. M.: Oil Muds in Large-Diameter, Highly Deviated Wells: Solving the Cuttings Removal Problem. SPE-paper 18635, 1989.
- 37) Shields A.: Anwendung der Aehnlichkeitsmechanik und der Turbulenzforschung auf die Geschiebebewegung. Mitteilungen der Preussischen Vesuchsanstalt fur Wasserbau und Schiffbau, heft 26, Berlin, 1936. (In german).
- 38) Sifferman T. R., Myers G. M., Haden E. L., Wahl H. A.: Drill-Cutting Transport in Full-Scale Vertical Annuli. Journal of Petroleum Technology, November 1974, pp.1295-1302.
- 39) Thomas R. P., Azar J. J., Becker T. E.: Drillpipe Eccentricity Effect on drilled Cuttings Behavior in Vertical Wellbores. Journal of Petroleum Technology, September 1982, pp.1929-1937.
- 40) Tomren P. H., Iyoho A. W., Azar J. J.: Experimental Study of Cuttings Transport in Directional Wells. SPE Drilling Engineering, February 1986, pp.43-56.
- 41) van Driest E.R.: On Turbulent Flow Near a Wall. Journal of the Aeronautical Sciences, 23 no.11, pp.1007-1011 and p.1036, 1956.
- 42) Wadell H.: The Coeffecient of Resistance as a Function of Reynolds Number for Solids of Various Shapes. Journal of the Franklin Institute, April 1934, pp.459-490.
- 43) Walker R. E., Mayes T. M.: Design of Muds for Carrying Capacity. Journal of Petroleum Technology, July 1975, pp.893-900.
- 44) Williams C. E., Bruce G. H.: Carrying Capacity of Drilling Muds. Petroleum Transactions, AIME, 192, pp.111-120, 1951.
- 45) Willmarth W. W., Hawk N. E., Harvey R. L.: Steady and Unsteady Motions and Wakes of Freely Falling Discs. The Physics of Fluids, 7 no.2, pp.197-208, 1964.
- 46) Wilson K. C.: Slip Point of Beds in Solid-Liquid Pipeline Flow. Journal of the Hydraulics Division, Proceedings of the American Society of Civil Engineers, HY 1, pp.1-12, 1970.
- 47) Wilson K. C.: A Unified Physically Based Analysis of Solid-Liquid Pipeline Flow, Hydrotransport 4, paper A1-1-16, 1976.

- 48) Zeidler H. U.: An Experimental Analysis of the Transport of Drilled Particles. Society of Petroleum Engineers Journal, February 1972, pp.39-48.
- 49) Zeidler H. U.: Fluid and Drilled Particle Dynamics Related to Drilling Mud Carrying Capacity. Ph.D. dissertation, The University of Tulsa, 1974.

Symbols

$A(n)$	empirical function defined by Artyushkov <i>et al.</i> ^{1 2} (Appendix 4)
A_c	cross sectional area of the lower (deposit) layer
A_i	polynomial coefficient in Appendix 4
A_m	cross sectional area of the upper (fluid) layer
A_p	characteristic surface area for a particle
B_i	polynomial coefficient in Appendix 4
c_a	annular cuttings concentration
c_b	particle concentration in deposit
C_d	drag coefficient
c_f	annular feed concentration
C_i	polynomial coefficients in Appendix 4
D	diameter of (outer) pipe
d	diameter of inner pipe
d_c	characteristic particle dimension
D_h	the hydraulic diameter of the upper layer
d_p	particle diameter
e	displacement between the centres of the inner- and outer pipe
f	friction factor defined for pipe flow
F	function defined in Appendix 3
F_f	frictional force between particle and deposit surface
F_{fd}	fluid drag force on a particle
F_{gax}	axial component of net gravity
f_i	interfacial friction factor
f_m	friction factor for the interaction between the fluid and the annular walls
Fr	Froude number
f_1	function defined in chapter 4.2.7
f_2	function defined in chapter 4.2.7
g	gravitational acceleration
h	height of roughness protrusions
h^*	non-dimensional height of the roughness protrusions (Appendix 4)
k	Power Law consistency index
K	non-dimensional quantity defined by <i>Martin et al.</i> ²⁵
l	mixing length
n	Power Law flow behavior index
N	number of subintervals (Appendix 4)
m_{feed}	particle feed rate to annular section
p	pressure
P	modified pressure ($P = p + \rho_m g z$)
Q	non-dimensional damping factor defined in Appendix 4

R	pipe radius
R_t	transport ratio (defined in chapter 1.3.1)
R^*	non dimensional quantity defined in Appendix 4
Re	Reynolds number for a Newtonian fluid
Re'	Reynolds number for a Power Law fluid
Re_{km}	Reynolds number for interstitial flow of a Power Law fluid, defined by <i>Kemblowski & Mertl</i> ²⁴
Re_m	Reynolds number based on the fluid velocity relative to the annular walls
Re_p	particle Reynolds number in Newtonian fluids
Re'_p	particle Reynolds number for a Power Law fluid defined by <i>Peden & Luo</i> ²⁹
Re'_{tr}	Re' at the point of transition between laminar and turbulent flow
Re^*_o	Reynolds number based on the friction velocity at the point of incipient particle motion (Appendix 3)
s	permeability of a granular deposit defined by <i>Kemblowski & Mertl</i> ²⁴
s_{c1}	length of the outer pipe perimeter in contact with the deposit
s_{c2}	length of the inner pipe perimeter in contact with the deposit
s_i	length of the interface between the upper and lower layer
s_{m1}	length of the outer pipe in contact with the upper layer
s_{m2}	length of the inner pipe in contact with the upper layer
u	average linear fluid velocity
u^*	friction velocity
u_b	deposit sliding velocity relative to the annular walls
u_c	nominal lower layer fluid velocity
u_k	nominal intergranular fluid velocity
u_m	average linear upper layer fluid velocity relative to the annular walls
u_o	characteristic fluid velocity at the point of incipient motion
u^*_o	friction velocity at the point of incipient particle motion defined in Appendix 3
V	volumetric flowrate
v_a	average linear fluid velocity
v_p	average linear particle transport velocity
v_s	average linear particle slip velocity
v_z	axial fluid velocity in pipe flow
y	radial coordinate
\bar{y}	non dimensional radial coordinate
z	axial coordinate
α	contact angle between the deposit surface and the inner pipe wall
α_1	polynomial coefficient in Appendix 4
α_2	polynomial coefficient in Appendix 4
α_3	polynomial coefficient in Appendix 4
β	the angle describing the position of the deposit surface in the SCSB-model
ϵ	porosity of the deposit

ζ	empirical parameter defined by <i>Peden & Luo</i> ²⁹
η	coefficient of friction
η_a	non dimensional position parameter in Appendix 4
η_d	coefficient of dynamic friction
η_p	coefficient of friction for particle resting on the deposit surface
η_s	coefficient of static friction
η_t	non-dimensional thickness of the viscous and transitional sublayers
η_v	non-dimensional thickness of the viscous sublayer
θ	integration variable in Appendix 2
κ_k	empirical function defined by <i>Kemblowski & Mertl</i> ²⁴
κ_0	von Karman constant
λ	empirical parameter defined by <i>Peden & Luo</i> ²⁹
μ	fluid viscosity
μ_k	empirical function defined by <i>Kemblowski & Mertl</i> ²⁴
μ_m	Newtonian fluid viscosity
ν	kinematic fluid viscosity
ξ	factor determining the characteristic surface area of a particle (Appendix 3)
ρ	fluid density
ρ_c	lower layer particle density
ρ_m	upper layer fluid density
ρ_p	particle density
σ	integration variable in Appendix 2
τ	fluid shear stress
τ_c	frictional stress between the deposit and the annular walls
τ_{cl}	frictional stress between the deposit and the outer pipe wall
τ_{c2}	frictional stress between the deposit and the inner pipe wall
τ_i	fluid shear stress exerted on the deposit surface
τ_{lam}	laminar contribution to fluid shear stress (Appendix 4)
τ_m	the fluid shear stress exerted on the annular walls
τ_n^i	normal stress exerted by the deposit on the inner pipe wall
τ_n^o	normal stress exerted by the deposit on the outer pipe wall
$\tau_{n\ av}$	average normal shear stress exerted by the deposit on the annular walls
$\tau_{n\ av}^i$	average normal stress exerted by the deposit on the inner pipe wall
$\tau_{n\ av}^o$	average normal stress exerted by the deposit on the outer pipe wall
τ_{turb}	turbulent contribution to fluid shear stress (Appendix 4)
τ_0	fluid shear stress on the deposit surface at the point of incipient particle motion
φ	annular inclination/deposit surface inclination with respect to vertical
φ_a	function defined by <i>Artyushkov et al.</i> ^{1 2}

ψ non-dimensional fluid velocity defined in Appendix 4
 $\dot{\psi}$ non-dimensional fluid velocity gradient in Appendix 4
 ψ_k parameter defined by *Kemblowski & Mertl* ²⁴
 ψ_r Angle of repose (measured relative to horizontal).